

REPORT 69-3

DETERMINATION OF THE DESIGN
PARAMETERS FOR OPTIMUM
HEAVILY LOADED DUCTED FANS

TERRY WRIGHT

This work was done in partial
fulfillment of the requirements
for the degree of Doctor of Philosophy

NOVEMBER 1969

Prepared for
U. S. Army Research Office, Durham
under
Project THEMIS
Contract No. DAHCO4 68 0004

School of Aerospace Engineering
Georgia Institute of Technology
Atlanta, Georgia 30332

AD-697 802

ACKNOWLEDGMENTS

I would like to express my appreciation to Dr. Robin B. Gray for his suggestion of the thesis topic and for his guidance during the course of this research. I would also like to thank Dr. A. Alvin Pierce and Professor James E. Hubbartt for their careful examination of the manuscript.

The numerous discussions with Dr. Robert K. Sigman, Mr. C. E. Hammond, Mr. Larry Wright, and my wife Mary Anne have provided me with valuable insight into the various aspects of the problem from time to time. Their advice is greatly appreciated. I thank Dr. Keaton D. Whitehead and Mr. Howard L. Durham for suggestions concerning the computational procedures of the thesis.

The financial support of the National Aeronautics and Space Administration, the U. S. Army Research Office, Durham, and the Georgia Institute of Technology are gratefully acknowledged.

Finally, I wish to thank my parents, Mr. and Mrs. Roy J. Wright, for their assistance and wholehearted support during the earlier years of my education.

TABLE OF CONTENTS

	Page
ACKNOWLEDGMENTS	ii
LIST OF TABLES	v
LIST OF ILLUSTRATIONS	vi
NOMENCLATURE	viii
SUMMARY	xiii
Chapter	
I. INTRODUCTION	1
II. DEVELOPMENT OF THE WAKE VORTEX MODEL	4
III. ANALYSIS AND SOLUTION OF THE WAKE MODEL	24
IV. CALCULATION OF THE THRUST, POWER, AND INDUCED EFFICIENCY	37
Thrust Power Efficiency	
V. NUMERICAL PROCEDURES	54
Evaluation of the Velocity Components System of Linear Equations Thrust and Power Integrations	
VI. RESULTS	74
Appendix	
I. GEOMETRY AND MOTION OF THE INNER HELICAL SHEETS	86
II. VELOCITY FIELD OF THE UNIFORM BOUNDARY SHEET	90
III. CHECK CASES FOR THE NUMERICAL PROCEDURES	98
IV. PERFORMANCE AND DESIGN TABLES	105

TABLE OF CONTENTS (Continued)

	Page
CITED LITERATURE.	139

LIST OF TABLES

Table		Page
1.	Accuracy of the Wake Integrations	103

LIST OF ILLUSTRATIONS

Figure		Page
1.	Conceptual Diagram of Vortex Shedding at the Duct Trailing Edge	6
2.	Helical Coordinate System	7
3.	Ultimate Wake System Showing Paths of the Line Integrals	9
4.	Velocity Diagram at an Inner Helical Vortex Filament of the Ultimate Wake.	10
5.	Ultimate Wake System Showing Paths of the Line Integrals	13
6.	Concept of the Ultimate Wake Vortex System.	19
	(a) Boundary Sheet of Uniform Strength	
	(b) Boundary Sheet of Varying Strength	
	(c) Result of Superposition	
7.	Velocity Diagram with respect to the Rotating Blades of the Outermost Filament of the Inner Vortex Sheet and at the Adjacent Point of the Boundary Sheet	21
8.	Control Volume used in Determining the Thrust	38
9.	A Path of Line Integration in the Ultimate Wake	44
10.	Schematic Diagram of the Arrangement of Vortex Filaments and Control Points in the Ultimate Wake of the Ducted Fan.	64
11.	Network Used in Calculating the Velocity Integrals on the $\bar{z}F$ - Surface.	71
12.	Comparison of Two Methods of Determining the Blade Bound Vorticity for a Lightly Loaded Ducted Fan	75
13.	Comparison of Two Methods for Determining the Blade Bound Vorticity for a Lightly Loaded Ducted Fan	76

LIST OF ILLUSTRATIONS (Continued)

Figure		Page
14.	Comparison of Two Methods of Calculating the Blade Bound Vorticity for a Lightly Loaded Ducted Fan	77
15.	Comparison of Two Methods of Calculating the Blade Bound Vorticity for a Lightly Loaded Ducted Fan	78
16.	Comparison of the Blade Bound Vorticity for a Lightly Loaded Ducted Fan for Successive Numbers of Blades (Digital Computer Solution) with the Infinite Blade Solution (Exact).	79
17.	Comparison of Mass Coefficients for Increasing Numbers of Blades (Digital Computer Solution) with the Mass Coefficient for the Infinite Blade Case (Exact)	80
18.	Blade Bound Vorticity Distributions for a Family of Lightly Loaded Ducted Fans.	82
19.	Variation of the Load Scaling Factor.	83
20.	Variation of Thrust Coefficient with Load for the Family of Ducted Fans	84
21.	Variation of the Power Coefficient with Load for the Family of Ducted Fans	85
22.	Incremental Thrust Efficiency Diagram	88
23.	Geometry of the Ring-Element Sheet.	92
24.	Geometry of the Straight-Line-Element Sheet	95
25.	Schematic Arrangement of Filaments and Control Point in the Ultimate Wake of a Free Propeller.	100
26.	Comparison of Two Methods for Calculating the Blade Bound Vorticity for a Free Propeller.	101
27.	Convergence of the Wake Integrations to the Exact Results for the Infinite Blade Case	104

NOMENCLATURE

a_n	coefficients of the trigonometric series for the non-uniform boundary sheet strength distribution
a, \bar{a}, \bar{b}	dummy variables used in Appendix II
A_1	defined as $A_1 = \sin(\varphi - \varphi_{r_B})$
A_2	defined as $A_2 = \cos(\varphi - \varphi_{r_B})$
$A_{i,j}$	elements of the coefficient matrix of a system of linear equations
b	number of blades
B_n	coefficients of the trigonometric series for $\Gamma(x)$
C_P	power coefficient, $C_P = P/[\rho(\Omega R)^3 \pi R^2]$
C_T	thrust coefficient, $C_T = T/[\rho(\Omega R)^2 \pi R^2]$
e	non-dimensional energy loss, $e = E/[\rho(\Omega R)^3 \pi R^2]$
E	energy loss in wake, $E = Q - TV_\infty$
$f(t)$	function of time
f_ζ	integrand of the Biot-Savart equation for u_ζ
f_ξ	integrand of the Biot-Savart equation for u_ξ
f_r	integrand of the Biot-Savart equation for u_r
g_n	defined as $g_n = \int_{-\infty}^{\infty} f_{\zeta n} d\psi'$
G	load scale factor $G = 1 - u_{\xi_0} / w$
h, h_2	distances used in Appendix II
i	integer subscript
I	integer
I_ζ	integral of f_ζ , equation (22)

NOMENCLATURE (Continued)

I_r	integral of f_r , equation (21)
j	integer subscript
J	integer
k	number of divisions of a turn of a helical filament
$K(x)$	non-dimensional blade bound vorticity, $K(x) = \frac{b\Gamma(x)}{2\pi R\omega\lambda}$
$K_0(x)$	$K(x)$ for $\bar{w} = 0$ case
l	integer subscript
L	characteristic axial length in wake, $L = 2\pi R\lambda/b$
n	integer subscript
p	static pressure
p_∞	static pressure in undisturbed flow
p_0	total pressure
\bar{P}	non-dimensional distance from a vortex element to a control point
P	induced or ideal power
\bar{P}_1, \bar{P}_2	non-dimensional distances used in half-range integrations
Q	torque
r, ψ, z	polar-cylindrical coordinates
r', ψ', z'	polar-cylindrical coordinates locating a vortex element
R	radius of the ultimate wake and the fan
R_-	inside surface of the wake cylindrical boundary
R_+	outside surface of the wake cylindrical boundary
s'	a length of a vortex element
S	surface area

NOMENCLATURE (Continued)

t	time
T	total thrust of the ducted fan
u	disturbance velocity component in direction of subscript
u_{ξ_0}	disturbance velocity along wake axis
\bar{u}	non-dimensional disturbance velocity, $\bar{u} = u/w$
u_{ζ_B}	velocity describing motion of filaments of uniform boundary sheet
v	total disturbance velocity
V	total velocity
V_{∞}	velocity of the undisturbed flow
w	apparent axial displacement velocity of blade trailing vortex system
w_B	apparent axial displacement velocity of uniform boundary sheet
\bar{w}	non-dimensional apparent axial displacement velocity, $\bar{w} = w/\Omega R$
x	non-dimensional blade radial station, $x = r/R$
x, y, z	Cartesian coordinates
x', y', z'	Cartesian coordinates locating a vortex element
z'_0	axial distance between the $z = 0$ plane and the point where vortex filament intersects the xz -plane
\tilde{z}_c	non-dimensional characteristic length on the wake boundary, $\tilde{z}_c = L/2\pi R = \lambda/b$
α	angle defining direction of induced velocity in Appendix 11

NOMENCLATURE (Continued)

β	angle between ds' and \bar{P}
γ	a vortex filament strength
$\bar{\gamma}$	non-dimensional vortex filament strength, $\bar{\gamma} = \gamma/(4\pi R w \lambda G)$
$\tilde{\gamma}$	vortex sheet strength per unit length normal to the filaments
$\gamma(\zeta_B)$	vortex sheet strength of the uniform boundary sheet
$\Gamma(x)$	blade bound vortex strength distribution
$\delta_\ell(\Delta u/w)$	contribution of the ℓ th turn of a helical vortex filament to $\Delta u/w$
ϵ	defined as $\epsilon = \epsilon_r + \epsilon_\psi + \epsilon_z$
ϵ_0	numerical factor for C_T , equation (45)
ϵ_r	defined as $\epsilon_r = \int_0^1 \int_0^1 \int_0^{2\pi} \bar{u}_r^2 \bar{r} \, d\bar{r} \, d\bar{z} \, d\bar{\psi} / 2\pi$
ϵ_ψ	defined as $\epsilon_\psi = \int_0^1 \int_0^1 \int_0^{2\pi} \bar{u}_\psi^2 \bar{r} \, d\bar{r} \, d\bar{z} \, d\bar{\psi} / 2\pi$
ϵ_z	defined as $\epsilon_z = \int_0^1 \int_0^1 \int_0^{2\pi} \bar{u}_z^2 \bar{r} \, d\bar{r} \, d\bar{z} \, d\bar{\psi} / 2\pi$
ϵ_{R_-}	defined as $\epsilon_{R_-} = \int_0^1 \int_0^1 \int_0^{2\pi} [\bar{u}_{z_{R_-}}^2 + \bar{u}_{\psi_{R_-}}^2] \bar{r} \, d\bar{r} \, d\bar{z} \, d\bar{\psi} / 2\pi$
ζ	helical coordinate normal to the filaments
η_i	induced efficiency, $\eta_i = (\lambda - \bar{w}) C_T / C_P$
K	mass coefficient, $K = 2 \int_0^1 K(x) x \, dx$
K_0	K for $\bar{w} = 0$ case
λ	pitch of the inner helical sheets, $\lambda = (V_\infty + w) / \Omega R$

NOMENCLATURE (Continued)

λ_B	pitch of the uniform boundary sheet filaments, $\lambda_B = (V_\infty + w_B)/\Omega R$
μ	defined as $\mu = 2 \int_0^1 K(x) \frac{x}{x^2 + \lambda^2} dx$
μ_0	μ for $\bar{w} = 0$ case
ρ	fluid density
φ	pitch angle of an inner helical sheet at r
φ_R	pitch angle of an inner helical sheet at $r = R$
φ_B	pitch angle of the uniform boundary sheet
φ'	pitch angle of a filament of an inner helical sheet at r'
φ_{r_B}	dummy pitch angle defined by $\varphi_{r_B} = \tan^{-1}(\tan \varphi_B / \bar{r})$
Φ	disturbance velocity potential
ψ_0	an arbitrarily fixed polar angle
ω	half-width of a strip element of a vortex sheet
Ω	blade rotational speed (radians per second)

SUMMARY

Like the free propeller in axial flight, a single-rotation ducted fan of highest induced efficiency is characterized by an ultimate wake vortex system shed from the blade trailing edges whose apparent motion is that of rigid helical surfaces. In addition and concentric with this inner sheet system there is a cylindrical surface of helical vortex filaments shed from the duct trailing edge. For zero hub diameter and neglecting compressibility, viscosity, and tip clearance, a consistent mathematical model of the constant-diameter vortex wake is developed and the compatibility relationships to be satisfied are presented. Using the Biot-Savart equation, the vortex strength distribution in the ultimate wake is determined and then related to the blade bound vortex strength distribution. In addition, expressions are developed for the thrust, power, and induced efficiency which depend on numerical integrations of velocity profiles in the ultimate wake. It is shown that the wake vorticity and the velocity distribution in the wake, for all loadings from the lightly loaded limit to the heavily loaded static thrust condition may be extracted from the lightly loaded result through the use of a simple algebraic scale factor. The performance parameters, thrust, power and blade bound vortex strength, are thus expressed in terms of a lightly loaded solution for a given freestream velocity, blade tip speed, blade number and the loading parameter. The lightly loaded case is compared to existing theoretical and experimental

results. Some sample results for heavily loaded performance parameters and design parameters are presented and compared to the exact results for a heavily loaded ducted fan with an infinite number of blades. Results for the heavily loaded system over a broad range of conditions are presented.

CHAPTER I

INTRODUCTION

In recent years there has been an increasing interest in low speed thrust and high-lift devices for application to aircraft with short or vertical take-off and landing characteristics. One of the devices under consideration for this role is the ducted fan or shrouded propeller. Analytical and experimental work in this field have been summarized in an excellent review of the state of the art through 1963 by Sacks and Burnell¹. As pointed out in the review, there have existed for some time adequate means of sizing and designing a duct for a given choice of fan blade design but there has been no method available for optimizing the blade design for the finite bladed system which operates at any but the lightest loadings. For the lightly loaded case the problem has been solved by Tachmindji², Theodorsen³, and Gray^{4,5}. In more recent years Morgan⁶, Ordway, Sluyter, and Sonnerup⁷, Chaplin⁸, and others have published papers in the field of ducted fans, still with primary emphasis on the shroud design. It is the purpose of this research to provide the information needed to size and design the optimum heavily loaded ducted fan.

The basis for this work stems from the classical analysis of the free propeller. It has been shown by Betz⁹ that an isolated propeller having the highest possible induced efficiency, that is, an optimum free propeller, will generate an ultimate wake vortex

system which moves through the fluid medium as if the vortex sheets of the wake formed a rigid helical structure of constant pitch. Application of this constraint to the motion of the sheets provides a straightforward means of determining the radial distribution of shed vortex sheet strength distribution. This determination has been carried out by Goldstein¹⁰ and Theodorsen¹¹.

It has been shown by Gray⁴ that, for the ducted fan having the highest possible induced efficiency, the same arguments and considerations are valid concerning the geometry and motion of those vortex sheets which are shed from the blade trailing edges. These arguments are reproduced in Appendix I for completeness.

In addition to this constraint, the system must satisfy the Kutta condition at the duct trailing edge; that is, the flow at the trailing edge must be tangent to the duct mean camber surface. As a consequence of this condition a sheet of vorticity must be shed from the trailing edge forming a boundary sheet enclosing the screw-like sheets shed from the blade trailing edges. It is the determination of the geometry, motion, and strength distribution of this boundary sheet and its mutual interaction with the inner sheets which constitute the development of the ultimate wake vortex model for the ducted fan.

When the geometry and motion of the vortex sheets of the ultimate wake have been defined, a straightforward application of the Biot-Savart equation determines the strength distribution of the vortex sheets. The blade bound circulation or vortex strength distribution is then obtained by integration of the inner helical sheet strength. This bound circulation is the basic information from which the fan blades

can be designed using any of the methods available in the literature (e.g. Theodorsen¹¹). In addition, the vortex sheet strength distributions enable a detailed calculation of the flow in the wake from which the thrust and induced power may be calculated.

In the development and analysis which follows the effects of hub diameter, blade tip clearance, compressibility and viscosity are neglected. The results will therefore give an upper limit on the performance of single-rotation fans without stator vanes for comparison with other design methods.

CHAPTER II

DEVELOPMENT OF THE WAKE VORTEX MODEL

Earlier analyses by Gray (see Appendix I) have shown that the optimum condition is obtained for the ducted fan when the helical vortex sheets shed from the blades appear to move as rigid screw surfaces in the ultimate wake. The principle difference between the arguments used by Gray and those for the free propeller is that the induced velocity in the wake, at the surface of a helical vortex sheet, need not be normal to the sheet surface. Beyond the need for satisfying the Kutta condition at the duct trailing edge no other information is obtained and additional relationships must be developed in order to assure a compatible vortex model.

Further information may be obtained through consideration of the flow associated with the vortex systems. A blade trailing vortex sheet has large radial velocity components associated with it and, with respect to a coordinate system fixed in the duct, this flow is periodic. Consequently, if the duct mean camber surface is to correspond to a streamline, a distribution of vorticity must be placed along this surface to cancel all normal velocity components. Part of this distribution must be periodic in nature and must also be a function of the number of blades in the fan and must rotate with the blades. A portion of this periodic distribution is considered to be a continuation of each blade bound vortex which passes directly from the blade tip onto the duct

contour where it spreads out over the duct mean camber surface. Then, in accordance with the Helmholtz theorems, it moves aft along the mean camber surface and is shed at the duct trailing edge as free vortex filaments of varying geometry and density wrapped on a cylindrical surface. While these filaments are within the duct contour it is assumed that they make all of the necessary adjustments in phase relationship and density with the blade trailing vortex system so that the motion of this wake boundary system is along the tangent to the mean camber surface at the trailing edge of the duct as shown in Fig. 1. In addition to the blade bound vortex continuation, a portion of the duct trailing vortex sheet is considered to be shed from bound vortices of varying strength rotating in the duct with the blades. It is also assumed that the duct is designed so that there is no contraction or expansion of the wake downstream of the fan. This is a feasible design problem⁸ and guarantees that the duct is compatible with the wake geometry of the analysis.

Continuing with the examination of the velocities associated with the wake vortex sheets, consider a helical coordinate system r, ξ, ζ defined in terms of the cylindrical coordinates r, ψ, z as shown in Fig. 2. At a given instant an inner helical vortex sheet in the ultimate wake coincides with the $\zeta = 0$ surface. Then

$$r = r \quad , \quad 0 \leq r \leq \infty$$

$$\xi = r\psi \cos \varphi + z \cos \varphi \quad , \quad -\infty \leq \xi \leq \infty$$

$$\zeta = -r\psi \sin \varphi + z \sin \varphi \quad , \quad \frac{-(V_\infty + w) \cos \varphi}{2b (\Omega/2\pi)} \leq \zeta \leq \frac{(V_\infty + w) \cos \varphi}{2b (\Omega/2\pi)}$$

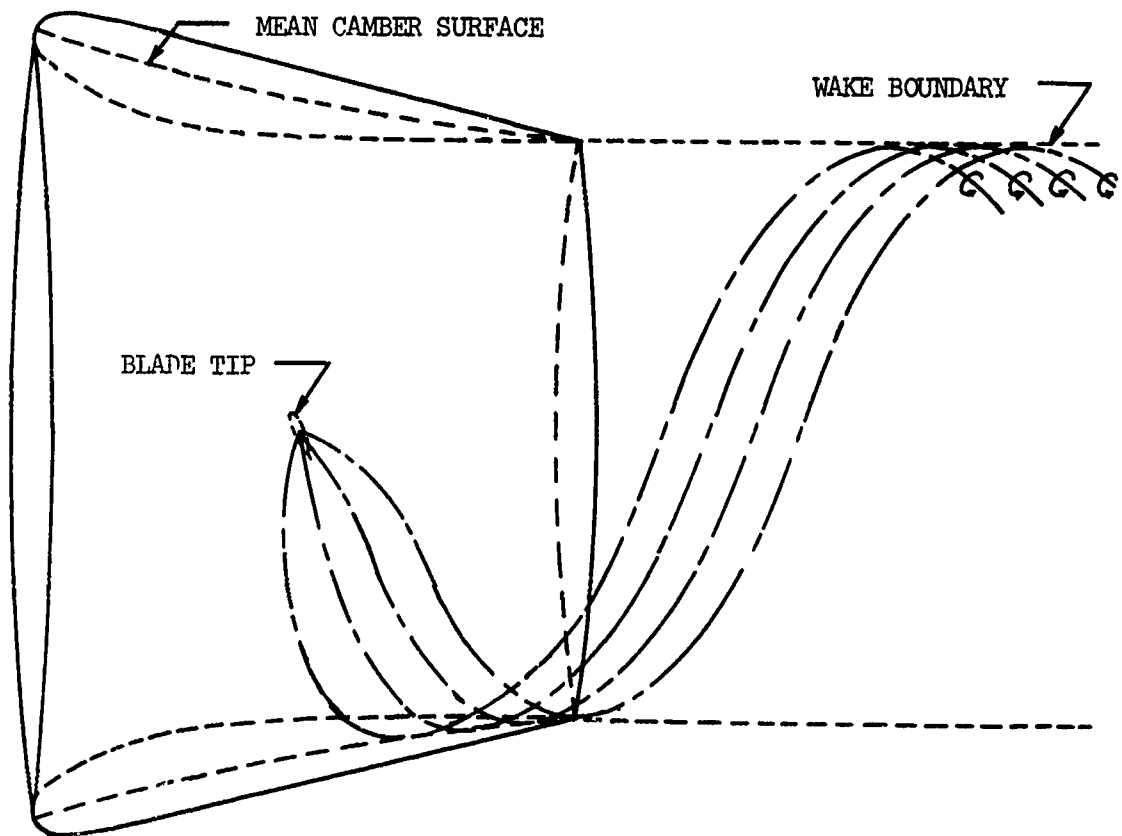


Figure 1. Conceptual Diagram of Vortex Shedding at the Duct Trailing Edge.

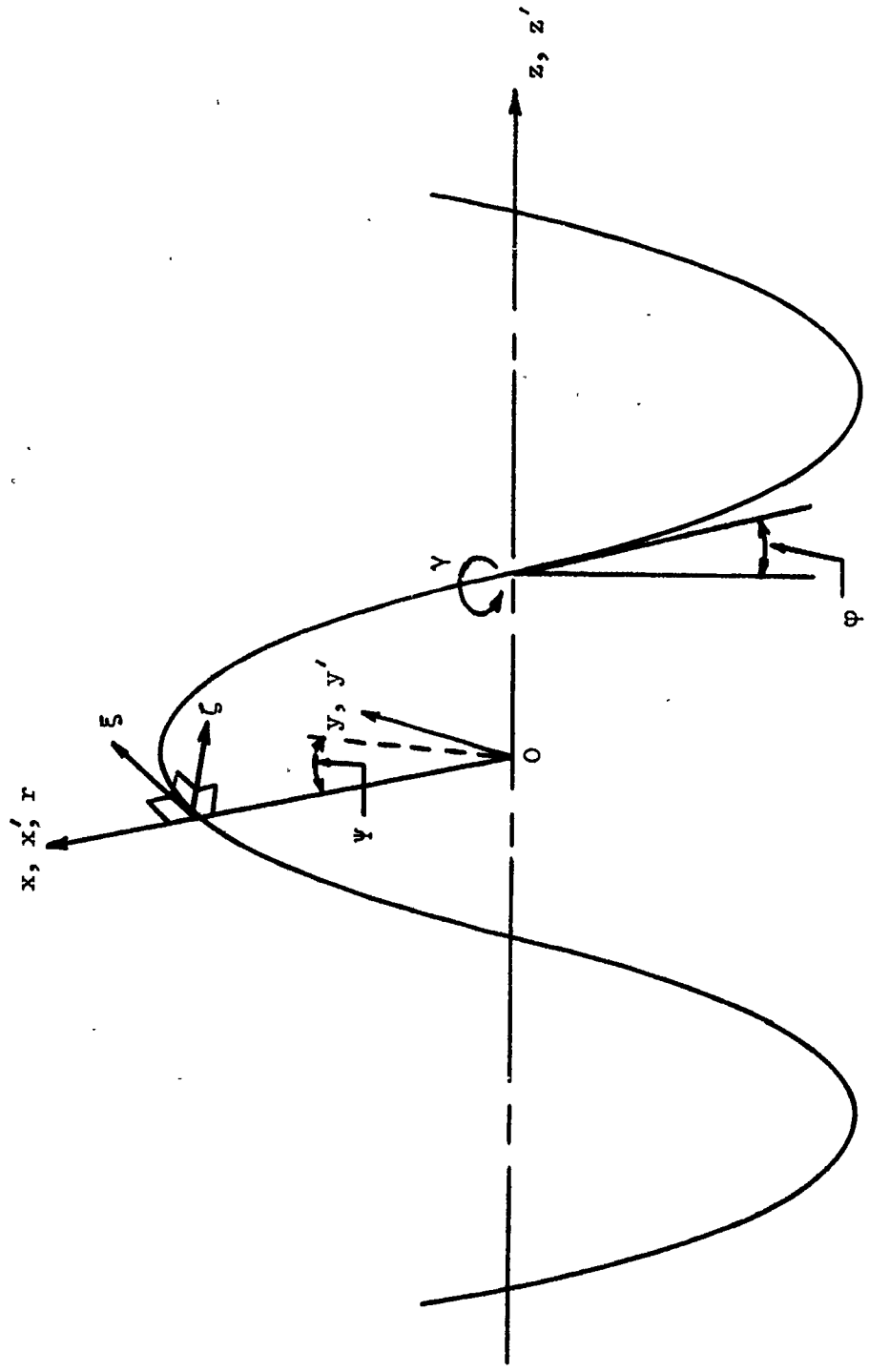


Figure 2. Helical Coordinate System.

where ξ is measured along the helical vortex filaments and ζ is measured along a helical line normal to the vortex filaments. It should be noted at the outset that w , the apparent velocity parameter, is not an actual disturbance velocity associated with the vortex sheets of the wake. Rather, it is the speed along the wake axis with which the inner helical sheets appear to be moving relative to a coordinate system fixed in space. Similarly $(V_\infty + w)$ is the axial speed with which the inner sheets appear to move relative to the ducted fan.

If the apparent rigid structure of the inner helical sheets in the ultimate wake is to be maintained, an observer fixed to any point on a sheet must see the same distribution of vorticity in the wake regardless of his angular position on the sheet. He must further see the same distribution above as he sees below. These constraints on the distribution of vorticity preclude the possibility of radial distortion of the inner sheets and amount to a requirement of helical symmetry of the wake vortex system. Subject to this helical symmetry the disturbance velocity vector will be constant along the helical lines $r = \text{constant}$ and $\zeta = \text{constant}$ both inside and outside the wake.

Now, consider a line integral of the velocity along the path \overline{ABCD} within the ultimate wake as shown in Fig. 3. The velocity diagram with respect to the rotating blades is shown in Fig. 4. Along \overline{BC} u_ξ is constant since r and ζ are constant. \overline{AB} and \overline{CD} are radial lines at two values of Ψ on the sheet surface and \overline{DA} coincides with the wake axis. Since no vorticity is enclosed by the path, the line integral is zero so that

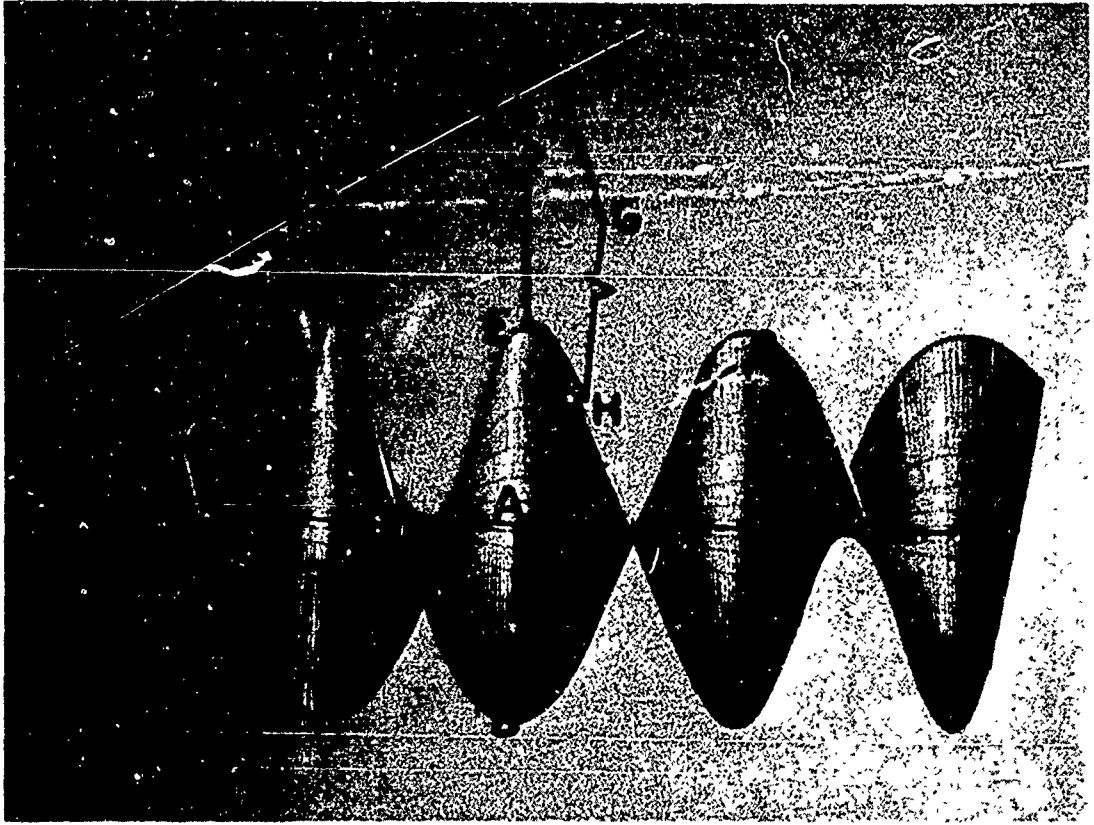


Fig. 3. Ultimate Wake System Showing Paths of Line Integrals.

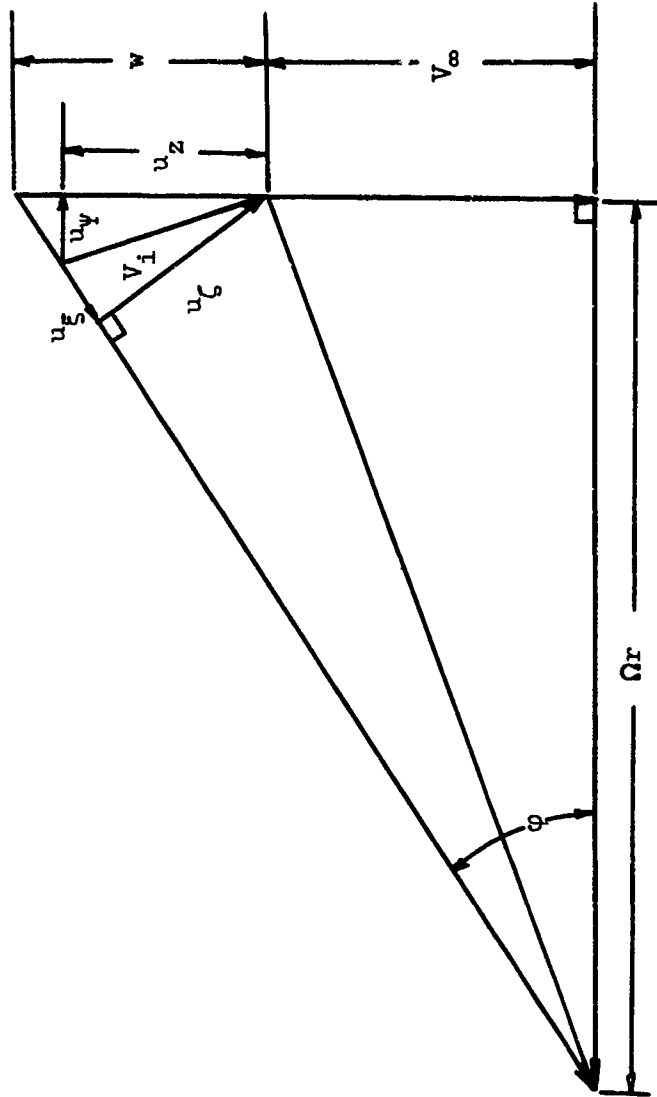


Figure 4. Velocity Diagram at an Inner Helical Vortex Filament of the Ultimate Wake.

$$\int_A^B u_r dr + \int_B^C u_\xi d\xi + \int_C^D u_r dr + \int_D^A u_\xi d\xi = 0$$

or

$$u_\xi (\xi_C - \xi_B) + u_{\xi_0} (z_A - z_D) = 0$$

where u_{ξ_0} is the value of u_ξ on the axis ($r = 0$).

Employing the helical coordinate relationships

$$- u_\xi \left(r \frac{2\pi}{b} \cos \varphi + \frac{V_\infty + w}{b(\Omega/2\pi)} \sin \varphi \right) + u_{\xi_0} \frac{V_\infty + w}{b(\Omega/2\pi)} = 0$$

Then

$$u_\xi = u_{\xi_0} \left\{ \frac{(V_\infty + w)/\Omega R}{\frac{r}{R} \cos \varphi + \frac{V_\infty + w}{\Omega R} \sin \varphi} \right\}$$

but $\tan \varphi_R = (V_\infty + w)/\Omega R$ and for the coordinate ζ

$r \tan \varphi = R \tan \varphi_P$ so that

$$u_\xi = u_{\xi_0} \left\{ \frac{\tan \varphi}{\cos \varphi + \tan \varphi \sin \varphi} \right\}$$

or

$$u_\xi = u_{\xi_0} \sin \varphi$$

Consider next the line integral along the path \overline{EFGHE} as shown in Fig. 3. The portion \overline{EH} is at $r = R_-$. From the requirement of helical symmetry, the filaments of the boundary vortex sheet must cross the line of intersection with an inner helical sheet at every

point on the intersection line at the same filament pitch angle regardless of angular position. In particular, if the pitch angle of the boundary sheet filaments is identical to that of the inner sheet as the boundary is reached ($r = R$) then no vorticity is enclosed by the path so that the line integral is zero. (The equal pitch constraint is a lightly loaded condition which will be relaxed later). Thus

$$u_{\xi} (\xi_G - \xi_F) + u_{\xi_0} \sin \varphi_R (\xi_E - \xi_H) = 0$$

or

$$u_{\xi} = u_{\xi_0} \sin \varphi$$

outside the wake as well as inside.

Further, the path \overline{ABCD} may be shifted axially so that the helical portion of the path lies along an arbitrary helical line at the pitch angle φ anywhere inside the wake. The restrictions of symmetry still require u_{ξ} to be constant along this path so that $u_{\xi} = u_{\xi_0} \sin \varphi$ throughout the wake.

These results are subject to the additional constraint that the line integral of velocity taken along a path enclosing the wake must be zero. The line integral may then be taken along the path \overline{ABCA} in Fig. 5 where u_{ξ} along \overline{ABC} is constant and known so that

$$\int_C^A u_z dz + 2\pi R u_{\xi_0} \tan \varphi_R = 0$$

The integral is then taken along \overline{ACDFA} . Subject to helical symmetry

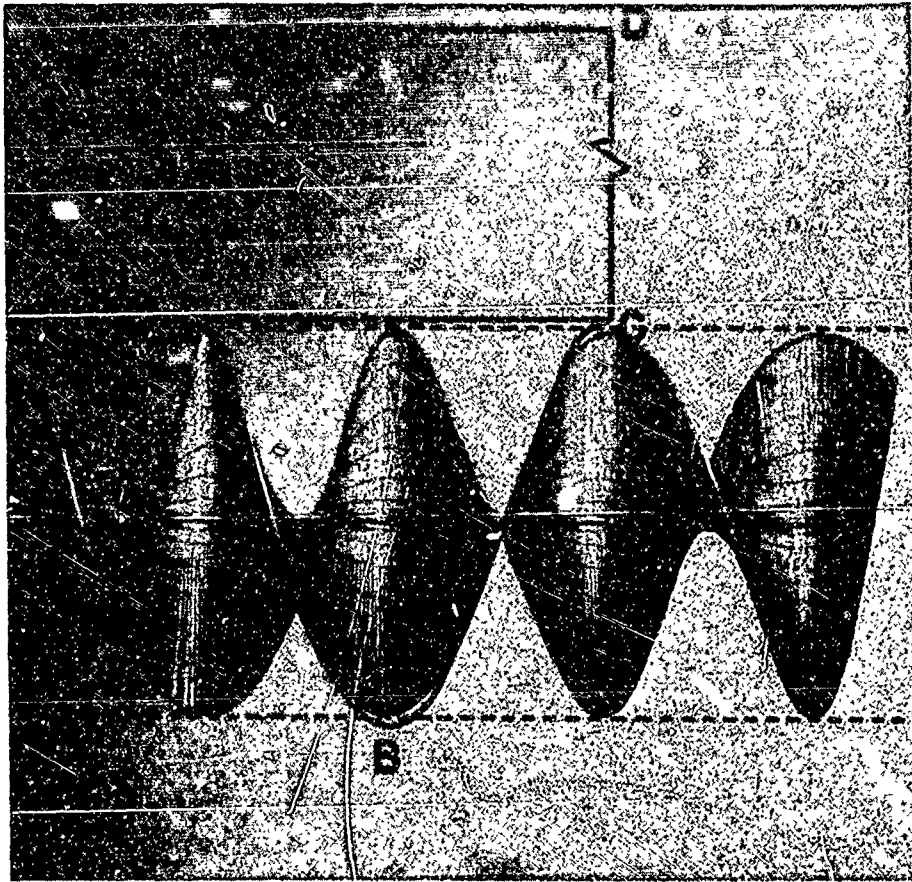


Fig. 5. Ultimate Wake System Showing Paths of Line Integrals.

the induced velocity is zero along the radial lines \overline{CD} and \overline{EA} . If \overline{DE} is allowed to approach infinity then u_z along \overline{DE} is zero. Since no vorticity is enclosed by the path

$$\int_C^A u_z dz = 0$$

Then, referring to the previous integration and subject to the condition of identical filament pitch angle along the intersection line, this result requires that u_{ξ_0} be zero. Thus, the induced velocity must be normal to the inner helical sheets. These two coexistent conditions of equal filament pitch and normal induced velocity characterize the lightly loaded conditions as discussed by Gray⁴.

The more general condition of load requires only that the filaments of the boundary sheet all cross the intersection line at the same pitch angle so that a relative motion between the inner and outer systems may exist. Thus, the path \overline{EFGHE} in Fig. 3 will enclose vorticity and no information will be obtained from the integral for a heavily loaded ducted fan. However, the requirements on u_{ξ} still apply inside the wake, and for the apparent rigid motion of the inner helical sheets u_{ζ} must be proportional to $\cos \varphi$. That is, from the previous results and the velocity diagram of Fig. 4

$$u_{\xi} = u_{\xi_0} \sin \varphi$$

$$u_{\zeta} = w \cos \varphi$$

A geometry and motion must now be established for the boundary sheet which will maintain helical symmetry of vortex strength distribution and which will permit the boundary sheet to have an axial motion relative to the inner sheets. Further, the disturbance velocities must be zero outside the wake in order that the flow be irrotational there. This may be shown by considering the line integral about \overline{ACDEA} as shown in Fig. 5. \overline{EA} and \overline{CD} are radial lines along which u_r must be zero by helical symmetry. \overline{ED} lies at $r = \infty$ so that u_z is zero along this path. Since the path encloses no vorticity the integral of u_z along \overline{AC} must be zero. For this to occur either u_z is identically zero or u_z is part positive and part negative. From considerations of continuity, for the latter condition to occur the flow must form closed streamlines within the area defined by the path of integration. However, integration of velocity along these closed streamlines would yield finite values of circulation. Thus, a contradiction is arrived at in terms of the irrotationality of the flow so that u_z must be zero along \overline{AC} . Another line integral is taken along \overline{ABCDEA} . For the helical portion of the path the velocity u_ξ must be constant due to helical symmetry. Since the velocities along the other branches of the path are zero and no net vorticity is enclosed, u_ξ must be identically zero along \overline{ABC} . The path \overline{ABC} may be shifted along the z -axis to any axial position with no change in the results. The path is closed by joining the helical part to the radial parts along the z -path \overline{AC} . Thus with u_ξ , u_z and u_r all identically zero on the outer surface it may be concluded that all induced velocities are zero on the outer surface of the wake boundary. This results may be extended to include the

entire region outside the wake by allowing the paths of integration to expand radially.

The strength of a vortex sheet is equal to the discontinuity in the velocity components as the sheet is crossed and the motion of the sheet along the line of discontinuity is equal to the mean value of the velocity at R_- and R_+ . At $r = R_-$, the induced velocity at the inner surface of the boundary sheet is given by the components

$$u_{\xi} = u_{\xi_0} \sin \varphi_R$$

$$u_{\zeta} = w \cos \varphi$$

while the induced velocity at R_+ is zero. Thus at the line of intersection with an inner helical sheet the boundary vortex sheet strength is given by

$$\gamma(\zeta_B) = (u_{\xi_0}^2 \sin^2 \varphi_R + w^2 \cos^2 \varphi_R)^{\frac{1}{2}} \quad (1)$$

The velocity of the filaments of the boundary sheet as they cross the intersection line must be in the direction of the induced velocity at R_- and normal to the filament direction; that is

$$u_{\zeta_B} = \frac{1}{2}(u_{\xi_0}^2 \sin^2 \varphi_R + w^2 \cos^2 \varphi_R)^{\frac{1}{2}} \quad (2)$$

The filaments of the boundary vortex sheet must then all cross the lines of intersection between the inner screw surface and the cylindrical boundary at a constant angle φ_B not equal to φ_R . This angle may be determined from the flight speed (V_{∞}), the blade rotational

speed (ΩR) and the total disturbance velocity of equation (1). The two vortex systems are related through equations (1) and (2) but only along their lines of intersection. On the wake boundary between these helical intersection lines, the filament density or sheet strength and the filament pitch angle will vary with the helical coordinate ζ .

The boundary sheet serves several basic purposes. First, it must cancel the radial velocity field at the boundary associated with the inner helical sheets. Second, it must accommodate the discontinuity in velocity as the boundary sheet is crossed. Third, it must not induce radial velocities, and hence radial distortions, at the inner sheet surfaces. Its remaining function is to preserve, in conjunction with the flow fields associated with the inner sheets, the apparent rigid axial motion of the inner sheets and to cancel the sum of vorticity of the inner sheets. The first and second requirements, along with the rigid axial motion constraint and the constraint on net vorticity, are satisfied by the strength distribution and the filament geometry both as yet unknown. The third condition may be automatically satisfied by a strength distribution and geometry that are symmetrical about the lines of intersection. This is simply a restatement of the helical symmetry requirements on the vortex systems.

Having to solve for both the strength distribution and the filament geometry of the boundary vortex sheet presents considerable difficulty and implies the need for some kind of iterative procedure for locating the compatible strengths and positions of the boundary sheet filaments. This difficulty may be eliminated through a consideration of the implications of the helical symmetry requirements.

It has been established that the boundary sheet strength and filament pitch angle are constant along an intersection line. At an arbitrary distance Δz below this line, the strength and filament pitch angle will be different. However, at any other angular position at the same Δz below the intersection line the pitch angle and strength must differ from the values at the intersection line by the same amounts due to the helical symmetry requirement. That is, at a z -position between intersection lines it is possible to change the sheet strength and filament pitch angle only through the addition of an infinitesimal strength vortex filament at the pitch angle φ_R . Thus, it is possible to replace the boundary sheet by two simpler systems whose combined effects satisfy all of the conditions mentioned above.

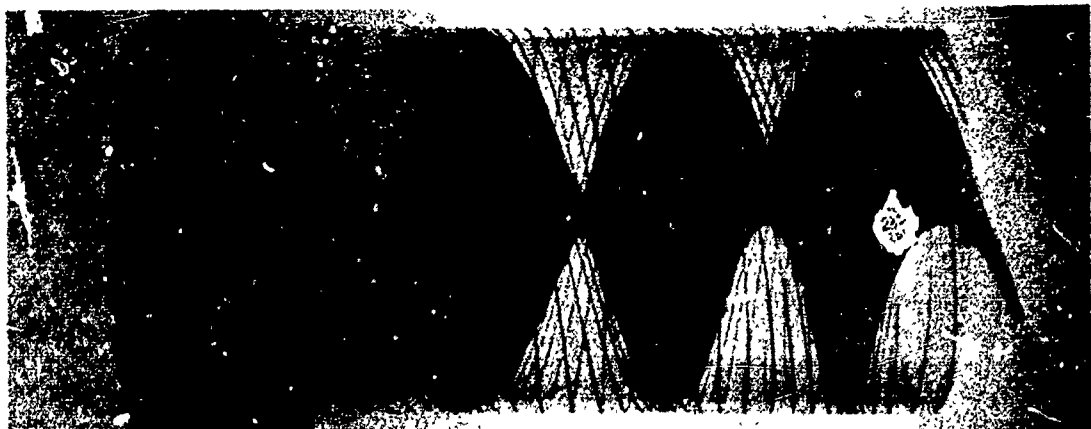
The first of these sheets is a uniform sheet of helical vortex filaments having constant density $\gamma(\zeta_B)$ and constant pitch angle φ_B as shown in Fig. 6a. This sheet satisfies the required compatibility conditions as previously discussed. The second is a cylindrical sheet of helical filaments of varying and unknown strength but having a constant and known pitch angle φ_R as shown in Fig. 6b. This sheet must have zero strength along the lines of intersection in order to preserve the compatibility established by the first sheet. It must have a symmetrical strength distribution about these lines and the lines midway between adjacent intersection lines and must cancel the radial velocities at the cylindrical boundary associated with the inner sheets. Superposition of the two sheets, as shown in Fig. 6c, must maintain the apparent rigid axial motion of the inner sheets in



(a) Boundary Sheet of Uniform Strength.



(b) Boundary Sheet of Varying Strength.



(c) Result of Superposition.

Fig. 6. Concept of Ultimate Wake Vortex System.

conjunction with the flow fields associated with those sheets, and must satisfy the net vorticity constraint. These are the conditions which will be placed on the solution.

It should be noted that to an observer fixed on an inner helical sheet the boundary vortex sheet (consisting of the superposition of the uniform boundary sheet and the non-uniform boundary sheet) appears in terms of the local strength distribution and geometry to be fixed relative to the inner sheet. Although the boundary sheet is actually slipping forward relative to the inner sheets, the observer sees the same local vortex sheet strength at a given point on the boundary at any instant while the identity of the filaments at the point is constantly changing.

Now consider the geometry and motion of the uniform boundary sheet relative to the last outboard filament of an adjacent inner helical vortex sheet. The velocity diagram of Fig. 7 illustrates the relationship between the velocities associated with the two systems according to the compatibility condition expressed in equations (1) and (2). From Fig. 7

$$\lambda = \tan \varphi_R = \frac{V_\infty + w}{\Omega R} \quad (3)$$

$$\lambda_B = \tan \varphi_B = \frac{V_\infty + w_B}{\Omega R}$$

where

$$w_B = \frac{1}{2} (u_{S_0}^2 \sin^2 \varphi_R + w^2 \cos^2 \varphi_R)^{\frac{1}{2}} \sec \varphi_B \quad (4)$$

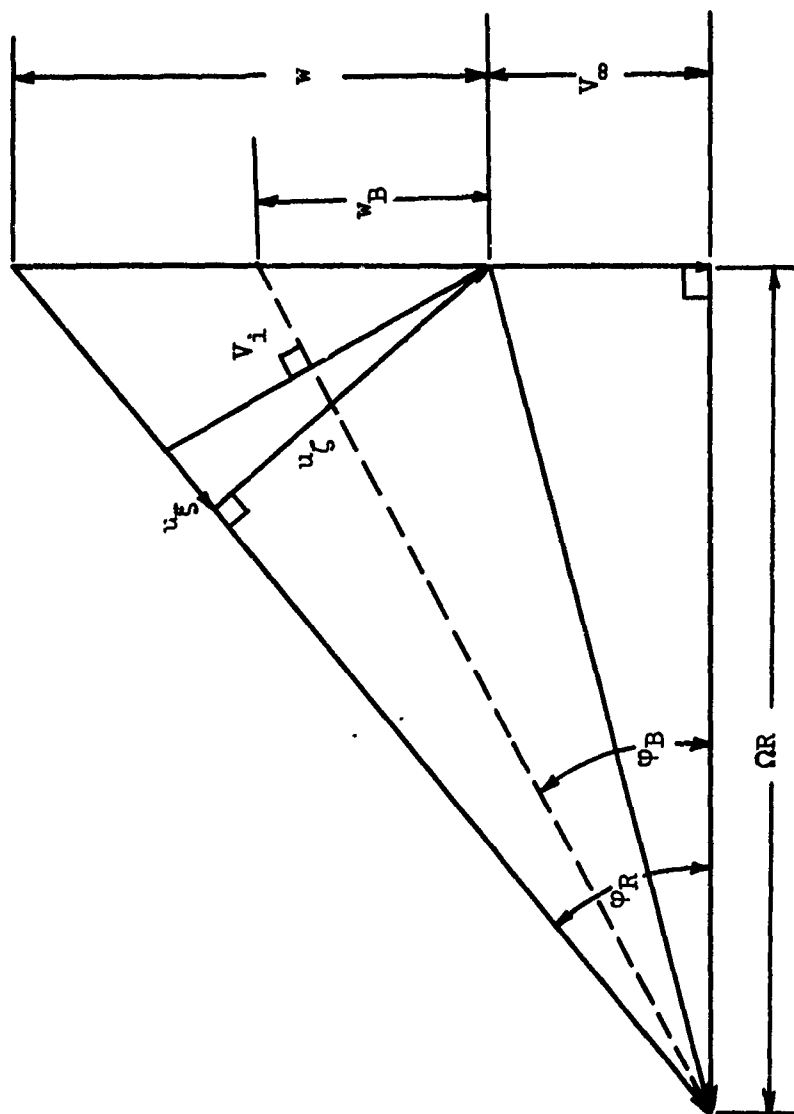


Figure 7. Velocity Diagram with respect to the Rotating Blades of the Outermost Filament of the Inner Vortex Sheet and at the Adjacent Point of the Boundary Sheet.

From the same figure

$$\frac{u_{\xi_0} \sin \varphi_R}{w \cos \varphi_R} = \tan (\varphi_R - \varphi_B) \quad (5)$$

Combining equation (4) and (5) to eliminate u_{ξ_0} and substituting for the functions of equations (3) yields

$$\lambda_B = \lambda - \bar{w} \left[1 + \frac{1}{2} \frac{1 + \lambda_B^2}{1 + \lambda \lambda_B} \right]$$

where $\bar{w} = w/\Omega R$, $0 \leq \bar{w} \leq \lambda$. This result shows that, for any choice of λ and \bar{w} , λ_B can be uniquely determined. It should be noted that for vanishingly small values of w , λ_B approaches λ which is in agreement with the lightly loaded case. Further, there would seem to be no simple redefinition of λ which would reduce the solutions to a single case for all values of \bar{w} . This is in agreement with the earlier analyses of Gray⁴.

Solving the last expression for the pitch of the uniform boundary sheet yields

$$\lambda_B = \lambda - \frac{1 + \lambda^2}{2\lambda - \bar{w}} + \left[\left(\lambda - \frac{1 + \lambda^2}{2\lambda - \bar{w}} \right)^2 + 1 \right]^{\frac{1}{2}} \quad (6)$$

Since $\varphi_B = \tan^{-1} \lambda_B$, the value of $\gamma(\zeta_B)$ is known according to

$$\gamma(\zeta_B) = w \cos \varphi_R \sec (\varphi_R - \varphi_B) \quad (7)$$

The ultimate wake vortex system of the heavily loaded ducted fan is thus defined in terms of the inner helical sheets of Fig. 5 (one for

each blade) having unknown strength but known geometry, a vortex sheet of uniform strength $\gamma(\zeta_B)$ and constant filament pitch angle φ_B lying on the cylindrical wake boundary as shown in Fig. 6a, and a sheet of varying strength but constant filament pitch angle φ_R also lying on the cylindrical wake boundary as shown in Fig. 6b. For a given blade number b , pitch λ , and loading parameter \bar{w} , the motion and geometry of the system are determined along with the strength of the uniform boundary sheet. The solution of this model for the unknown strength distributions of the inner sheets and the non-uniform boundary sheet proceeds directly through the application of the Biot-Savart equation.

CHAPTER III

ANALYSIS AND SOLUTION OF THE WAKE MODEL

From the discussion of the preceding chapter, the geometry and motion of the ultimate wake vortex system of infinite length are known. The problem is now to find the distribution of vorticity in the wake which will satisfy the velocity boundary conditions implied by this geometry and motion. In this analysis, the Biot-Savart equation supplies the required relationship between the geometry, motion, and vortex sheet strengths. For an elemental length of an arbitrary vortex filament

$$dv_i = \frac{\gamma}{4\pi} \frac{\cos \beta ds'}{\bar{r}^2} \quad (8)$$

The integral relations for the velocity components in Cartesian coordinates are given by Lamb¹² and are repeated here for a single finite strength vortex filament.

$$\Delta u_x = \frac{\gamma}{4\pi} \int \left(\frac{dy'}{ds'} \frac{z - z'}{\bar{r}} - \frac{dz'}{ds'} \frac{y - y'}{\bar{r}} \right) \frac{ds'}{\bar{r}^2}$$

$$\Delta u_y = \frac{\gamma}{4\pi} \int \left(\frac{dz'}{ds'} \frac{x - x'}{\bar{r}} - \frac{dx'}{ds'} \frac{z - z'}{\bar{r}} \right) \frac{ds'}{\bar{r}^2}$$

$$\Delta u_z = \frac{\gamma}{4\pi} \int \left(\frac{dx'}{ds'} \frac{y - y'}{\bar{r}} - \frac{dy'}{ds'} \frac{x - x'}{\bar{r}} \right) \frac{ds'}{\bar{r}^2}$$

A vortex sheet of the wake system is divided into a number of equal width strips. These strips are replaced by vortex filaments of finite but unknown strengths lying on the centerlines of the strips. The strength of the filament must be equal to the integral of the sheet strength across the strip width. For purposes of numerical calculation, an adequate representation of the vortex sheet is achieved by placing a filament along the centerline of its corresponding strip, provided the strip width is sufficiently small compared to a characteristic sheet width.

The integrals for the velocity components associated with the finite strength helical vortex filaments introduced in this manner are more conveniently expressed in polar coordinates so that the following transformation is made. (See Fig. 2.)

$$x' = r' \cos \Psi'$$

$$x = r \cos \Psi$$

$$y' = r' \sin \Psi'$$

$$y = r \sin \Psi$$

$$z' = z'_0 + r' \Psi' \tan \phi'$$

$$z = z$$

$$s' = r' \Psi' \sec \phi'$$

Employing the transformation yields

$$u_x = -\frac{\gamma}{4\pi} \int \left[r' \tan \varphi' (r \sin \Psi - r' \sin \Psi') - r' \cos \Psi' (z - z'_0 - r' \Psi' \tan \varphi') \right] \frac{d\Psi'}{\bar{p}^3}$$

$$u_y = \frac{\gamma}{4\pi} \int \left[r' \tan \varphi' (r \cos \Psi - r' \cos \Psi') + r' \sin \Psi' (z - z'_0 - r' \Psi' \tan \varphi') \right] \frac{d\Psi'}{\bar{p}^3}$$

$$u_z = \frac{\gamma}{4\pi} \int \left[r'^2 - r r' \cos (\Psi' - \Psi) \right] \frac{d\Psi'}{\bar{p}^3}$$

where

$$\bar{p}^2 = r^2 + r'^2 - 2 r r' \cos (\Psi' - \Psi) + (z - z'_0 - r' \Psi' \tan \varphi')^2$$

The boundary conditions are more conveniently expressed in terms of the velocity components along the vortex sheets and perpendicular to the sheets. Thus

$$u_r = u_x \cos \Psi + u_y \sin \Psi$$

$$u_\xi = (u_y \cos \Psi - u_x \sin \Psi) \cos \varphi + u_z \sin \varphi$$

$$u_\zeta = u_z \cos \varphi - (u_y \cos \Psi - u_x \sin \Psi) \sin \varphi$$

The integrals for these velocities due to a single finite strength filament become

$$\Delta u_r = \frac{\gamma}{4\pi} \int_{-\infty}^{\infty} \left[r'^2 \tan \varphi' \sin (\Psi' - \Psi) \right. \\ \left. + r' [z - z'_0 - r'\Psi' \tan \varphi'] \cos (\Psi' - \Psi) \right] \frac{d\Psi'}{P^3}$$

$$\Delta u_\xi = \frac{\gamma}{4\pi} \int_{-\infty}^{\infty} \left[\left\{ r' \tan \varphi' [r - r' \cos (\Psi' - \Psi)] \right. \right. \\ \left. \left. + r' [z - z'_0 - r'\Psi' \tan \varphi'] \sin (\Psi' - \Psi) \right\} \cos \varphi \right. \\ \left. + \left\{ r'^2 - rr' \cos (\Psi' - \Psi) \right\} \sin \varphi \right] \frac{d\Psi'}{P^3}$$

$$\Delta u_\zeta = \frac{\gamma}{4\pi} \int_{-\infty}^{\infty} \left[\left\{ r'^2 - rr' \cos (\Psi' - \Psi) \right\} \cos \varphi \right. \\ \left. - \left\{ r' \tan \varphi' [r - r' \cos (\Psi' - \Psi)] \right. \right. \\ \left. \left. + r' [z - z'_0 - r'\Psi' \tan \varphi'] \sin (\Psi' - \Psi) \right\} \sin \varphi \right] \frac{d\Psi'}{P^3}$$

where the limits on the integrals refer to the infinite extent of the ultimate wake.

Now, non-dimensionalizing these equations with w and R , and employing the helical relation

$$r \tan \varphi = r' \tan \varphi' = R \tan \varphi_R ,$$

the elemental velocities associated with one filament become

$$\frac{\Delta u_r}{w} = \frac{\gamma}{4\pi R w} \int_{-\infty}^{\infty} \left[\bar{r}' \tan \varphi_R \sin (\Psi' - \Psi) + \bar{r}' [\bar{z} - \bar{z}'_0 - \Psi' \tan \varphi_R] \cos (\Psi' - \Psi) \right] \frac{d\Psi'}{\bar{p}^3} \quad (9)$$

$$\frac{\Delta u_\xi}{w} = \frac{\gamma \cos \varphi}{4\pi R w} \int_{-\infty}^{\infty} \left[\bar{r}' \tan \varphi_R \left(\frac{\bar{r}}{\bar{r}'} + \frac{\bar{r}'}{\bar{r}} - 2 \cos (\Psi' - \Psi) \right) + [\bar{z} - \bar{z}'_0 - \Psi' \tan \varphi_R] \sin (\Psi' - \Psi) \right] \frac{d\Psi'}{\bar{p}^3} \quad (10)$$

$$\frac{\Delta u_\zeta}{w} = \frac{\gamma \cos \varphi}{4\pi R w} \int_{-\infty}^{\infty} \left[\bar{r}'^2 - \bar{r}\bar{r}' \cos (\Psi' - \Psi) - \tan^2 \varphi_R \left[1 - \frac{\bar{r}'}{\bar{r}} \cos (\Psi' - \Psi) \right] - \frac{\bar{r}'}{\bar{r}} \sin (\Psi' - \Psi) \tan \varphi_R [\bar{z} - \bar{z}'_0 - \Psi' \tan \varphi_R] \right] \frac{d\Psi'}{\bar{p}^3} \quad (11)$$

where

$$\bar{p}^2 = \bar{r}^2 + \bar{r}'^2 - 2 \bar{r}\bar{r}' \cos (\Psi' - \Psi) + [\bar{z} - \bar{z}'_0 - \Psi' \tan \varphi_R]^2$$

$$\varphi = \tan^{-1} \left[\frac{1}{\bar{r}} \tan \varphi_R \right]$$

and \bar{r} , \bar{r}' , \bar{z} , \bar{z}'_0 are non-dimensionalized by R .

The boundary conditions may be written by summing the contributions of every filament of the system. They are,

on the inner sheet:

$$\sum \left(\frac{\Delta u_{\zeta}}{w} \right) = \cos \varphi \quad (12)$$

$$\sum \left(\frac{\Delta u_r}{w} \right) = 0 \quad (13)$$

and on the cylindrical boundary:

$$\sum \left(\frac{\Delta u_r}{w} \right) = 0 \quad (14)$$

The uniform boundary sheet induces no radial velocities anywhere in the ultimate wake and the non-uniform boundary sheet induces no radial velocities on an inner sheet due to its symmetry above and below a line of intersection. Examination of the integrand of equation (9) reveals that no radial velocities are induced at an inner helical sheet by the evenly spaced inner sheets themselves. Thus, equation (13) is satisfied identically. The condition on the cylindrical boundary, equation (14) involves only the inner sheets and the non-uniform boundary sheet. The condition of equation (12) involves all three systems. The remaining constraint requires that the sum of the strengths of all of the vortex filaments comprising the wake be zero. The boundary conditions may now be written on the inner sheet (from equation (12))

$$\sum_1 \left(\frac{\Delta u_{\zeta}}{w} \right) + \sum_2 \left[\left(\frac{\Delta u_{\zeta}}{w} \right)_{A_1} - \left(\frac{\Delta u_{\zeta}}{w} \right)_{A_2} \right] + \sum_3 \left(\frac{\Delta u_{\zeta}}{w} \right) = \cos \varphi \quad (15)$$

on the cylindrical boundary (from equation (14))

$$\sum_1 \left(\frac{\Delta u_r}{w} \right) + \sum_3 \left(\frac{\Delta u_r}{w} \right) = 0 \quad (16)$$

and

$$\sum_1 \left(\frac{\gamma}{4\pi R w} \right) + \sum_2 \left(\frac{\gamma}{4\pi R w} \right) + \sum_3 \left(\frac{\gamma}{4\pi R w} \right) = 0 \quad (17)$$

where \sum_1 refers to the inner sheets, \sum_2 refers to the uniform boundary sheet, \sum_3 refers to the non-uniform boundary sheet and

$$A_1 = \cos (\varphi - \varphi_{r_B}) \quad ,$$

$$A_2 = \sin (\varphi - \varphi_{r_B})$$

$$\tan \varphi_{r_B} = \frac{1}{r} \tan \varphi_B \quad \text{and} \quad \tan \varphi = \frac{1}{r} \tan \varphi_R \quad .$$

For a fixed choice of λ and \bar{w} , the contributions of the uniform boundary sheet to equations (15) and (17) are fixed in terms of the sheet strength $\gamma(\zeta_B)$ and the pitch angle φ_B . Thus the system of equations can be written more conveniently as

$$\sum_1 \left(\frac{\Delta u_\zeta}{w} \right) + \sum_3 \left(\frac{\Delta u_\zeta}{w} \right) = \cos \varphi - \sum_2 \left\{ \left(\frac{\Delta u_\zeta}{w} \right) A_1 - \left(\frac{\Delta u_\xi}{w} \right) A_2 \right\} \quad (18)$$

$$\sum_1 \left(\frac{\Delta u_r}{w} \right) + \sum_3 \left(\frac{\Delta u_r}{w} \right) = 0 \quad (19)$$

and

$$\sum_1 \left(\frac{\gamma}{4\pi R w} \right) + \sum_3 \left(\frac{\gamma}{4\pi R w} \right) = - \sum_2 \left(\frac{\gamma}{4\pi R w} \right) \quad (20)$$

Equation (18) can be evaluated at a number of control points on an inner sheet. These points are placed between the filaments comprising the sheet and are equal in number to the number of filaments on the sheet (the final point being placed at $r = R$). Equation (19) can be evaluated at control points on the cylindrical boundary between an intersection line and the point midway between intersection lines. The points are again placed between filaments with one less point than filaments. Equation (20) includes the filaments on one inner sheet, the filaments on the non-uniform boundary sheet lying between an intersection line and the adjacent intersection line, and those filaments of the uniform boundary sheet passing through a line connecting two adjacent intersection lines. These filaments comprise a characteristic portion of the vortex wake, although the velocities must be calculated using all of the filaments of the wake system.

Now, the integrals of equations (9) and (11) may be defined respectively as

$$I_r = \left(\frac{\Delta u_r}{w} \right) / \left(\frac{\gamma}{4\pi R w} \right) \quad (21)$$

$$I_\zeta = \left(\frac{\Delta u_\zeta}{w} \right) / \left(\frac{\gamma}{4\pi R w} \cos \varphi \right) \quad (22)$$

and the system of equations may be written as follows:

for the control points on an inner sheet

$$\sum_1 I_\zeta \left(\frac{Y}{4\pi R w} \right) + \sum_3 I_\zeta \left(\frac{Y}{4\pi R w} \right) = 1 - \sum_2 \left\{ \left(\frac{\Delta u_\zeta}{w} \right) A_1 - \left(\frac{\Delta u_\zeta}{w} \right) A_2 \right\} / \cos \varphi \quad (23)$$

for the control points on the cylindrical boundary

$$\sum_1 I_r \left(\frac{Y}{4\pi R w} \right) + \sum_3 I_r \left(\frac{Y}{4\pi R w} \right) = 0 \quad (24)$$

and

$$\sum_{1_c} \left(\frac{Y}{4\pi R w} \right) + \sum_{3_c} \left(\frac{Y}{4\pi R w} \right) = - \sum_{2_c} \left(\frac{Y}{4\pi R w} \right) \quad (25)$$

where

\sum_{1_c} is over the filaments of one inner sheet,

\sum_{3_c} is over the filaments of a characteristic portion of the non-uniform boundary sheet,

and

\sum_{2_c} is over the filaments of a characteristic portion of the uniform boundary sheet.

With the equations in this form, the influence of \bar{w} is confined to the right hand sides of the equations through the velocity field of the uniform boundary sheet, and the coefficients I_r and I_ζ depend only on the choice for λ (the pitch of the inner sheets) and b (the number of blades).

Owing to the simplicity of the uniform boundary sheet, the velocity field inside the wake associated with this sheet has been evaluated explicitly in terms of λ and \bar{w} in Appendix II. The result is

$$\frac{u_z}{w} = \frac{\gamma(\zeta_B)}{w} \cos \varphi_B$$

$$\frac{u_\psi}{w} = \frac{u_r}{w} = 0 .$$

Using equation (7), $\frac{u_z}{w}$ can be written as

$$\frac{u_z}{w} = \cos \varphi_R \sec (\varphi_R - \varphi_B) \cos \varphi_B$$

or

$$\frac{u_z}{w} = \frac{1}{1 + \lambda \lambda_B} .$$

Then, the right hand side of equation (23) becomes

$$1 - \sum_2 \left\{ \left(\frac{\Delta u_\zeta}{w} \right)_{A_1} - \left(\frac{\Delta u_\xi}{w} \right)_{A_2} \right\} / \cos \varphi = 1 - \frac{1}{1 + \lambda \lambda_B} \quad (26)$$

Further, the right hand side of equation (25) becomes

$$- \sum_2 \left(\frac{\gamma}{4\pi R w} \right) = - \frac{\gamma(\zeta_B)}{4\pi R w} (2\pi R \lambda_B \cos \varphi_B / b)$$

Since $2\pi R \lambda_B / b$ is the length of the line defining the characteristic portion of the uniform boundary sheet and $\gamma(\zeta_B)$ is the sheet strength

per unit length. Thus

$$-\sum_{2c} \left(\frac{\gamma}{4\pi R w} \right) = -\frac{1}{2b} \left(\frac{\lambda_B}{1 + \lambda \lambda_B} \right) \quad (27)$$

Some rearrangement of the terms of equations (26) and (27) yields

$$1 - 1/(1 + \lambda \lambda_B) = \frac{\lambda^2}{1 + \lambda^2} \left[1 - \frac{1}{\lambda} \left(\frac{\lambda - \lambda_B}{1 + \lambda \lambda_B} \right) \right] \quad (28)$$

$$-\sum_3 \left(\frac{\gamma}{4\pi R w} \right) = \frac{-1}{2b} \left(\frac{\lambda}{1 + \lambda^2} \right) \left[1 - \frac{1}{\lambda} \left(\frac{\lambda - \lambda_B}{1 + \lambda \lambda_B} \right) \right] \quad (29)$$

From equation (5)

$$\frac{u_{\xi_0} \sin \varphi_R}{w \cos \varphi_R} = \tan (\varphi_R - \varphi_B)$$

or

$$\frac{u_{\xi_0}}{w} = \frac{1}{\lambda} \left(\frac{\lambda - \lambda_B}{1 + \lambda \lambda_B} \right)$$

So that, defining

$$G = 1 - \frac{u_{\xi_0}}{w} \quad (30)$$

equations (28) and (29) may be rewritten as

$$1 - 1/(1 + \lambda \lambda_B) = G \frac{\lambda^2}{1 + \lambda^2}$$

$$-\sum_3 \left(\frac{\gamma}{4\pi R w} \right) = -\frac{G}{2b} \left(\frac{\lambda}{1 + \lambda^2} \right)$$

Thus, the system of equations can be written

at the inner sheet control points

$$\sum_1 I_c \left(\frac{\gamma}{4\pi R w} \right) + \sum_3 I_c \left(\frac{\gamma}{4\pi R w} \right) = G \frac{\lambda^2}{1 + \lambda^2}$$

at the cylindrical boundary control points

$$\sum_1 I_r \left(\frac{\gamma}{4\pi R w} \right) + \sum_3 I_r \left(\frac{\gamma}{4\pi r w} \right) = 0$$

and

$$\sum_{1c} \left(\frac{\gamma}{4\pi R w} \right) + \sum_{3c} \left(\frac{\gamma}{4\pi R w} \right) = -G \frac{1}{2b} \left(\frac{\lambda}{1 + \lambda^2} \right)$$

Since the right hand side of every equation is multiplied by G (or is zero) a new vortex filament strength can be defined as

$$\bar{\gamma} = \frac{1}{G} \left(\frac{\gamma}{4\pi R w} \right)$$

and the system written

at the inner sheet control points

$$\sum_1 I_c \bar{\gamma} + \sum_3 I_c \bar{\gamma} = \frac{\lambda^2}{1 + \lambda^2} \quad (31)$$

at the cylindrical boundary control points

$$\sum_1 I_r \bar{\gamma} + \sum_3 I_r \bar{\gamma} = 0 \quad (32)$$

and

$$\sum_{1_c} \bar{\gamma} + \sum_{3_c} \bar{\gamma} = -\frac{1}{2b} \left(\frac{\lambda}{1 + \lambda^2} \right) \quad (33)$$

The system of equations in this form does not contain the \bar{w} parameter, so that a solution may be obtained which may be scaled directly for any value of \bar{w} . That is, the equations are solved for $G = 1$ ($\bar{w} = 0$) and the wake vorticity distribution for any value of \bar{w} is obtained by multiplying the result by the appropriate value of G .

The blade bound vortex strength is found at any radial station by summing the filaments of an inner sheet lying inboard of the radial station in the ultimate wake. The remaining elements of the solution, the strengths of the filaments of the non-uniform boundary sheet, are required in the calculation of the power and thrust. The evaluation of the coefficients I_r and I_c of the unknown filament strengths, the positioning of the filaments and control points on the sheets, and the simultaneous solution of the system of linear equations for the unknown strengths are all considered in some detail in Chapter V.

CHAPTER IV

CALCULATION OF THRUST, POWER, AND INDUCED EFFICIENCY

The solution for the distribution of vorticity in the ultimate wake allows a detailed calculation of the induced velocities within the wake. A knowledge of these velocities, and hence of the momentum and energy in the wake, leads to a straightforward calculation of the thrust, power and efficiency.

Thrust

Following the analysis of Theodorsen¹¹ consider a control volume enclosing the ducted fan and its ultimate wake as shown schematically in Fig. 8. Using the momentum theorem the thrust of the ducted fan may be found by considering the average pressure forces acting on the control surface and the average flux of momentum through the surface. These averages are taken over a time $\Delta t = 2\pi/b\Omega$ and the integration is with respect to time, $dt = dz/(V_\infty + w)$. Thus, from Fig. 8

$$T + \frac{1}{\Delta t} \int_{S_1, S_2} p \, dt \, dS = \frac{1}{\Delta t} \int_{S_2} \rho (V_\infty + u_z) \, dt (V_\infty + u_z) \, dS$$

$$- \frac{1}{\Delta t} \int_{S_1} \rho V_\infty \, dt V_\infty \, dS$$

which can be written as

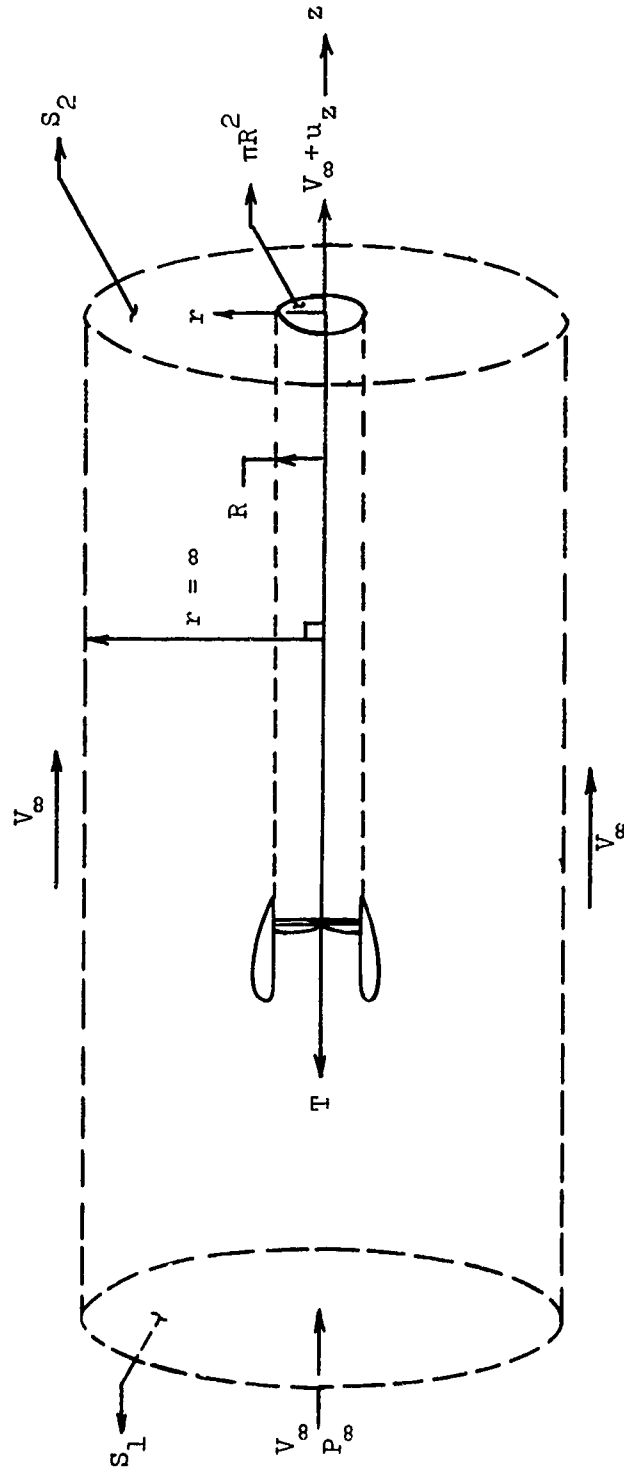


Figure 8. Control Volume Used in Determining the Thrust.

$$T + \frac{b\Omega}{2\pi(V_\infty + w)} \int (p_\infty - p) dz dS = \frac{b\Omega\rho}{2\pi(V_\infty + w)} \int (V_\infty u_z + u_z^2) dz dS \quad (34)$$

In order to integrate equation (34) the pressure term must first be eliminated by employing the equation of motion for an unsteady, incompressible, potential flow.

$$\frac{\partial\phi}{\partial t} + \frac{p}{\rho} + \frac{1}{2} V^2 = f(t)$$

Since there can be no induced velocities at an infinite radial distance from the wake axis

$$\frac{\partial\phi}{\partial t} + p/\rho + V^2/2 = p_o/\rho \quad (35)$$

The unsteady term may be eliminated by considering the potential field in a steady coordinate system such that

$$\phi(r, \psi, z) = \phi(r, \psi_o + \Omega r t, z)$$

Then

$$\frac{\partial\phi}{\partial t} = \frac{\partial\phi}{\partial\psi} \frac{\partial\psi}{\partial t} = u_\psi \Omega r = x u_\psi \Omega R$$

Now u_ψ may be written as

$$u_\psi = u_{\xi_o} \sin \varphi \cos \varphi - u_\xi \sin \varphi$$

and

$$u_z = u_{\xi_0} \sin^2 \varphi + u_r \cos \varphi ,$$

Thus

$$u_\zeta \sin \varphi = u_z \tan \varphi - u_{\xi_0} \sin^2 \varphi \tan \varphi .$$

u_ψ becomes

$$u_\psi = \tan \varphi w(1 - G) - u_z \tan \varphi$$

and, since $\tan \varphi = \lambda/x = \left(\frac{V_\infty + w}{\Omega R}\right)/x$, $\frac{\partial \phi}{\partial t}$ inside the wake becomes

$$\frac{\partial \phi}{\partial t} = - (V_\infty + w)u_z + w(V_\infty + w) (1 - G) .$$

Then inside the wake equation (35) is

$$p/\rho + V^2/2 - (V_\infty + w)u_z + w(V_\infty + w) (1 - G) = p_{O_{R_-}}/\rho \quad (36)$$

The pressure must also be constrained by a static pressure balance at the wake boundary. Since all disturbances vanish outside the wake, the constraint becomes $p_{R_-} = p_\infty$ or

$$p_\infty = p_{O_{R_-}} - \frac{1}{2} \rho V_{R_-}^2 + \rho (V_\infty + w) u_{z_{R_-}} - \rho (V_\infty + w) w(1 - G)$$

Then using equation (36) to eliminate $p_{O_{R_-}}$ yields

$$(p_{\infty} - p) = \frac{1}{2} \rho (V^2 - V_{R_-}^2) - \rho (V_{\infty} + w) (u_z - u_{z_{R_-}}) \quad (37)$$

where

$$V^2 = (V_{\infty} + u_z)^2 + u_r^2 + u_{\psi}^2$$

$$V_{R_-}^2 = (V_{\infty} + u_{z_{R_-}})^2 + u_{\psi_{R_-}}^2$$

Substitution of equation (37) into equation (34) yields

$$T = \frac{b \rho p}{2\pi (V_{\infty} + w)} \int_{\substack{\text{Volume} \\ \text{Inside} \\ \text{Wake}}} \left[V_{\infty} u_z + u_z^2 - \frac{1}{2} ([V_{\infty} + u_z]^2 - [V_{\infty} + u_{z_{R_-}}]^2 + u_r^2 + u_{\psi}^2 - u_{\psi_{R_-}}^2) + (V_{\infty} + w) (u_z - u_{z_{R_-}}) \right] r dr dz d\psi$$

The limits of integration are taken over a characteristic volume of the wake such that

$$0 \leq z \leq 2\pi R \lambda / b$$

$$0 \leq r \leq R$$

$$0 \leq \psi \leq 2\pi$$

Then defining non-dimensional lengths as

$$\bar{z} = z/(2\pi R\lambda/b) \quad , \quad 0 \leq \bar{z} \leq 1$$

$$\bar{r} = r/R \quad , \quad 0 \leq \bar{r} \leq 1$$

the thrust can be written as

$$T = \frac{b\Omega\rho}{2\pi(V_\infty + w)} R^2(2\pi R\lambda/b) \int_0^1 \int_0^1 \int_0^{2\pi} \left[V_\infty u_z + u_z^2 - \frac{1}{2} [(V_\infty + u_z)^2 \right. \\ \left. - (V_\infty + u_{z_{R_-}})^2 + u_r^2 + u_\psi^2 - u_{z_{R_-}}^2] + (V_\infty + w)(u_z - u_{z_{R_-}}) \right] \bar{r} d\bar{r} d\bar{z} d\psi/2\pi$$

Now, non-dimensionalizing the velocities according to $\bar{u} = u/w$ and $\bar{w} = w/\Omega R$ yields

$$T = 2 \bar{w}^2 (\Omega R)^2 \int_0^1 \int_0^1 \int_0^{2\pi} \left[\frac{V_\infty}{\bar{w}} \bar{u}_z + \bar{u}_z^2 - \frac{1}{2} \left[\left(\frac{V_\infty/\Omega R}{\bar{w}} + \bar{u}_z \right)^2 \right. \right. \\ \left. \left. - \left(\frac{V_\infty/\Omega R}{\bar{w}} + \bar{u}_{z_{R_-}} \right)^2 + \bar{u}_r^2 + \bar{u}_\psi^2 - \bar{u}_{\psi_{R_-}} \right] \right. \\ \left. + \left(\frac{V_\infty/\Omega R}{\bar{w}} + 1 \right) (\bar{u}_z - \bar{u}_{z_{R_-}}) \right] \bar{r} d\bar{r} d\bar{z} d\psi/2\pi$$

Noting that $(V_\infty/\Omega R) = (\lambda - \bar{w})$ and defining a thrust coefficient as

$$C_T = T/[\rho(\Omega R)^2 \pi R^2] \quad (38)$$

the result may be reduced to

$$C_T = 2 \bar{w}^2 \int_0^1 \int_0^1 \int_0^{2\pi} \left[\frac{\lambda}{\bar{w}} \bar{u}_z + \bar{u}_z^2 - \frac{1}{2} [\bar{u}_z^2 + \bar{u}_r^2 + \bar{u}_\psi^2] + \frac{1}{2} [\bar{u}_{zR}^2 + \bar{u}_{\psi R}^2] \right. \\ \left. - \bar{u}_{zR} \right] \bar{r} \, d\bar{r} \, d\bar{z} \, d\psi / 2\pi \quad (39)$$

Some of the terms may be integrated immediately as follows. Consider a line integral within the wake as shown in Fig. 9. The integral about the path \overline{ABCD} encloses those filaments shed by a blade bound vortex between $x = 0$ and $x = x$ ($x = \bar{r}$) so that the line integral yield $\Gamma(x)$ and

$$\int_A^B u_r \, dr + \int_B^C u_z \, dz + \int_C^D u_r \, dr + \int_D^A u_z \, dz = \Gamma(x)$$

But, from the requirement on velocity discontinuity across the sheet (for which u_r of the filaments is zero)

$$\int_A^B u_r \, dr = - \int_C^D u_r \, dr$$

so that

$$\int_D^A u_z \, dz - u_{z0} (2\pi R \lambda / b) = \Gamma(x)$$

or

$$\int_0^1 \bar{u}_z \, d\bar{z} = \frac{b \Gamma(x)}{2\pi R \lambda} + \bar{u}_{z0}$$

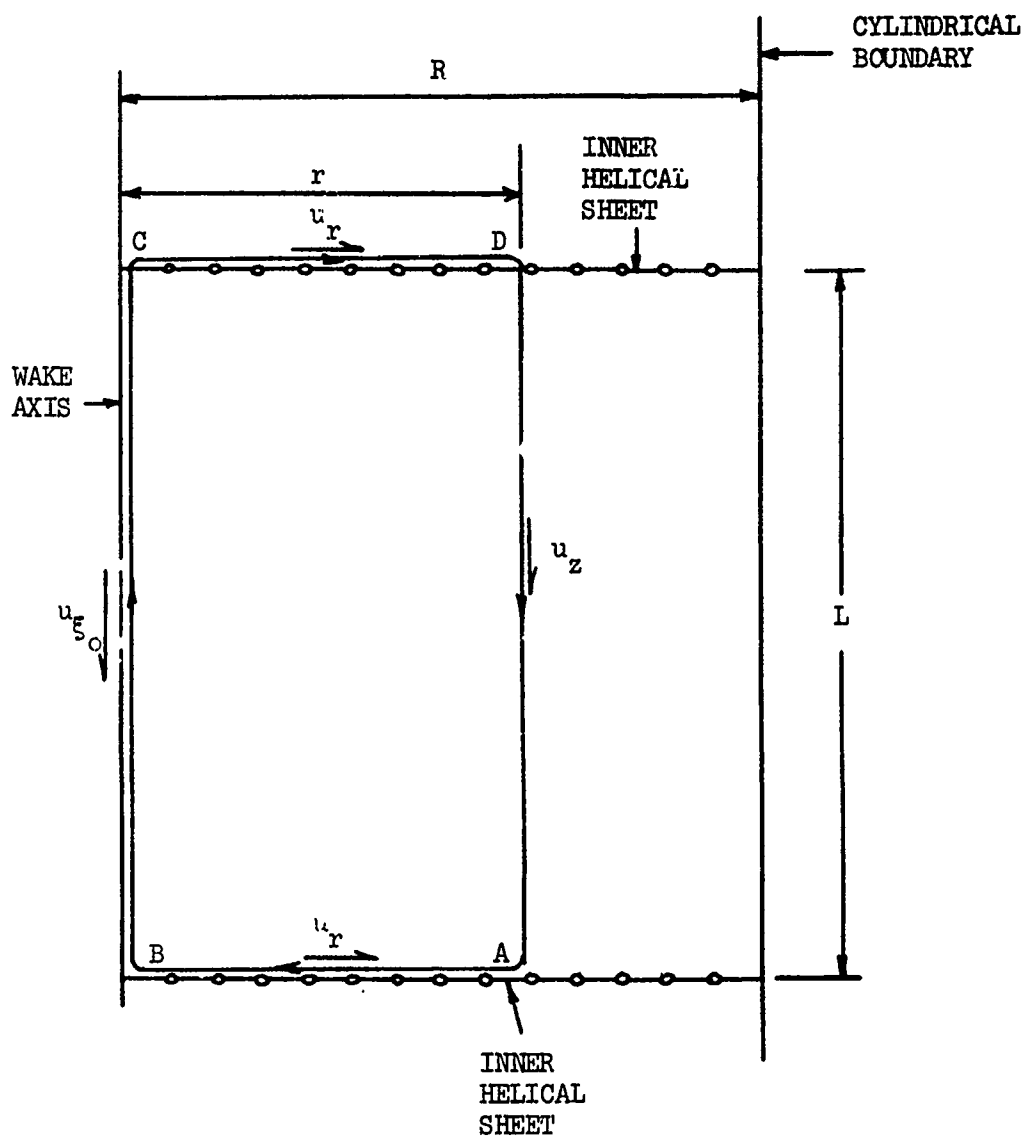


Figure 9. A Path of Line Integration in the Ultimate Wake.

Employing the definition of Theodorsen for the non-dimensional blade bound vortex strength as

$$K(x) = \frac{b \Gamma(x)}{2\pi k w \lambda} \quad (40)$$

yields

$$\int_0^1 \bar{u}_z d\bar{z} = K(x) + \bar{u}_{\xi_0}$$

so that

$$\begin{aligned} \int_0^1 \int_0^1 \int_0^{2\pi} \bar{u}_z \bar{r} d\bar{r} d\bar{z} d\psi / 2\pi &= \int_0^1 \int_0^{2\pi} [K(x) + \bar{u}_{\xi_0}] x dx d\psi / 2\pi \\ &= \frac{1}{2} \left[2 \int_0^1 K(x) x dx + \bar{u}_{\xi_0} \right] . \end{aligned}$$

But the integral term is defined¹¹ as \mathcal{K} , the propeller mass coefficient,

$$\mathcal{K} = 2 \int_0^1 K(x) x dx \quad (41)$$

Thus

$$\int_0^1 \int_0^1 \int_0^{2\pi} \bar{u}_z \bar{r} d\bar{r} d\bar{z} d\psi / 2\pi = \frac{1}{2} [\mathcal{K} + \bar{u}_{\xi_0}] \quad (42)$$

If \bar{r} is taken as $\bar{r} = x = 1$ then \bar{u}_z becomes \bar{u}_{zR} so that the integration of the last term of equation (39) becomes

$$\int_0^1 \int_0^1 \int_0^{2\pi} \bar{u}_{z_{R_-}} \bar{r} \, d\bar{r} \, d\bar{z} \, d\bar{\psi} / 2\pi = \frac{1}{2} [K(1) + \bar{u}_{\xi_0}] \quad (43)$$

The remaining terms of the integral of equation (39), which must be evaluated numerically, may be defined as

$$\epsilon_z = \int_0^1 \int_0^1 \int_0^{2\pi} \bar{u}_z^2 \bar{r} \, d\bar{r} \, d\bar{z} \, d\bar{\psi} / 2\pi$$

$$\epsilon_r = \int_0^1 \int_0^1 \int_0^{2\pi} \bar{u}_r^2 \bar{r} \, d\bar{r} \, d\bar{z} \, d\bar{\psi} / 2\pi$$

$$\epsilon_\psi = \int_0^1 \int_0^1 \int_0^{2\pi} \bar{u}_\psi^2 \bar{r} \, d\bar{r} \, d\bar{z} \, d\bar{\psi} / 2\pi$$

$$\epsilon_{R_-} = \int_0^1 \int_0^1 \int_0^{2\pi} [\bar{u}_{z_{R_-}}^2 + \bar{u}_{\psi_{R_-}}^2] \bar{r} \, d\bar{r} \, d\bar{z} \, d\bar{\psi} / 2\pi$$

and $\epsilon = \epsilon_z + \epsilon_r + \epsilon_\psi$. Employing these definitions and equations (42) and (43), equation (39) becomes

$$C_T = \bar{w}^2 \left[\frac{\lambda}{\bar{w}} K - K(1) + \left(\frac{\lambda}{\bar{w}} - 1 \right) \bar{u}_{\xi_0} + 2 \epsilon_z - \epsilon + \epsilon_{R_-} \right] \quad (44)$$

It has been established that the flow field of the uniform boundary sheet is known and that the vortex sheet strength distributions, and hence the flow fields, of the sheets of varying strength need only

be solved for the lightly loaded condition. It is possible, then, to calculate the thrust coefficient in terms of the $\bar{w} = 0$ wake solution and the scale factor G . Referring to equation (39) the integral terms can be modified as follows. The velocities are separated into those associated with the inner helical and non-uniform boundary sheets (variable strength, subscript $vs_{\bar{w}}$) and those associated with the uniform boundary sheet. The $vs_{\bar{w}}$ velocities can be scaled according to

$$\bar{u}_{vs_{\bar{w}}} = G \bar{u}_{vs_0} = G \bar{u}_{vs}$$

Further $K(x) = G K(x)_{\bar{w}=0} = G K_0(x)$ and $M = G M_0$. From equation (28) the velocity associated with the uniform boundary sheet is simply $\bar{u}_z = 1 - \frac{G \lambda^2}{1 + \lambda^2}$ for all \bar{r} . For simplicity in the following development $\int d(\text{vol})$ will be taken to represent $\int_0^1 \int_0^1 \int_0^{2\pi} \bar{r} d\bar{r} d\bar{z} d\psi / 2\pi$.

The integrals in equation (39) can then be written as

$$\begin{aligned} \int \bar{u}_z^2 d(\text{vol}) &= \int \left[G \bar{u}_{z_{vs}} + \left(1 - \frac{G \lambda^2}{1 + \lambda^2} \right) \right]^2 d(\text{vol}) \\ &= G^2 \int \bar{u}_{z_{vs}}^2 d(\text{vol}) + 2G \left(1 - \frac{G \lambda^2}{1 + \lambda^2} \right) \int \bar{u}_{z_{vs}} d(\text{vol}) \\ &\quad + \frac{1}{2} \left(1 - \frac{G \lambda^2}{1 + \lambda^2} \right)^2 \int d(\text{vol}) \end{aligned}$$

$$\int \bar{u}_\psi^2 d(\text{vol}) = G^2 \int \bar{u}_{\psi_{vs}}^2 d(\text{vol}) ,$$

$$\int \bar{u}_R^2 d(\text{vol}) = G^2 \int \bar{u}_{R_{VS}}^2 d(\text{vol}) ,$$

$$\int \bar{u}_{z_{R_-}}^2 d(\text{vol}) = G^2 \int \bar{u}_{z_{VS_{R_-}}} d(\text{vol}) + 2G \left(1 - \frac{G \lambda^2}{1 + \lambda^2}\right) \int \bar{u}_{z_{VS_{R_-}}} d(\text{vol}) \\ + \frac{1}{2} \left(1 - \frac{G \lambda^2}{1 + \lambda^2}\right)^2 ,$$

$$\int \bar{u}_{Y_{R_-}} d(\text{vol}) = G^2 \int \bar{u}_{Y_{VS_{R_-}}} d(\text{vol}) .$$

From equation (42)

$$\int \bar{u}_{z_{VS}} d(\text{vol}) = \frac{1}{2} \left[K_0 - \frac{1}{1 + \lambda^2} \right]$$

and from equation (43)

$$\int \bar{u}_{z_{VS_{R_-}}} d(\text{vol}) = \frac{1}{2} \left[K_0(1) - \frac{1}{1 + \lambda^2} \right]$$

Substituting these results and the results of equations (42) and (43) into equation (39) yields

$$C_T = 2\bar{w}^2 \left[\frac{1}{2} \frac{\lambda}{\bar{w}} (G K_0 + 1 - G) \right. \\ \left. + \frac{1}{2} \left[G^2 \int \bar{u}_{z_{VS}}^2 d(\text{vol}) + G \left(1 - \frac{G \lambda^2}{1 + \lambda^2}\right) \left(K_0 - \frac{1}{1 + \lambda^2} \right) \right] \right]$$

$$\begin{aligned}
& + \frac{1}{2} \left(1 - \frac{G \lambda^2}{1 + \lambda^2}\right)^2 - \frac{1}{2} G^2 \left[\int_{vs} \bar{u}_r^2 d(\text{vol}) + \int_{vs} \bar{u}_y^2 d(\text{vol}) \right] \\
& + \frac{1}{2} \left[G^2 \int_{vsR} \bar{u}_z^2 d(\text{vol}) + G \left(1 - \frac{G \lambda^2}{1 + \lambda^2}\right) \left(K_0(1) - \frac{1}{1 + \lambda^2} \right) \right. \\
& \qquad \qquad \qquad \left. + \frac{1}{2} \left(1 - \frac{G \lambda^2}{1 + \lambda^2}\right)^2 \right. \\
& \left. + G^2 \int_{vsR} \bar{u}_y^2 d(\text{vol}) \right] - \frac{1}{2} (G K_0(1) + 1 - G)
\end{aligned}$$

The remaining integrals, which must be evaluated numerically, may be regrouped and defined as

$$\epsilon_0 = \int_0^1 \int_0^1 \int_0^{2\pi} \left[\bar{u}_{zs}^2 - \bar{u}_{rs}^2 - \bar{u}_{ys}^2 + \bar{u}_{zsR}^2 \right] \bar{r} d\bar{r} d\bar{z} d\psi / 2\pi \quad (45)$$

Using the definition of equation (45), the thrust coefficient may be written as

$$\begin{aligned}
C_T = \bar{w}^2 \left[G \left(\frac{\lambda}{\bar{w}} + 1 - \frac{G \lambda^2}{1 + \lambda^2} \right) K_0 - \frac{G^2 \lambda^2}{1 + \lambda^2} K_0(1) + G^2 \epsilon_0 \right. \\
\left. + (1 - G) \left(\frac{\lambda}{\bar{w}} + 1 - \frac{2G \lambda^2}{1 + \lambda^2} \right) - \left(1 - \frac{G \lambda^2}{1 + \lambda^2}\right)^2 \right] \quad (46)
\end{aligned}$$

where, for a given b and λ , K_0 , $K_0(1)$ and ϵ_0 are calculated from the $\bar{w} = 0$ solution. Since G is calculated algebraically for a given λ and \bar{w} , equation (46) provides an entire family of values for C_T whereas equation (44) provides only a single value.

Power

The ideal power required by the heavily loaded ducted fan may be determined through a consideration of the induced energy loss in the ultimate wake. Following Theodorsen¹¹ the energy loss, E , is given by the methods of classical mechanics as

$$E = Q\Omega - TV_\infty = \frac{b\Omega}{2\pi(V_\infty + w)} \int \left[\frac{1}{2} \rho V_\infty v^2 + \left(\frac{1}{2} \rho v^2 + p - p_\infty \right) u_z \right] d(\text{vol}) \quad (47)$$

where Q is the torque of the fan and v^2 is the magnitude of the total induced velocity, $v^2 = u_z^2 + u_r^2 + u_\psi^2$. Substituting from equation (37) for $(p - p_\infty)$, the energy loss becomes

$$E = \frac{b\Omega\rho}{2\pi(V_\infty + w)} \int \left[\frac{1}{2} V_\infty v^2 + w u_z^2 + u_z \left(\frac{1}{2} v_{R-}^2 - w u_{zR-} \right) \right] d(\text{vol})$$

Then, defining a non-dimensional energy loss as

$$e = E / [\rho (\Omega R)^3 \pi R^2] \quad (48)$$

and non-dimensionalizing velocities and lengths as was done for the thrust coefficient, e becomes

$$e = 2\bar{w}^3 \int_0^1 \int_0^1 \int_0^{2\pi} \left[\bar{u}_z^2 + \frac{1}{2} \left(\frac{\lambda}{\bar{w}} - 1 \right) \bar{v}^2 + \frac{1}{2} \bar{u}_z \left(\bar{v}_{R-}^2 - \bar{u}_{zR-} \right) \right] \bar{r} d\bar{r} d\bar{z} d\bar{\psi} / 2\pi$$

Again, dividing the induced velocities into those associated with the uniform boundary sheet and those associated with the variable strength sheets, the expression for e can be calculated in terms of G and the $\bar{w} = 0$ solution. All manipulations and integrations are similar to those performed in the thrust analysis. The result is given as

$$\begin{aligned}
 e = \bar{w}^3 & \left[G \left(\frac{\lambda}{\bar{w}} + \frac{1}{2} \left[1 - \frac{G \lambda^2}{1 + \lambda^2} \right] \right) \left(1 - \frac{G \lambda^2}{1 + \lambda^2} \right) \left(K_0 - \frac{1}{1 + \lambda^2} \right) \right. & (49) \\
 & - \frac{G^2 \lambda^2}{1 + \lambda^2} \left(1 - \frac{G \lambda^2}{1 + \lambda^2} \right) \left(K_0 (1) - \frac{1}{1 + \lambda^2} \right) \\
 & + \frac{1}{2} \left(\frac{\lambda}{\bar{w}} - 1 \right) \left(1 - \frac{G \lambda^2}{1 + \lambda^2} \right)^2 + \frac{1}{2} \left(1 - \frac{G \lambda^2}{1 + \lambda^2} \right)^3 \\
 & + G^2 \left(\frac{\lambda}{\bar{w}} + 1 \right) \int \bar{u}_{z_{vs}} d(\text{vol}) \\
 & + G^2 \left(\frac{\lambda}{\bar{w}} - 1 \right) \int [\bar{u}_{y_{vs}}^2 + \bar{u}_{r_{vs}}^2] d(\text{vol}) \\
 & + G^2 \left(1 - \frac{G \lambda^2}{1 + \lambda^2} \right) \int [\bar{u}_{z_{vsR_-}}^2 + \bar{u}_{y_{vsR_-}}^2] d(\text{vol}) \\
 & - 2 \frac{G^3 \lambda^2}{1 + \lambda^2} \int \bar{u}_{z_{vs}} \bar{u}_{z_{vsR_-}} d(\text{vol}) \\
 & \left. + G^3 \int \bar{u}_{z_{vs}} [\bar{u}_{z_{vs}}^2 + \bar{u}_{y_{vsR_-}}^2] d(\text{vol}) \right]
 \end{aligned}$$

Of the remaining integral terms the first three are evaluated in the calculation of ϵ_0 for the thrust coefficient. The last two must be numerically integrated for the $\bar{w} = 0$ case in a similar manner.

From equation (47) the power can be written as

$$P = Q\Omega = TV_\infty + E$$

so that defining a power coefficient as

$$C_P = P / [\rho (\Omega R)^3 \pi R^2] \quad (50)$$

yields

$$C_P = (\lambda - \bar{w}) C_T + e \quad (51)$$

The power requirement for a constant diameter wake can also be calculated directly by the Kutta-Joukowski theorem. An increment of torque is given by $dQ = b\rho V_{\text{axial}} \Gamma r dr$ where V_{axial} is given by

$$\begin{aligned} V_{\text{axial}} &= V_\infty + u_\xi \sin \varphi + u_\zeta \cos \varphi \\ &= V_\infty + w \left(1 - \frac{G \lambda^2}{x^2 + \lambda^2} \right) \end{aligned}$$

Then

$$dQ = \rho (2\pi R w \lambda) K(x) \left[V_\infty + w \left(1 - \frac{G \lambda^2}{x^2 + \lambda^2} \right) \right] R^2 x dx$$

and

$$Q = \rho (\pi R)^2 R w \lambda \left[(V_\infty + w) \int_0^1 K(x) x dx - 2 G w \lambda^2 \int_0^1 K(x) \frac{x}{x^2 + \lambda^2} dx \right]$$

From equation (41)

$$\mathcal{K} = 2 \int_0^1 K(x) x \, dx$$

Defining the remaining integral as

$$\mu = 2 \int_0^1 K(x) \frac{x}{x^2 + \lambda^2} \, dx$$

the power can be written as

$$P = Q\Omega = \rho (\pi R^2) (\Omega R)^3 \bar{w} \lambda^2 [\mathcal{K} - G\bar{w} \mu] .$$

Then, since $\mathcal{K} = G\mathcal{K}_0$ and $\mu = G\mu_0$, the power coefficient is given by

$$C_P = G\bar{w} \lambda^2 [\mathcal{K}_0 - G\bar{w} \mu_0] . \quad (52)$$

Efficiency

The induced efficiency is defined as $\eta_i = TV_\infty/P$. Thus from equation (50)

$$\eta_i = \frac{(\lambda - \bar{w})C_T}{(\lambda - \bar{w})C_T + e} . \quad (53)$$

Efficiency may also be written as

$$\eta_i = (\lambda - \bar{w})C_T/C_P .$$

CHAPTER V

NUMERICAL PROCEDURES

In the preceding chapters the model and its mathematical solution have been outlined in terms of the basic procedures and developments required. To obtain such a solution it is necessary to evaluate the velocity contributions of a filament of unknown strength at an arbitrary location in the flow field of that filament. This evaluation will be carried out by numerically calculating the integrals of equations (9), (10) and (11). Using these results a system of linear equations will be developed in terms of the unknown filament strengths of the system by equating the sums of velocities at control points in the ultimate wake to the required normal velocities at these points. In order to specify the parameters of these equations, decisions will be made about the manner of subdividing the vortex sheets into finite strength filaments and the placement of control points on the sheets.

After the system of equations is determined and solved, the integrals of equations (45) and (46) will be evaluated in order to calculate the thrust and power of the ducted fan. In addition the values of $K_0(x)$, K_0 and μ_0 will be evaluated.

Evaluation of Velocity Components

The evaluation of the velocity components associated with a single finite strength helical vortex filament at an arbitrary location in the flow field of the filament depends (in this analysis) on a

numerical integration of an integrand which is solely a function of the geometry of the filament and the point at which the velocity is to be calculated. The expressions for the components, equations (9), (10), and (11), are repeated here for convenience.

$$\frac{\Delta u_r}{w} = \frac{\gamma}{4\pi R w} \int_{-\infty}^{\infty} \left\{ \bar{r}' \tan \varphi_R \sin (\Psi' - \Psi) + \bar{r}' (\bar{z} - \bar{z}'_0 - \Psi' \tan \varphi_R) \cos (\Psi' - \Psi) \right\} \frac{d\Psi'}{P^3}$$

$$\frac{\Delta u_s}{w} = \frac{\gamma \cos \varphi}{4\pi R w} \int_{-\infty}^{\infty} \left\{ \bar{r}' \tan \varphi_R \left(\frac{\bar{r}}{\bar{r}'} + \frac{\bar{r}'}{\bar{r}} - 2 \cos (\Psi' - \Psi) \right) + (\bar{z} - \bar{z}'_0 - \Psi' \tan \varphi_R) \sin (\Psi' - \Psi) \right\} \frac{d\Psi'}{P^3}$$

$$\frac{\Delta u_z}{w} = \frac{\gamma \cos \varphi}{4\pi R w} \int_{-\infty}^{\infty} \left\{ \bar{r}'^2 - \bar{r}\bar{r}' \cos (\Psi' - \Psi) - \tan^2 \varphi_R \left(1 - \frac{\bar{r}'}{\bar{r}} \cos (\Psi' - \Psi) \right) - \frac{\bar{r}'}{\bar{r}} \sin (\Psi' - \Psi) \tan \varphi_R (\bar{z} - \bar{z}'_0 - \Psi' \tan \varphi_R) \right\} \frac{d\Psi'}{P^3}$$

where

$$\bar{P}^2 = \bar{r}^2 + \bar{r}'^2 - 2 \bar{r}\bar{r}' \cos (\Psi' - \Psi) + [\bar{z} - \bar{z}'_0 - \Psi' \tan \varphi_R]^2 ,$$

$$\varphi = \tan^{-1} \left(\frac{1}{\bar{r}} \tan \varphi_R \right) ,$$

and the primed dimensions \bar{r}' , \bar{z}'_0 , Ψ' refer to the location of an elemental length of the vortex filament. The unprimed dimensions refer to the location of the point at which the velocity is to be calculated.

The computations needed to numerically evaluate these integrals may be simplified by converting their limits from $-\infty \leq \Psi' \leq \infty$ to $0 \leq \Psi' \leq \infty$. This is done in the usual manner by splitting the integral at $\Psi' = 0$, switching the limits on the $-\infty \leq \Psi' \leq 0$ portion and redefining Ψ' to $-\Psi'$ in the negative range. The resulting velocity component relations are (using the substitution $\lambda = \tan \phi_R$)

$$\begin{aligned} \frac{\Delta u_r}{w} = \frac{\gamma}{4\pi R w} \int_0^\infty \left\{ \left[\bar{r}' \lambda \sin (\Psi' - \Psi) \right. \right. \\ \left. \left. + \bar{r}' [\bar{z} - \bar{z}'_0 - \lambda \Psi'] \cos (\Psi' - \Psi) \right] \frac{1}{P_1^3} \right. \\ \left. - \left[\bar{r}' \lambda \sin (\Psi' + \Psi) \right. \right. \\ \left. \left. - \bar{r}' [\bar{z} - \bar{z}'_0 + \lambda \Psi'] \cos (\Psi' + \Psi) \right] \frac{1}{P_2^3} \right\} d\Psi \quad , \end{aligned}$$

$$\begin{aligned} \frac{\Delta u_\xi}{w} = \frac{\gamma \cos \phi}{4\pi R w} \int_0^\infty \left\{ \bar{r}' \left[\lambda \left(\frac{\bar{r}'}{\bar{r}} + \frac{\bar{r}}{\bar{r}'} - 2 \cos (\Psi' - \Psi) \right) \right. \right. \\ \left. \left. + [\bar{z} - \bar{z}'_0 - \lambda \Psi'] \sin (\Psi' - \Psi) \right] \frac{1}{P_1^3} \right. \end{aligned}$$

$$+ \bar{r}' \left[\lambda \left(\frac{\bar{r}'}{\bar{r}} + \frac{\bar{r}}{\bar{r}'} - 2 \cos (\Psi' + \Psi) \right) \right. \\ \left. - [\bar{z} - \bar{z}'_0 + \lambda \Psi'] \sin (\Psi' - \Psi) \right] \frac{1}{\bar{r}_2^3} \} d\Psi' ,$$

$$\frac{\Delta u_c}{w} = \frac{\gamma \cos \varphi}{4\pi R w} \int_0^\infty \left\{ \left[\bar{r}'^2 - 2 \bar{r} \bar{r}' \cos (\Psi' - \Psi) \right. \right. \\ \left. \left. - \lambda^2 \left[1 - \frac{\bar{r}'}{\bar{r}} \cos (\Psi' - \Psi) \right] \right. \right. \\ \left. \left. - \frac{\bar{r}'}{\bar{r}} \lambda \sin (\Psi' - \Psi) [\bar{z} - \bar{z}'_0 - \lambda \Psi'] \right] \frac{1}{\bar{r}_1^3} \right. \\ \left. + \left[\bar{r}'^2 - 2 \bar{r} \bar{r}' \cos (\Psi' + \Psi) \right. \right. \\ \left. \left. - \lambda^2 \left[1 - \frac{\bar{r}'}{\bar{r}} \cos (\Psi' + \Psi) \right] \right. \right. \\ \left. \left. + \frac{\bar{r}'}{\bar{r}} \lambda \sin (\Psi' + \Psi) [\bar{z} - \bar{z}'_0 + \lambda \Psi'] \right] \frac{1}{\bar{r}_2^3} \right\} d\Psi' ,$$

where

$$\bar{r}_1^2 = \bar{r}^2 + \bar{r}'^2 - 2 \bar{r} \bar{r}' \cos (\Psi' - \Psi) + [\bar{z} - \bar{z}'_0 - \lambda \Psi']^2$$

$$\bar{r}_2^2 = \bar{r}^2 + \bar{r}'^2 - 2 \bar{r} \bar{r}' \cos (\Psi' + \Psi) + [\bar{z} - \bar{z}'_0 + \lambda \Psi']^2 .$$

For convenience in the ensuing discussion the integrands of the velocity components are defined by f_r , f_ξ and f_ζ such that

$$\frac{\Delta u_r}{w} = \frac{\gamma}{4\pi R w} \int_0^\infty f_r (\Psi'; \bar{r}, \bar{r}', \bar{z}, \bar{z}', \Psi, \lambda) d\Psi'$$

$$\frac{\Delta u_\xi}{w} = \frac{\gamma \cos \varphi}{4\pi R w} \int_0^\infty f_\xi (\Psi'; \bar{r}, \bar{r}', \bar{z}, \bar{z}', \Psi, \lambda) d\Psi'$$

$$\frac{\Delta u_\zeta}{w} = \frac{\gamma \cos \varphi}{4\pi R w} \int_0^\infty f_\zeta (\Psi'; \bar{r}, \bar{r}', \bar{z}, \bar{z}', \Psi, \lambda) d\Psi'$$

The numerical integrations proceed in a straightforward manner; $\frac{\Delta u_r}{w}$ will be used as the illustrative example. The integration is performed by subdividing each turn of the helix ($\Delta\Psi' = 2\pi$) into k subintervals of included angle $2\pi/k$. f_r is calculated at $\Psi' = 0, 2\pi/k, 2(2\pi/k), \dots, k(2\pi/k)$ and these values are stored as they are calculated. Then the contributions of these segments of the helical filament are summed by a trapezoidal rule integration such that

$$\begin{aligned} \delta_1 \left(\frac{\Delta u_r}{w} \right) &= (2\pi/k) \left[f_r(0) + \frac{1}{2} \left(f_r(0) + f_r(2\pi/k) \right) \right. \\ &\quad + f_r(2\pi/k) + \frac{1}{2} \left(f_r(2\pi/k) + f_r(2 \frac{2\pi}{k}) \right) + \\ &\quad \dots + f_r([k-1] \frac{2\pi}{k}) \\ &\quad \left. + \frac{1}{2} \left(f_r([k-1] \frac{2\pi}{k}) + f_r(k \frac{2\pi}{k}) \right) \right] . \end{aligned}$$

(Note that δ_1 is a coefficient of velocity subject to multiplication by the non-dimensional filament strength $\gamma/4\pi R w$.) δ_1 measures the contribution of the first turn of the helical filament (and its reflection for $-2\pi \leq \Psi' \leq 0$) to the radial velocity associated with the filament. This result is stored and the contribution of the turn defined by $2\pi \leq \Psi' \leq 4\pi$ (and its reflection) is calculated in the same manner yielding $\delta_2 \left(\frac{\Delta u_r}{w} \right)$. Then δ_2 is compared to the sum of δ_1 and δ_2 . A percent change is defined as $100 \times \left| \frac{\delta_2}{\delta_1 + \delta_2} \right|$. If this change is not sufficiently small then δ_3 is calculated and the comparison is made again according to $100 \times \left| \frac{\delta_3}{\sum_1 \delta_i} \right|$. The process is continued until the percent change in the coefficient of $\frac{\Delta u_r}{w}$ is less than some specified tolerance. The coefficient is then set equal to the sum of the contributions of all terms for which δ_i was calculated.

Clearly, the accuracy of this result depends on the choice for k and the specified tolerance. The magnitudes of these parameters depend in general on the geometrical values \bar{r} , \bar{r}' , ϕ_R and on the number of blades in the fan. It would be possible to control these values very closely by a process of repeated calculations and comparisons within a given integration. For example, δ_1 could be evaluated with $k = 90$, then reevaluated with $k = 120$, again with $k = 150, 180$ and so on until two successive values were identical to an arbitrarily specified number of significant digits. Then δ_2 would be handled in the same manner. Similarly the δ_i contributions would be summed until the final contribution failed to change the sum in the chosen number

of significant digits. It is apparent that such a procedure could be enormously time consuming, and the choice for the number of significant digits to be carried must be made very conservatively. Choosing the best alternative at hand, reliance is made on the specification of minimum requirements over a broad range of cases.

The values of k and the tolerances for the velocity components were sized somewhat subjectively on the basis of their effects on solutions of the wake vorticity distribution. The method of sizing a parameter consists of fixing all but one of these at very conservative levels and systematically varying the remaining parameter over a wide range. This procedure is repeated for various values of b and λ and the resulting wake vortex strength distributions are compared. For example, k was varied over a range from 90 to 720. It was found that for k greater than 180 the solutions for wake vorticity were essentially identical for b and λ taken over very wide ranges. That is, the value of $K_0(1)$ at b and λ was changed by less than 1/2 of one percent by increasing k from 180 to 720. On the basis of this result k was fixed at 180 for all subsequent solution, obviating the need for any repetitive calculations.

The permissible tolerances for summing the δ_i contributions to $\frac{\Delta u_x}{w}$ and $\frac{\Delta u_y}{w}$ were treated in a similar manner. The minimum values were found to vary with the choice of b and λ but in general could be fairly large due to a favorable compensation of the truncation errors. For example, the value for $\frac{\Delta u_x}{w}$ for ten turns of a filament might be only 95 percent of the value for 30 turns, but the errors for the $\frac{\Delta u_y}{w}$ values for the other filaments would be nearly the same so that solutions for

wake vorticity (or for $K(1)$) would differ by perhaps 1/4 of one percent. Thus it was decided that the tolerances on $\frac{\Delta u_x}{W}$ and $\frac{\Delta u_z}{W}$ could be set at two percent for all subsequent solutions without incurring significant errors.

For the calculation of $\frac{\Delta u_r}{W}$ the truncation tolerance was found to be strongly dependent on the characteristic axial separation of two adjacent inner helical sheets as measured at the wake boundary. This characteristic length may be non-dimensionalized by the wake circumference to yield

$$\tilde{z}_c = \frac{2\pi R \lambda/b}{2\pi R} = \lambda/b \quad (55)$$

When \tilde{z}_c is small problems arise in accurately calculating the radial velocities. That is, when a calculation point lies on the cylindrical boundary, the radial velocity due to a filament in a helical sheet lying to one side of the point must be summed with the velocity contribution of a filament at the same radial station of the helical sheet lying to the other side of the point. The radial velocity contributions of two such filaments will be nearly equal in magnitude but large and opposite in sign. Thus an acceptable calculation of the sum of these contributions requires accuracy to a large number of significant digits.

The primary influence of these calculations on the wake vorticity solution occurs in the sizing of the non-uniform boundary sheet strength. If the percent change of $|\delta_e \sqrt{\frac{b}{\lambda}} \delta_i|$ is not held sufficiently small the strength distribution of this sheet may become quite irregular, changing sign and generally degenerating. Fortunately, the magnitude of the

non-uniform boundary sheet strength becomes very small (as compared to $K(x)$) when \tilde{z}_c becomes small so that the effect of inaccuracies in this sheet strength is of secondary importance to the solution for $K(x)$ and to the calculation of velocity profiles in the wake. (When \tilde{z}_c becomes zero the model reduces to the infinite blade case for which the radial velocities vanish along with the strength of the non-uniform boundary sheet.) It was found that the solutions could be adequately controlled if, for $\tilde{z}_c < 1/4$ the tolerance was held to 0.1 percent; for $1/4 < \tilde{z}_c < 1/2$ the tolerance was 1/2 percent; and for $1/2 < \tilde{z}_c < 1$ the tolerance was held to 1.5 percent. Higher values of \tilde{z}_c are not considered to be of practical interest.

System of Linear Equations

As may be seen in the preceding section, the velocity component contribution of a single filament at any point in its flow field is a linear function of the vortex strength of the filament. If the contribution of n filaments to a velocity component, say $\Delta u_c/w$, at a given point are summed then the result is of the form

$$g_1 \bar{v}_1 + g_2 \bar{v}_2 + g_3 \bar{v}_3 + \dots + g_n \bar{v}_n = \bar{u}_c / \cos \varphi$$

where g_i is the integrated functions of geometry, f_c , related to the set of filaments (one for each blade) of strength \bar{v}_i and to the calculation point, \bar{r}, ψ, \bar{z} . If the filament strengths (\bar{v}_i) are unknown and the geometry of the filaments is known, then specifying a value for \bar{u}_c at the calculation point yields a linear equation in $\bar{v}_1, \bar{v}_2, \dots, \bar{v}_n$. If n such calculation points are chosen and the

velocity component is specified at each point, the result is a system of n linear equations in n unknowns. Such a system of equations is used in the solution for the distribution of vorticity in the ultimate wake. The inner helical sheets and the non-uniform boundary sheets must be divided into strips and the strips replaced by finite strength vortex filaments. In order to arrive at some criterion for a minimum number of finite strength vortex filaments to be used to represent a sheet, the blade circulation for an optimum free propeller was calculated using the methods of this chapter for comparison with the results of Goldstein.¹⁰ Solutions were generated using 4, 6, 8, 10, 12, and 18 filaments per sheet. The results, which are considered in greater detail in Appendix III, indicated that ten filaments constituted an adequate approximation to the vortex sheet (i.e., a maximum value of $K(x)$ of about 98 percent of Goldstein's value).

Initial calculations for the ducted fan wake model were performed using ten filaments to replace an inner helical sheet and eight filaments to replace a characteristic portion of the non-uniform boundary sheet. Because of the symmetry of vortex strength in the boundary sheet the eight filaments introduce only four unknowns. Control points were placed between adjacent filaments using ten points on the inner sheet at $\psi' = 0$ and three points on the cylindrical boundary. This arrangement is illustrated schematically in Fig. 10. At the ten control points on the inner sheet the contributions to $\bar{u}_\zeta / \cos \varphi = 1$ are calculated and summed to yield ten equations. At the three control points on the cylindrical boundary the contributions to $\bar{u}_r = 0$ are summed to yield three equations. A final (14th) equation is written in terms of the

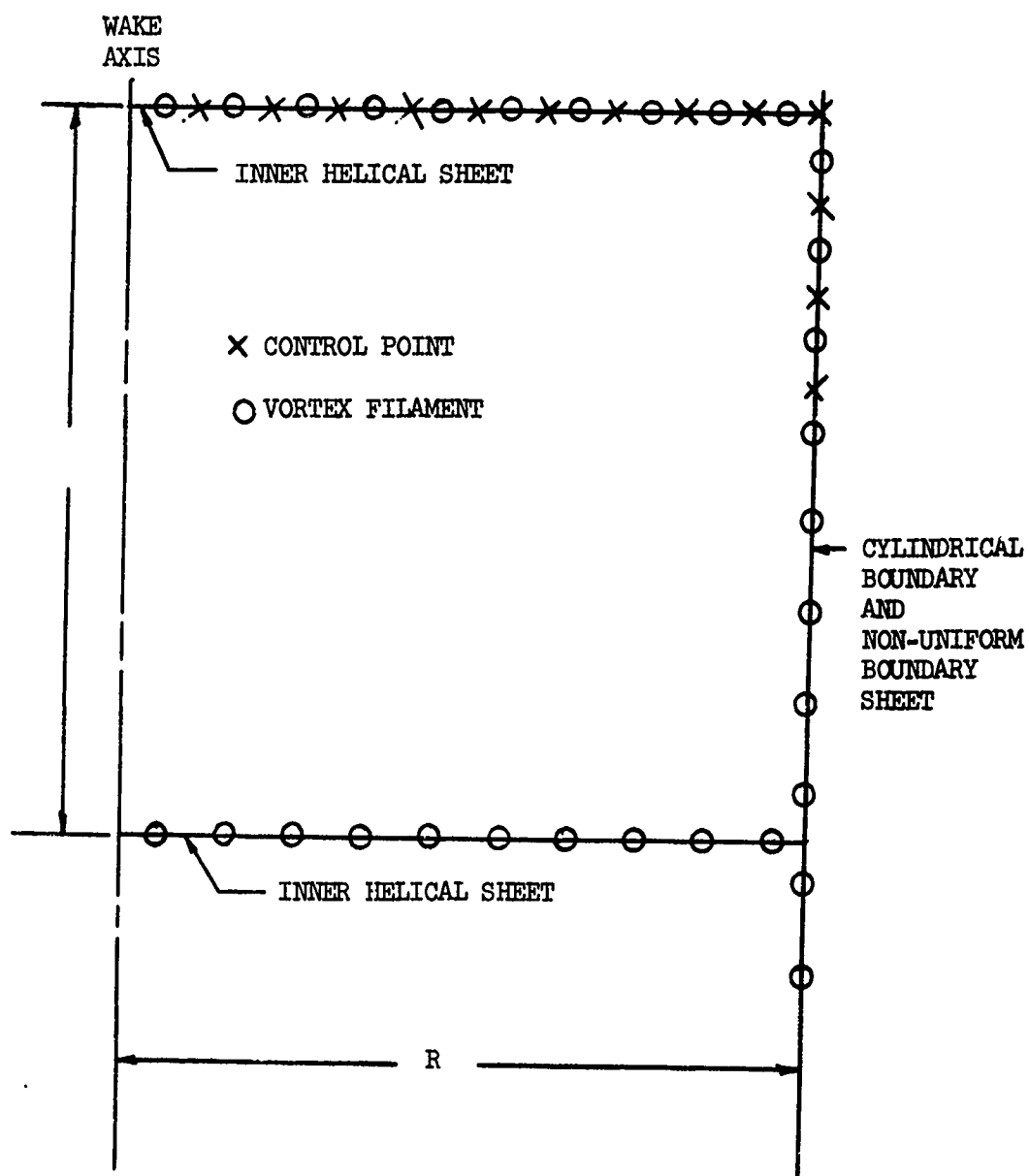


Figure 10. Schematic Diagram of the Arrangement of Vortex Filaments and Control Points in the Ultimate Wake of the Ducted Fan.

net vorticity. The forms of the right hand elements of the equations are modified to include the effect of the uniform boundary sheet as discussed in Chapter III so that the system of equations takes the form

$$A_{1,1} \bar{v}_1 + A_{1,2} \bar{v}_2 + \dots + A_{1,14} \bar{v}_{14} = \lambda^2 / (1 + \lambda^2)$$

$$A_{2,1} \bar{v}_1 + A_{2,2} \bar{v}_2 + \dots + A_{2,14} \bar{v}_{14} = \lambda^2 / (1 + \lambda^2)$$

⋮

⋮

$$A_{10,1} \bar{v}_1 + A_{10,2} \bar{v}_2 + \dots + A_{10,14} \bar{v}_{14} = \lambda^2 / (1 + \lambda^2)$$

$$A_{11,1} \bar{v}_1 + A_{11,2} \bar{v}_2 + \dots + A_{11,14} \bar{v}_{14} = 0$$

⋮

⋮

$$A_{13,1} \bar{v}_1 + A_{13,2} \bar{v}_2 + \dots + A_{13,14} \bar{v}_{14} = 0$$

$$A_{14,1} \bar{v}_1 + A_{14,2} \bar{v}_2 + \dots + A_{14,14} \bar{v}_{14} = - \left(\frac{\lambda}{2b} \right) / (1 + \lambda^2) .$$

$A_{1,1}$ through $A_{10,10}$ are sums of b of the integrated function, f_c , with the sum taken over the corresponding filaments of each inner helical sheet. $A_{1,11}$ through $A_{10,14}$ are the sums of b integrations of f_c for the corresponding filaments of the characteristic portions of the non-uniform boundary sheet. Similarly, $A_{11,1}$ through $A_{13,10}$ are integrations of f_r for the inner sheets and $A_{11,11}$ through $A_{13,14}$ are the integrated coefficients for the non-uniform boundary sheet. $A_{14,1}$ through $A_{14,10}$ are 1.0 and $A_{14,11}$ through $A_{14,14}$ are 2.0. \bar{v}_1 through \bar{v}_{10} are the

unknown strengths, $\gamma/(4\pi R\omega G)$ of the inner sheet filaments and $\bar{\gamma}_{11}$ through $\bar{\gamma}_{14}$ are the unknown strengths for the non-uniform boundary sheet filaments.

Thorough investigations of the effect of the total numbers of filaments and control point locations and their spacing on the inner sheets indicate that the arrangement shown in Fig. 10 is satisfactory and does not require modification with \bar{z}_c (i.e., λ and b). The satisfactory numbers of filaments and control points on the cylindrical boundary were found to be clearly dependent on \bar{z}_c . That is, for $\bar{z}_c < 1/4$ 6 filaments and 2 control points suffice; for $1/4 < \bar{z}_c < 1/2$ 8 filaments and 3 control points suffice; and for $1/2 < \bar{z}_c < 1$, 12 filaments and 5 control points are adequate. The decisions for adequate arrangements were made rather subjectively on the basis of comparisons of a blade number family of solutions to the exact infinite blade solution by Gray¹³. A further criterion which involves the smoothness of the vorticity distributions on the sheets was used as a measure of the convergence of the sheet strength distributions.

In Chapter II it was noted that the strength of the non-uniform boundary sheet must be zero at the lines of intersection and must maintain helical symmetry between lines of intersection. In order to meet these requirements the sheet strength was defined as a series of trigonometric functions such that

$$\bar{\gamma} = \sum_{n=1}^N a_n \sin \left[\frac{2n-1}{2} \pi \bar{z} \right]$$

where $N + 1$ is the number of control points on the sheet. The series is integrated over a strip width of the sheet to yield the corresponding finite filament strength. If $2w$ represents the strip width such that $w = 1/4N$ then the filament strength is

$$\bar{\gamma} = \int_{\bar{z} - w}^{\bar{z} + w} \gamma \, d\bar{z} = \sum_{n=1}^N \left[a_n \left(\frac{4/\pi}{2n-1} \right) \sin \left[\frac{2n-1}{2} \pi w \right] \cos \left[\frac{2n-1}{2} \pi \bar{z} \right] \right]$$

The strength distribution of an inner sheet is also expressed in series form. As \bar{r} approaches 1.0 it is necessary that $\tilde{\gamma}$ become zero so that for points immediately above and below the sheet \bar{u}_r may vanish. Since the strength of the sheet is $\tilde{\gamma} = -\frac{d\Gamma(x)}{dx}$ this restriction requires that $\frac{d\Gamma}{dx}$ be zero at $x = 1.0$. Thus the bound vortex strength may be written as

$$\frac{\Gamma(x)}{2\pi R w \lambda} = \sum_{n=1}^{N-1} B_n \sin \left[\frac{2n-1}{2} \pi x \right] . \quad (55)$$

To calculate the strength of a filament of the inner sheet the difference in bound strength is taken at the radial stations corresponding to the edges of the strip which the filament replaces. Thus

$$\bar{\gamma} = - \sum_{n=1}^{N-1} 2 B_n \sin \left[\frac{2n-1}{2} \pi w \right] \cos \left[\frac{2n-1}{2} \pi x \right] .$$

The system of linear equations is formed in the same manner as before by summing the velocity component contributions at a given point due to all of the filaments of unknown strength. However, the unknowns now become the coefficients of the two series for $\bar{\gamma}$. That is, at the point $(\bar{r}, \bar{y}, \bar{z})$ n is fixed and the contributions of all filaments for

B_n (or a_n) are summed to yield the coefficient $A_{i,j}$. For example, set $n = 1$ in the B_n series so the coefficient for B_1 is

$$A_{1,1} = - \sum_{i=1}^N \frac{1}{2\pi R w} \int_0^{\infty} f_{\zeta_i} d\psi' \left[\sin\left(\frac{\pi}{2} \omega\right) \cos\left(\frac{\pi}{2} x\right) \right] .$$

The system formed in this manner is equivalent to the previous system (with discrete filament strengths) with the additional constraints on the end values of the vorticity distributions.

Solution of the linear system for either the filament strengths or the series coefficients is carried out by the Gauss method of successive eliminations as presented by Fadeeva¹⁴. Having solved for the wake vorticity the blade bound vortex strength distribution may be calculated directly from the series of equation (55). K_0 may be calculated by integration of the series to yield

$$K_0 = \frac{4b}{\lambda} \sum_{n=1}^{N-1} \left(\frac{2n-1}{n} \pi\right)^{-1} \left[(-1)^{n+1} - \left(\frac{2n-1}{\pi}\right)^{-1} \right] B_n ,$$

and

$$K_0(x) = \frac{2b}{\lambda} \sum_{n=1}^{N-1} B_n \sin \left[\frac{2n-1}{2} \pi x \right] .$$

μ_0 may be obtained by a simple strip integration based on filament strength such that

$$\mu_0 = \frac{4b}{\lambda} \left\{ \sum_{i=1}^{N-1} (-\bar{v}_i) \frac{x_i}{(x_i^2 + \lambda^2)^2} 2w \right\}$$

Thrust and Power Integrations

In Chapter IV the thrust and power coefficients were shown to contain integrals of the velocity distribution through a characteristic volume of the wake. These integrals, which must be evaluated numerically are

$$\epsilon_o = \int_0^1 \int_0^1 \int_0^{2\pi} \left[\bar{u}_{zvs}^2 - \bar{u}_{rvs}^2 - \bar{u}_{\psi vs}^2 + \bar{u}_{zvsR}^2 + \bar{u}_{\psi vsR}^2 \right] \bar{r} \, d\bar{r} \, d\bar{z} \, d\bar{\psi} / 2\pi$$

and the integrals occurring in the power calculation

$$\int_0^1 \int_0^1 \int_0^{2\pi} \bar{u}_{zvs} \bar{u}_{zvsR} \bar{r} \, d\bar{r} \, d\bar{z} \, d\bar{\psi} / 2\pi$$

and

$$\int_0^1 \int_0^1 \int_0^{2\pi} \bar{u}_{zvs} \left[\bar{u}_{zvsR}^2 + \bar{u}_{\psi vsR}^2 \right] \bar{r} \, d\bar{r} \, d\bar{z} \, d\bar{\psi} / 2\pi$$

When the strengths of all of the vortex filaments comprising the ultimate wake are known, the components of induced velocity can be calculated at any point in the wake by evaluating the integrals for each of the filaments and multiplying the result by the filament strength. The procedures for integrating and summing the contributions of the filaments are the same as those used in setting up the system of linear equations. These results are then projected to yield the components of induced velocity in the r -, z -, and ψ - directions. Due to the helical symmetry of the vorticity and velocity distributions in the ultimate wake, the volume integrations may be performed by

obtaining a detailed knowledge of the flow field on a $\bar{z}\bar{r}$ - surface. This surface is bounded by the wake axis, the cylindrical boundary, an inner helical sheet, and the radial line midway between two adjacent inner helical sheets. The surface is divided into a network or grid. At the intersection points of the grid the induced velocity components are calculated, their squares are calculated, and all of this information is formed into two-dimensional arrays of data. A typical integration surface is shown schematically in Fig. 11.

Since the motion and vorticity of the wake are known, numerical evaluation of the velocity components at the edges of the $\bar{z}\bar{r}$ - surface is not required. Specifically, at $\bar{r} = 0$ $\bar{u}_y = \bar{u}_r = 0$ and $\bar{u}_z = \bar{u}_{z_0}$. At $\bar{z} = 0$, $\bar{u}_z = 1 - G\lambda^2/(\bar{r}^2 + \lambda^2)$, $\bar{u}_y = -G\lambda \bar{r}/(\bar{r}^2 + \lambda^2)$, and $\bar{u}_r = -\frac{\lambda}{2b} \frac{d\Gamma(x)}{dx}$. At $\bar{r} = 1$ $\bar{u}_r = 0$, $\bar{u}_z = 1 - G\lambda^2/(\bar{r}^2 + \lambda^2) + 2\tilde{\gamma} \cos \varphi_R$, $\bar{u}_y = -G\lambda \bar{r}/(\bar{r}^2 + \lambda^2) + 2\tilde{\gamma} \sin \varphi_R$. (Here, $\tilde{\gamma}$ is the strength of the non-uniform boundary sheet.) At $\bar{z} = 1/2$ $\bar{u}_r = 0$ but \bar{u}_z and \bar{u}_y must be evaluated numerically. For the arrangement shown in Fig. 11, all of the velocity components must be evaluated at the internal grid points of which there are 27, and the \bar{u}_y and \bar{u}_z values must be calculated at the 9 lower edge points.

The elements of these two-dimensional arrays of data are then squared to form three new arrays denoted by $\bar{u}_{z,i,j}^2$, $\bar{u}_{r,i,j}^2$ and $\bar{u}_{y,i,j}^2$. Taking the $\bar{u}_{z,i,j}^2$ array as an example, the integration may be performed by a simple strip method such that

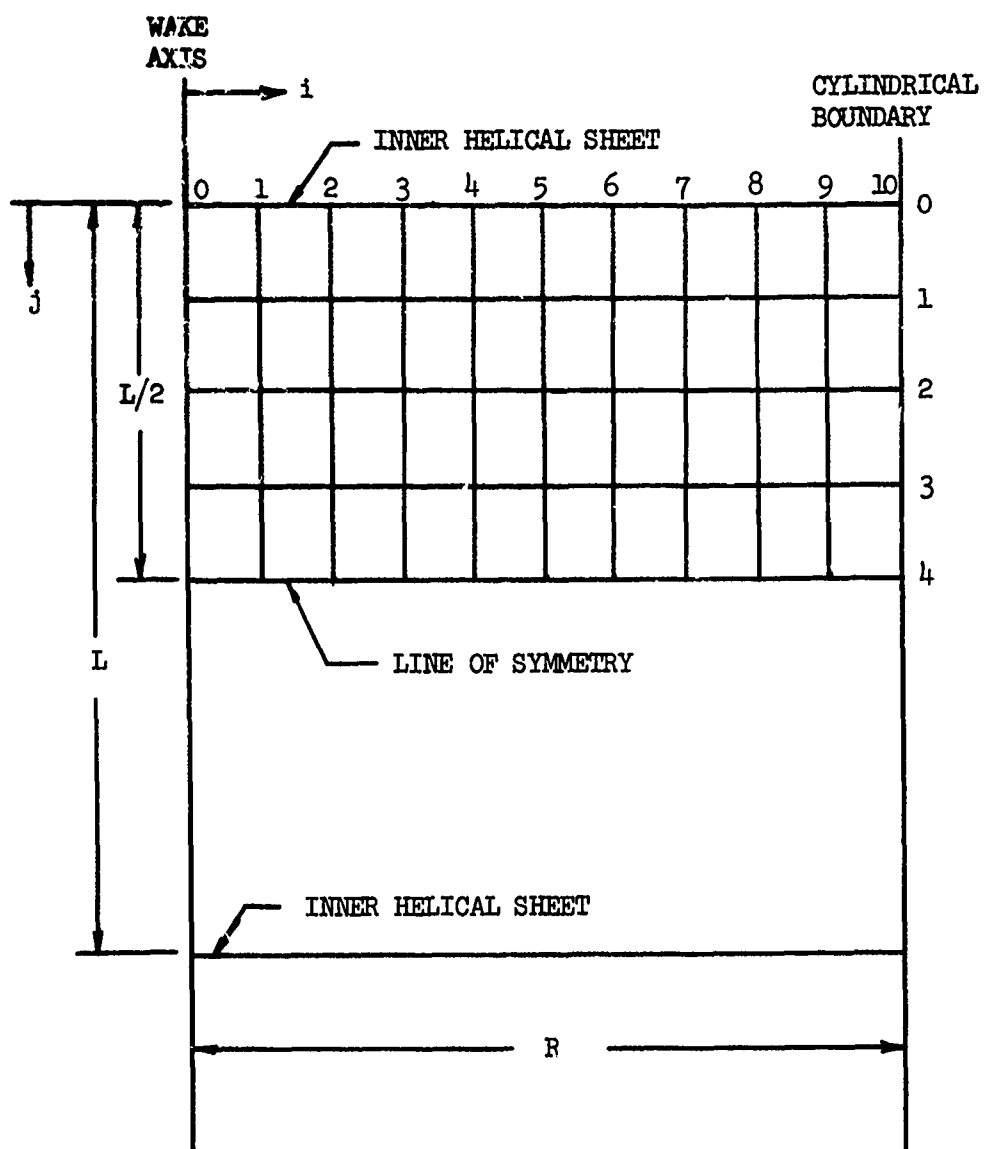


Figure 11. Network Used in Calculating the Velocity Integrals on the $\bar{z}\bar{r}$ - surface.

$$\int_0^1 \int_0^1 \int_0^{2\pi} \bar{u}_z \bar{r} d\bar{r} d\bar{z} d\psi / 2\pi = \sum_{i=0}^I \sum_{j=0}^J \frac{(2i-1)}{4I^2J} \left[\bar{u}_{z,i,j}^2 + \bar{u}_{z,i+1,j}^2 \right. \\ \left. + \bar{u}_{z,i,j+1}^2 + \bar{u}_{z,i+1,j+1}^2 \right]$$

where $(I + 1)$ is the number of grid points in the \bar{r} - direction and $(J + 1)$ is the number of grid points in the \bar{z} - direction. For the network illustrated in Fig. 9, $I = 10$, $J = 4$ and $4I^2J = 1600$.

For the integrations involving the (vs) velocities, calculation of the array members is restricted to the filaments associated with the inner helical sheets and the non-uniform boundary sheet. The edge values become: at $\bar{r} = 0$ $\bar{u}_{\psi_{vs}} = \bar{u}_{r_{vs}} = 0$, $\bar{u}_{z_{vs}} = -1/(1 + \lambda^2)$; at $\bar{z} = 0$ $\bar{u}_{z_{vs}} = \frac{1}{1 + \lambda^2} - \frac{\lambda^2}{\bar{r}^2 + \lambda^2}$, $\bar{u}_{\psi_{vs}} = -G\lambda \bar{r}/(\bar{r}^2 + \lambda^2)$ and $\bar{u}_{r_{vs}} = -\frac{\lambda}{2b} \frac{d\Gamma(x)}{dx}$; at $\bar{r} = 1$ $\bar{u}_{r_{vs}} = 0$, $\bar{u}_{\psi_{vs}} = -G\lambda/(1 + \lambda^2) + 2\tilde{\gamma} \sin \phi_R$, $\bar{u}_{z_{vs}} = 2\tilde{\gamma} \cos \phi_R$. At $\bar{z} = 1/2$ $\bar{u}_{r_{vs}} = 0$ and $\bar{u}_{z_{vs}}$ and $\bar{u}_{\psi_{vs}}$ must be evaluated numerically.

The accuracy of the integration technique is clearly dependent on the choice for I and J and on the strip method employed. As a check on the method the \bar{u}_z velocity distribution was calculated for several values of λ and b and integrated using the method outlined above. From equation (42) of Chapter IV

$$\int \bar{u}_z d \text{ vol} = \frac{1}{2} [N + \bar{u}_{\xi_0}]$$

Using values of $I = 5$ and $J = 4$ the numerical results agreed with the more exact results of equation (42) to within about 1 percent in all cases. (See Appendix III.) As a further check the values of ϵ_r , ϵ_y and ϵ_z were calculated in the same manner for $\lambda = 1.356$ and for increasingly large blade number. Their convergence to the exact value for the infinite blade case¹³ was satisfactorily observed and is considered in more detail in Appendix III.

CHAPTER VI

RESULTS

Following the initial checkouts of the numerical procedures, the methods for the generation and solution of the system of equations for the wake vorticity distribution of the lightly loaded ducted fan were programmed for the digital computer. The system was solved first for a value of $\lambda = 1.356$ with $b = 2$ and 4 . The results for the blade bound circulation, $K(x)$, were compared to the electro-potential analogy results of Gray⁴. These comparisons are shown in Fig. 12 and Fig. 13. In both cases the agreement is considered to be good.

Solutions were also generated for comparison to the theoretical results of Tachmindji² who used the velocity potential approach. $K(x)$ is shown for the two methods in Fig. 14 and Fig. 15, with $\lambda = 1/3$ and $2/3$ and $b = 4$ in both cases. The agreement is again considered to be good.

For comparison to the exact theory³ for a ducted fan having an infinite number of blades, solutions were obtained for $b = 2, 4, 6, 8, 12, 16,$ and 24 with $\lambda = 1.356$. The results for the blade bound vortex strength show excellent convergence to the exact solution as seen in Fig. 16. Since the measure of convergence may be seen more easily in terms of the mass coefficient, the values of K_0 for increasing blade number are shown in Fig. 17.

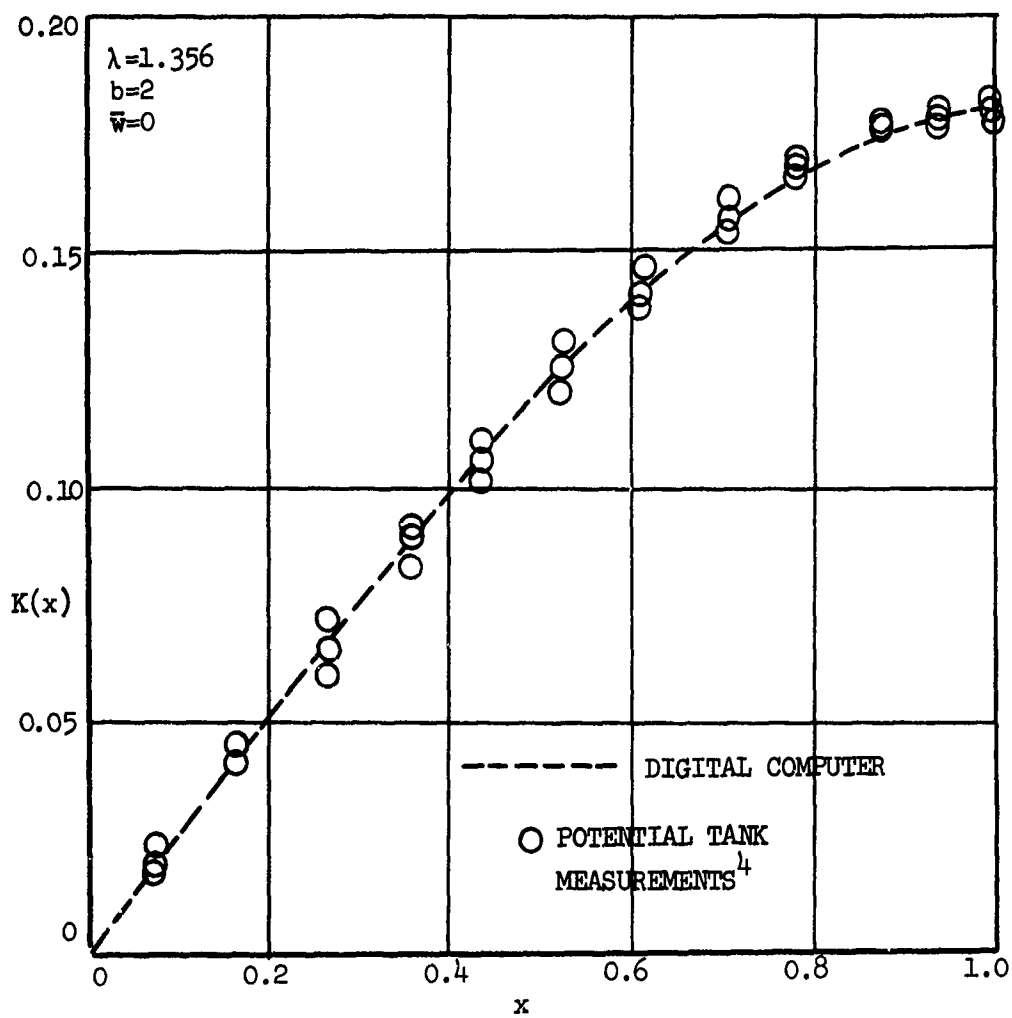


Figure 12. Comparison of Two Methods for Determining the Blade Bound Vorticity for a Lightly Loaded Ducted Fan.

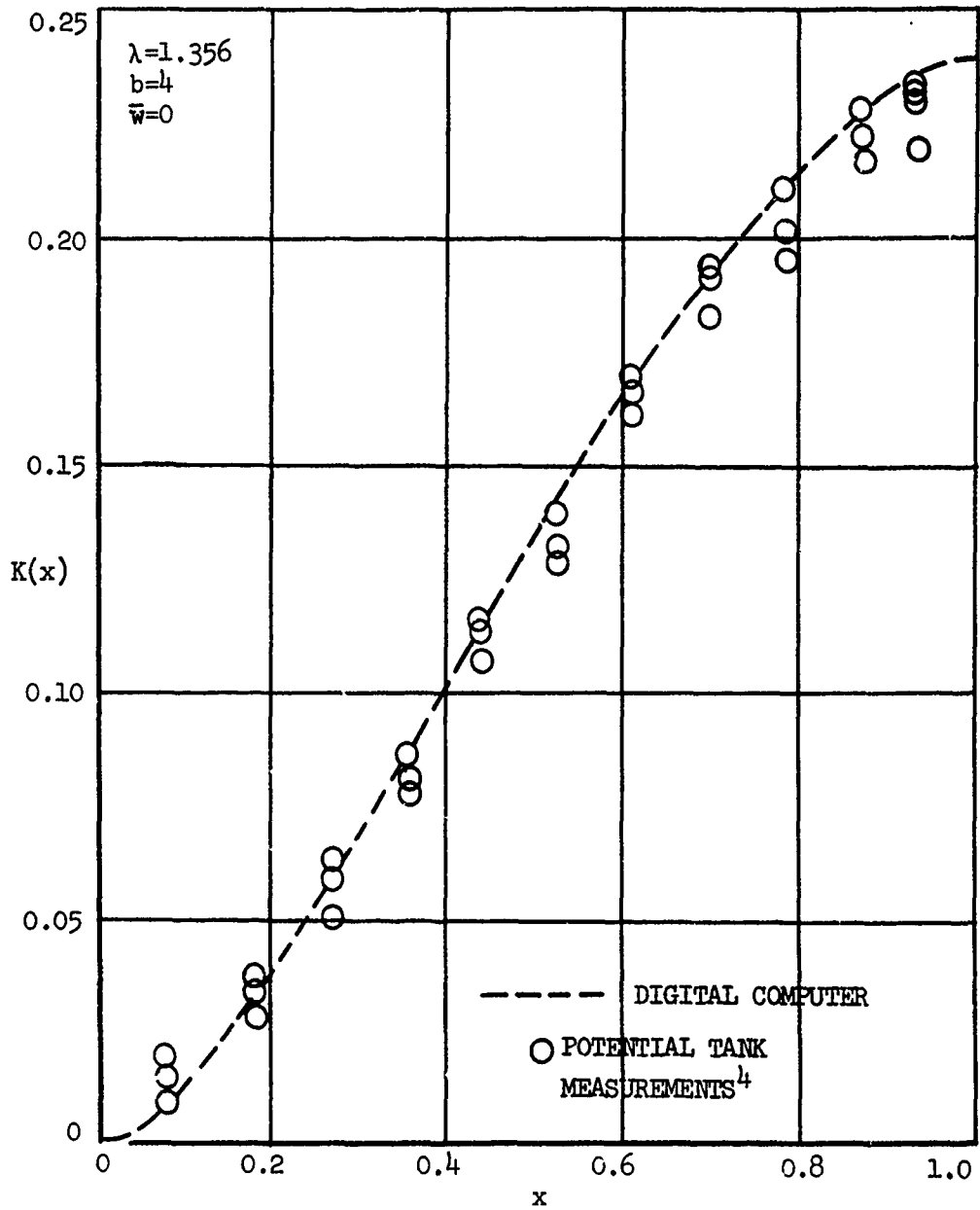


Figure 13. Comparison of Two Methods for Determining the Blade Bound Vorticity for a Lightly Loaded Ducted Fan.

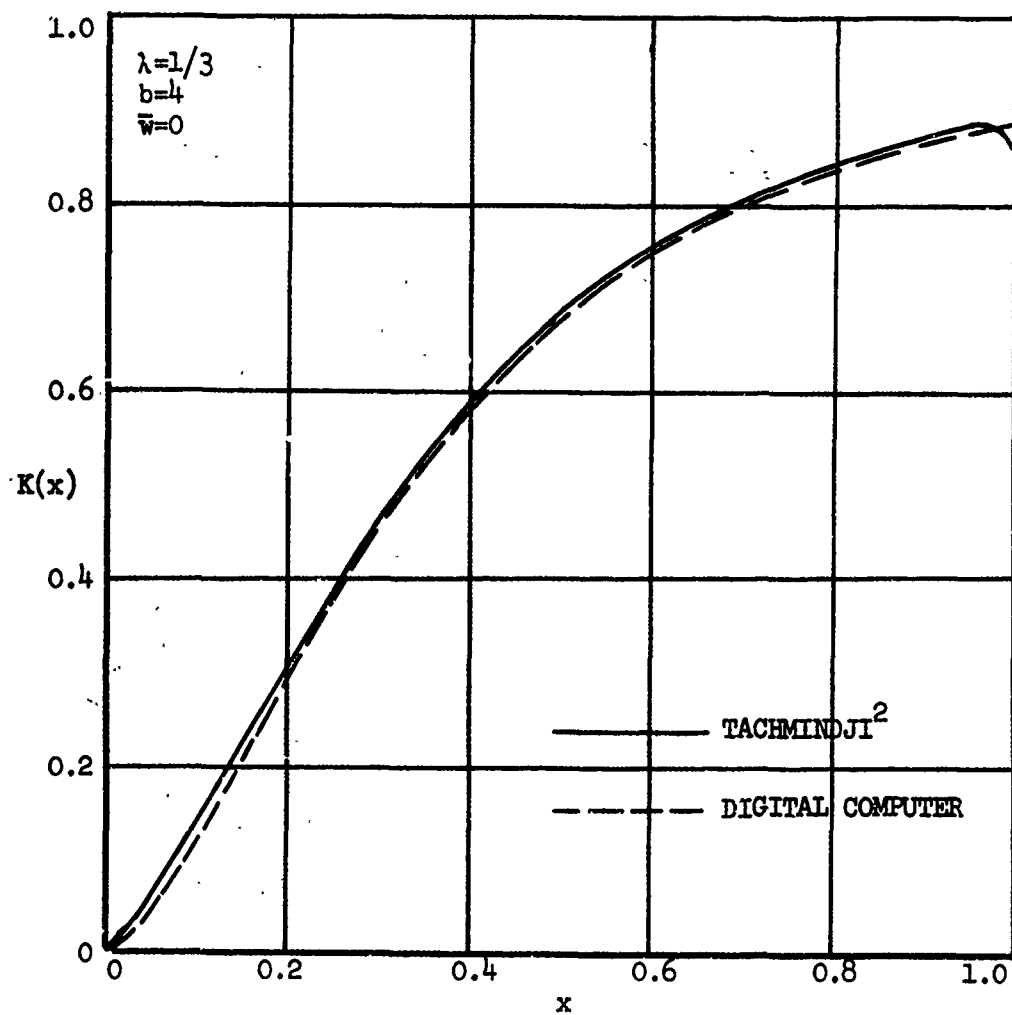


Figure 14. Comparison of Two Methods of Calculating the Blade Bound Vorticity for a Lightly Loaded Ducted Fan.

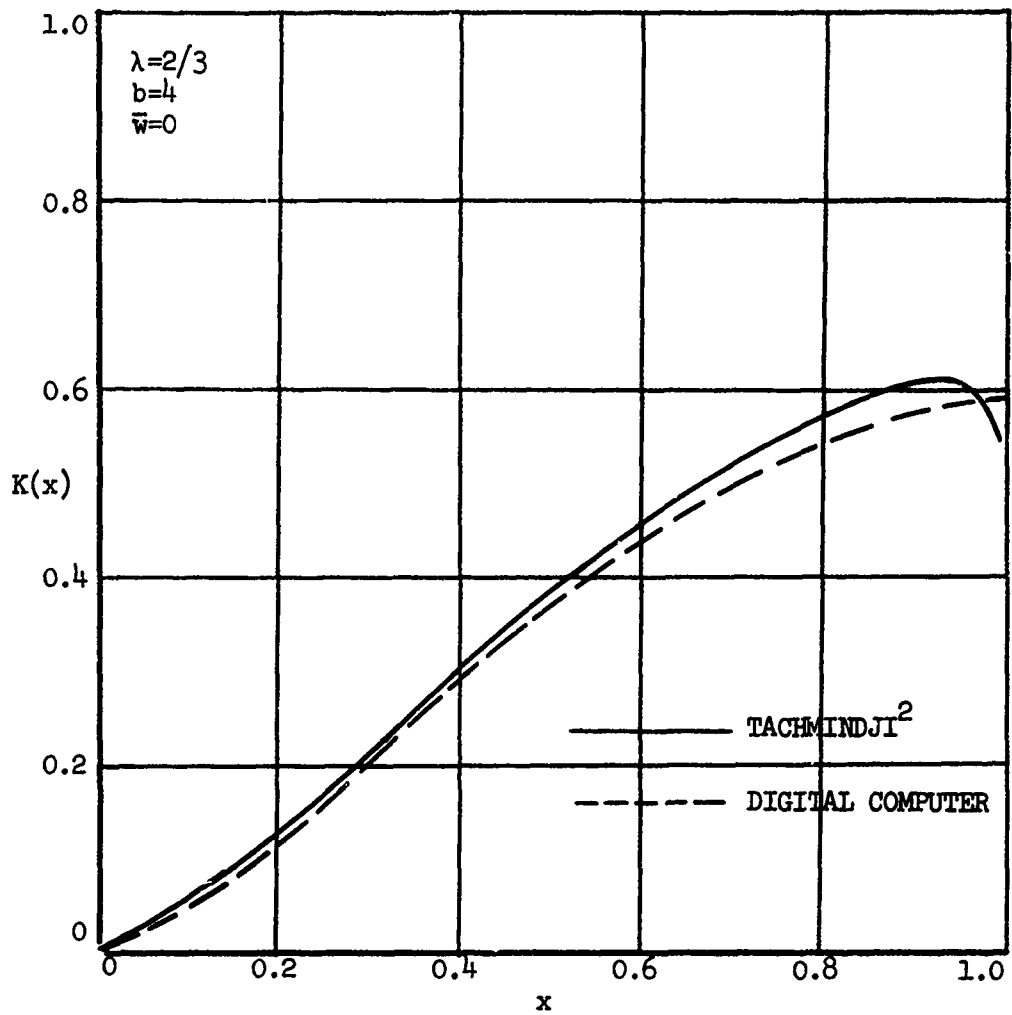


Figure 15. Comparison of Two Methods of Calculating the Blade Bound Vorticity for a Lightly Loaded Ducted Fan.

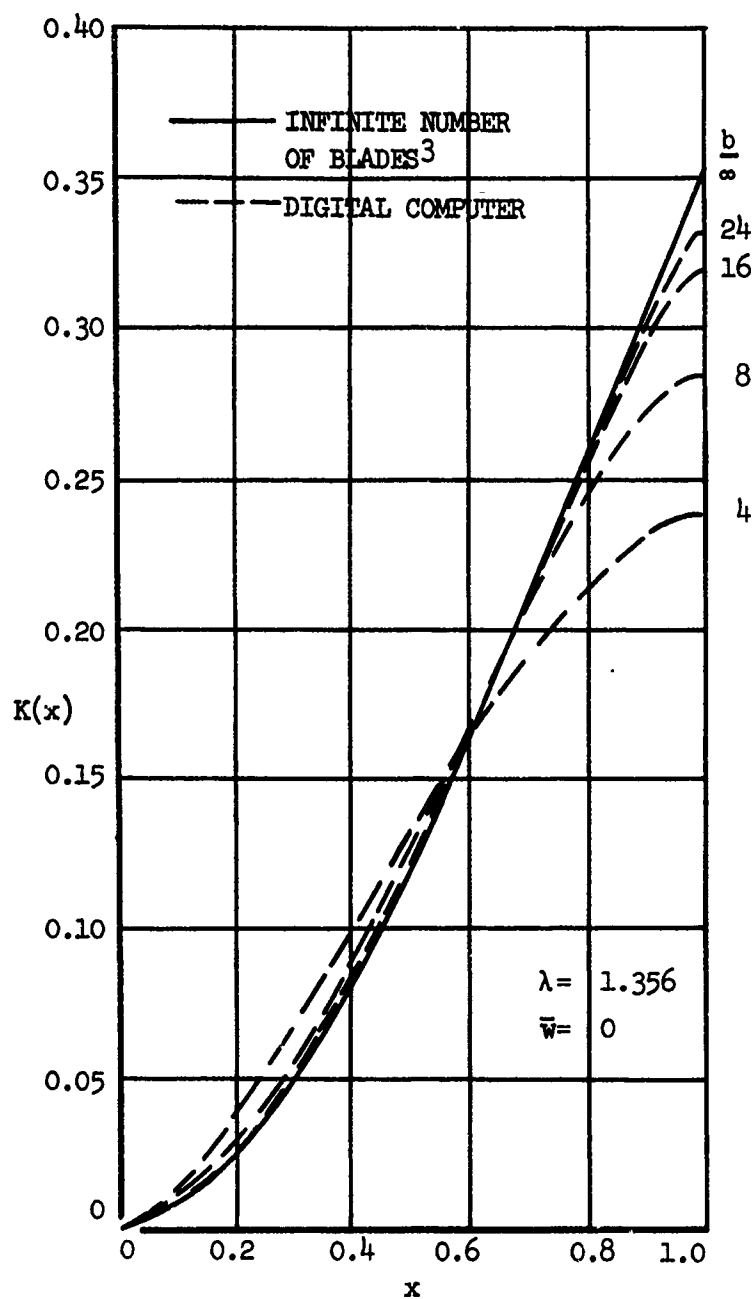


Figure 16. Comparison of the Blade Bound Vorticity for a Lightly Loaded Ducted Fan for Successive Numbers of Blades (Digital Computer) with the Infinite Blade Solution (Exact³).

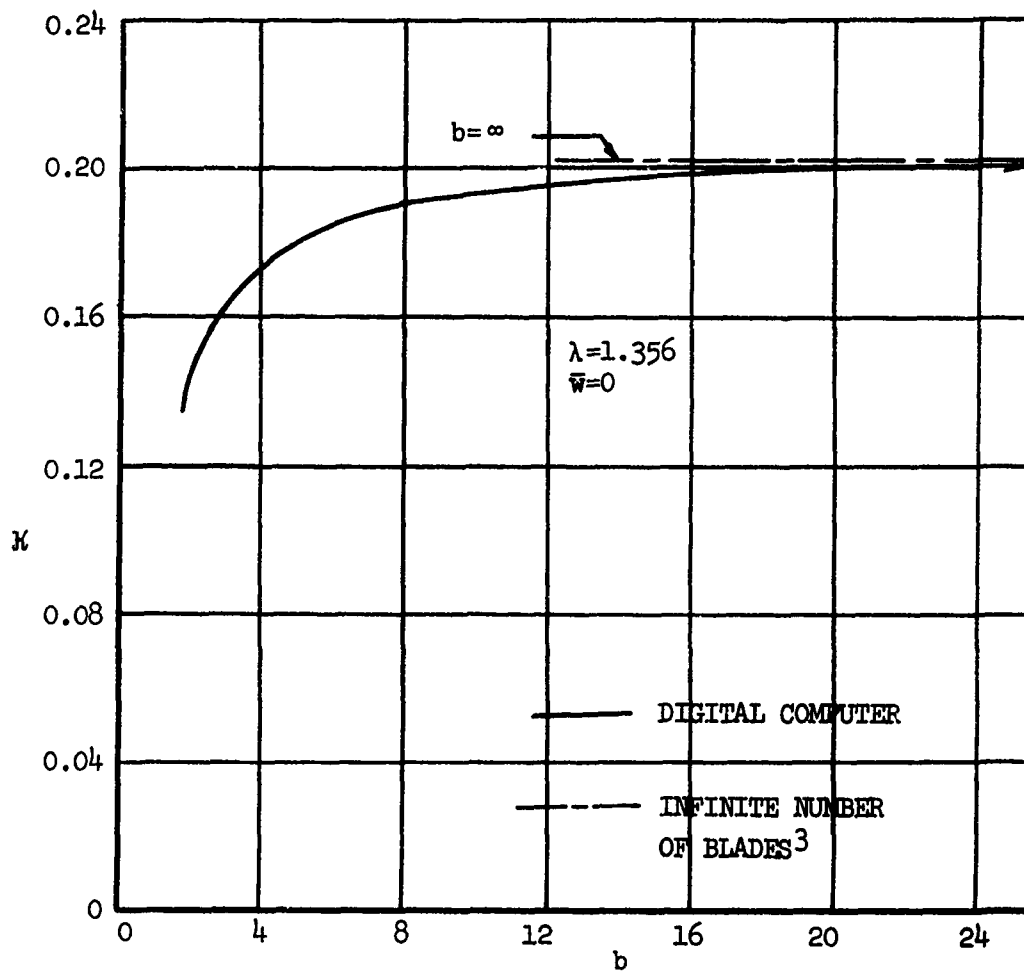


Figure 17. Comparison of Mass Coefficients for Increasing Number of Blades (Digital Computer) with the Mass Coefficient for the Infinite Blade Case (Exact3).

In order to illustrate the behavior of the design and performance parameters with the variation of the load parameter, a family of solutions is presented in Figures 18 through 21. Fig. 18 shows the basic lightly loaded circulation curves, $K_0(x)$, for $\lambda = 1/2$ and $b = 2, 3, 4, 6, \text{ and } 8$. The variation of the scale factor G with \bar{w} is illustrated in Fig. 19. This result is plotted versus \bar{w}/λ ; since \bar{w} ranges from zero to λ , \bar{w}/λ yields the convenient range of zero to 1.0 with $\bar{w}/\lambda = 1.0$ corresponding to the static thrust condition. The variations of C_T and C_P with \bar{w}/λ are shown in Fig. 20 and Fig. 21 for the heavily loaded ducted fans corresponding to the lightly loaded fans of Fig. 18. The exact results for the infinite blade case are included in these figures for comparison and to illustrate the convergence of the results, with increasing blade number, to the exact solution.

In Appendix IV a collection of results is presented in several tables. The range taken for λ was $0 < \lambda \leq 1$, and for \bar{w}/λ from zero to 1.0. For the values of λ considered, the blade numbers were taken as 2, 3, 4, 6, 8, 12 and 16. As may be seen in the tables, the higher blade numbers were not considered in the calculations for the smaller values of λ . Rather, the blade number was increased until the results had closely approached the exact infinite blade solution.

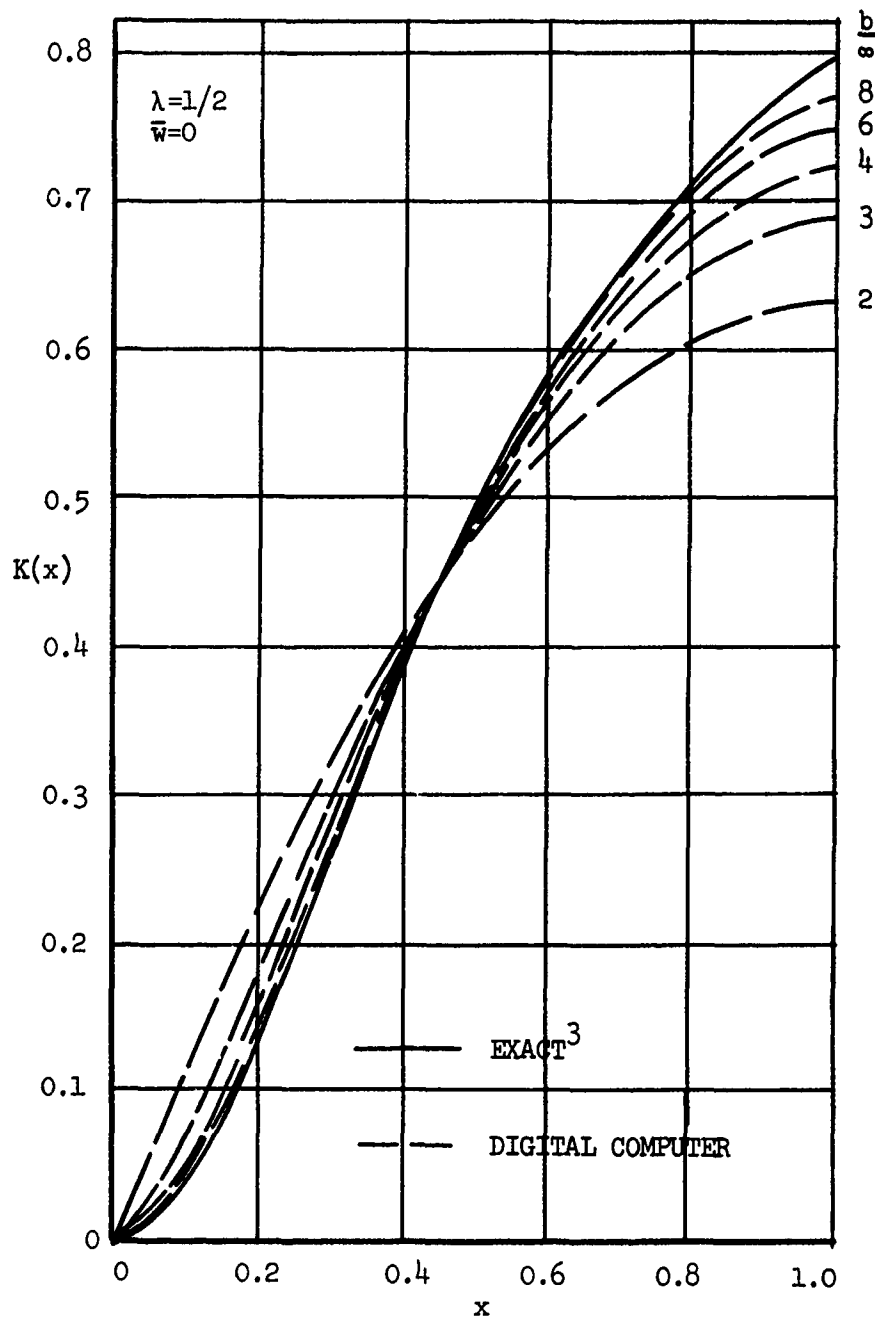


Figure 18. Blade Bound Vorticity for a Family of Lightly Loaded Ducted Fans.

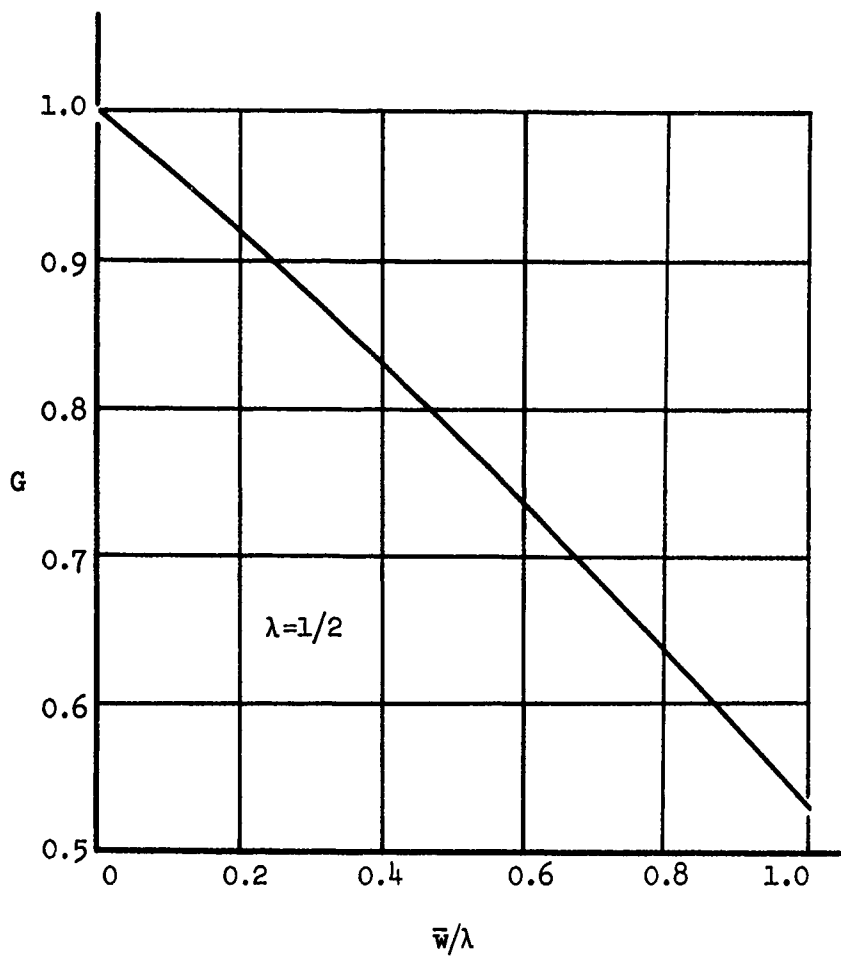


Figure 19. Variation of the Load Scaling Factor.

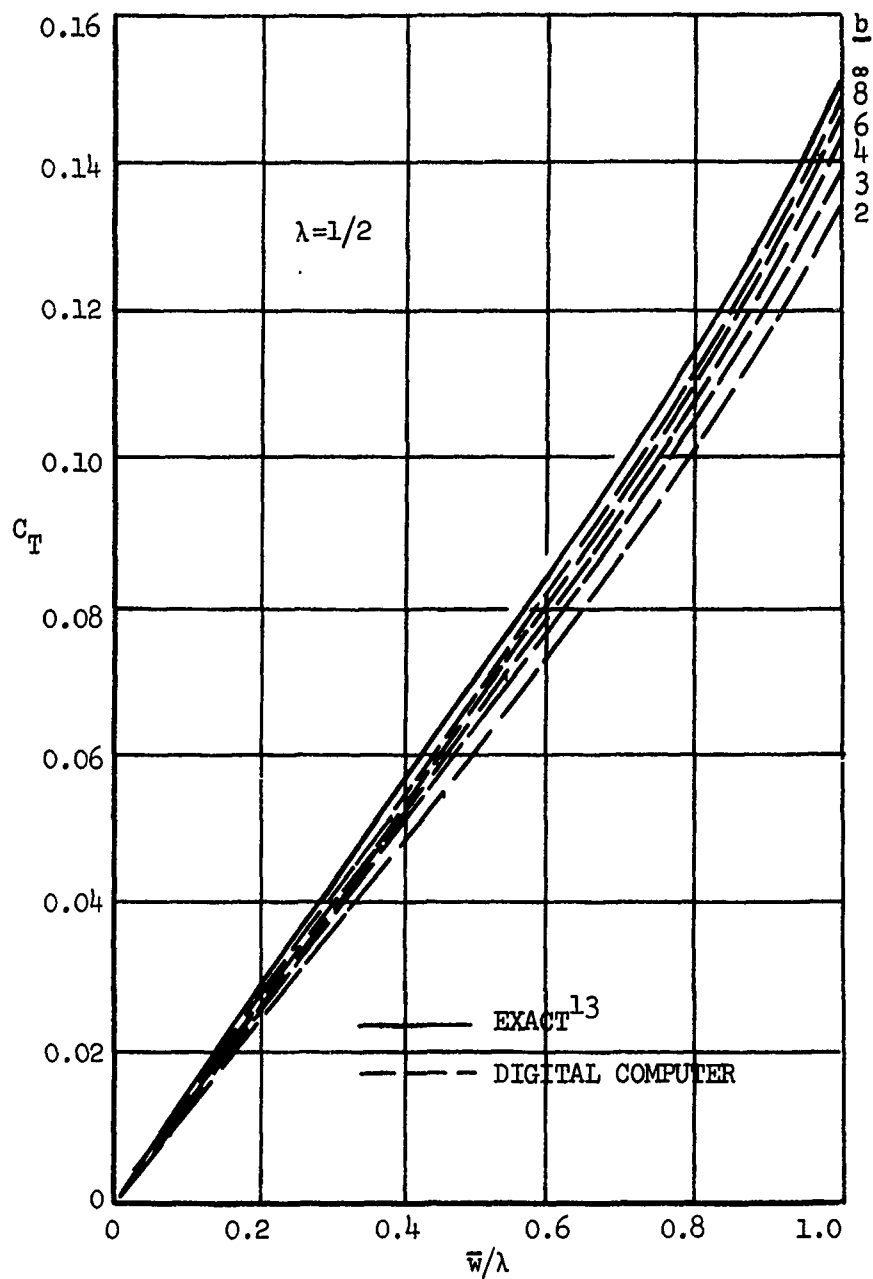


Figure 20. Variation of Thrust Coefficient with Load for the Family of Ducted Fans.

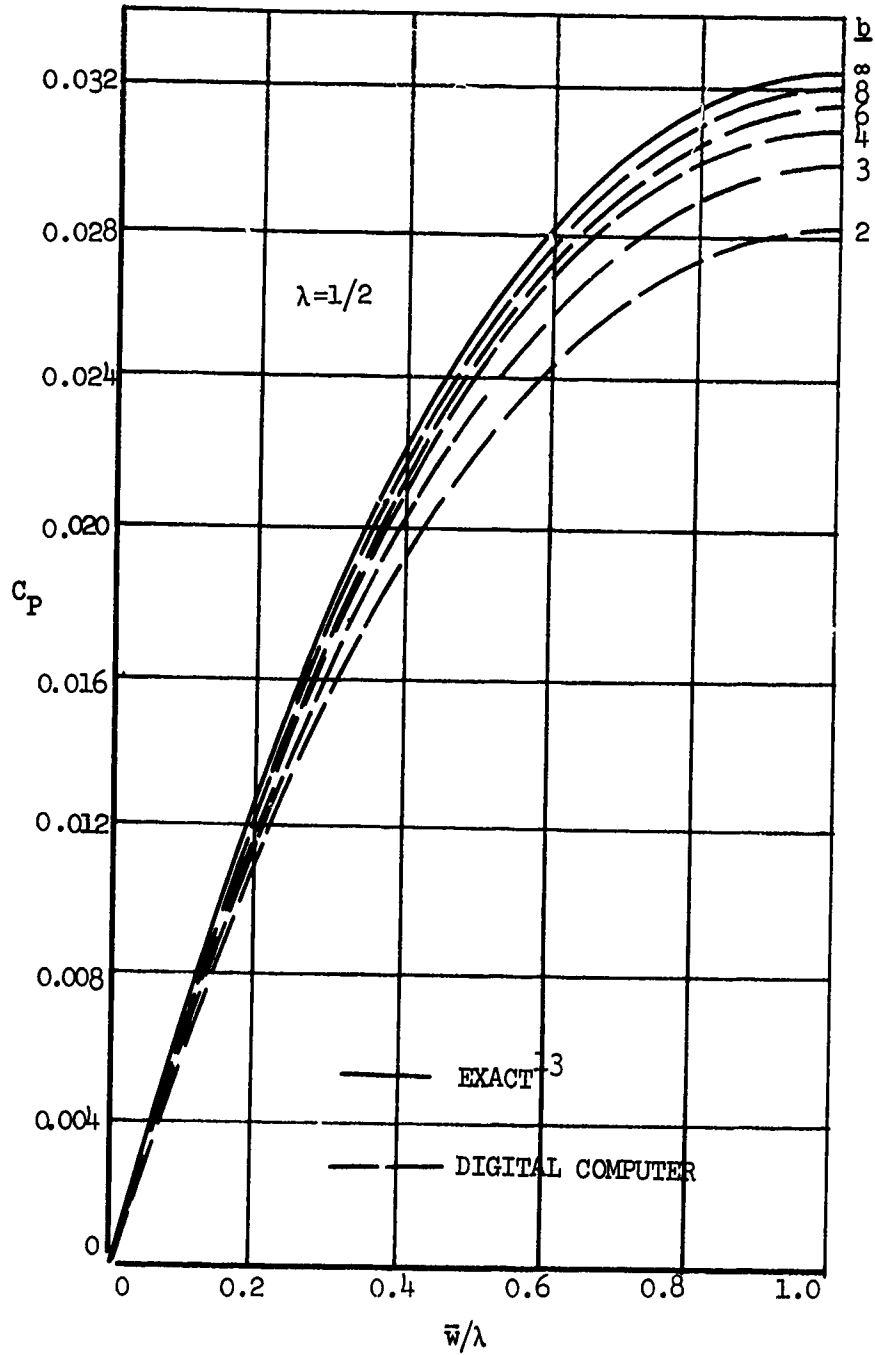


Figure 21. Variation of the Power Coefficient with Load for the Family of Ducted Fans.

APPENDIX I

GEOMETRY AND MOTION OF THE INNER HELICAL SHEETS⁴

The argument as to the geometry and motion of the wake vortex pattern of an optimum ducted single-rotation fan is essentially the same as that presented by Betz⁹ and Theodrosen³. Following these approaches, consider a non-optimum ducted fan which is producing the required thrust at the expenditure of the necessary amount of power. At a distance behind the first ducted fan system such that the duct interference velocities are negligible, arrange a second ducted fan having the same number of blades and rotational speed as the first fan and so phased with the first fan that each blade intercepts one of the sheet of discontinuity that are shed from the former fan's blade trailing edges. The diameter of the duct of this second system is set equal to the wake diameter so that it intercepts the sheet of discontinuity that is shed from the first duct's trailing edge. Assume that the second fan is mounted on an extension of the shaft of the first fan and assume further that neither the second fan nor the duct contribute to the motion of the wake nor disturb the flow in any way. Similarly, place a third ducted fan, and so forth, until a large number of ducted fans are arranged in tandem, all mounted on the shaft of the first fan, all having the required phase relation, and none contributing to the motion of the wake nor to the thrust or power required.

In general, certain of the blade elements of the first fan will be operating at relatively high efficiencies while other elements will be operating at relatively low efficiencies. This will be evident in the wake, as will be seen later, by the pitch of the wake spiral with the efficiency being higher where the pitch is lower and vice versa. Suppose now that on the second ducted fan a positive increment of thrust is added to a blade element where the pitch is low and an equal increment of negative thrust is added on the third fan to an element operating in a region where the pitch is high. The thrust of the complete system remains unchanged but the third fan adds more power to the shaft acting as a windmill than the second fan requires to produce the thrust increment so that a net reduction of the power required by the system is realized. (Of course skin friction is neglected and it is assumed that the thrust increments are very small so that the power recovery factor is 100%.) The efficiency of these added increments may be obtained by considering Fig. 22. Using the Kutta-Joukowski theorem, the increment of thrust is

$$\Delta T = \rho \Delta \Gamma (\Omega r - u_y) \quad .$$

The increment of torque is

$$\Delta Q = \rho \Delta \Gamma (V_\infty + u_z) r \quad .$$

This gives for the efficiency

$$\eta = \frac{V_\infty \Delta T}{\Omega \Delta Q} = \frac{\rho \Delta \Gamma (\Omega r - u_y) V_\infty}{\rho \Delta \Gamma (V_\infty + u_z) \Omega r}$$

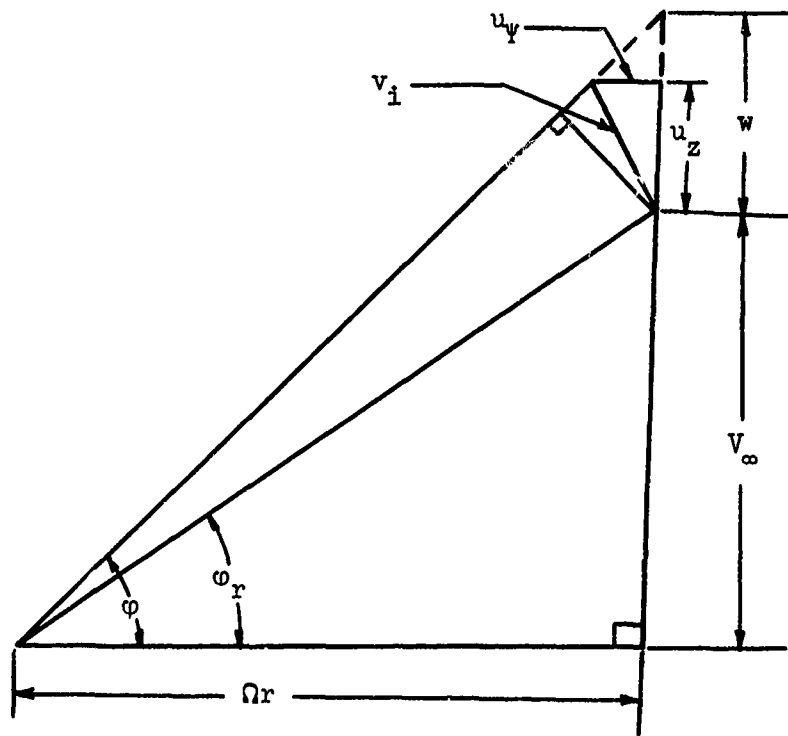


Figure 22. Incremental Thrust Efficiency Diagram.

$$= \frac{V_{\infty}}{V_{\infty} + w} \left(\frac{\Omega r - u_{\psi}}{V_{\infty} + u_z} \right) \tan \varphi$$

$$= \frac{V_{\infty}}{V_{\infty} + w}$$

or
$$\eta = \frac{1}{1 + w/V_{\infty}} \quad (56)$$

The elemental efficiency is thus simply a function of the ratio of the apparent velocity of the helical vortex sheet element to the free stream velocity. The process of adding an increment of thrust on a blade element of one fan and removing the same amount on the following fan with a net reduction in power required is continued until no further reduction is realized. At this point the efficiency of the added element of thrust will be the same regardless of the radius at which it is added. From equation (56) this occurs when w/V_{∞} is the same at each blade station for the last fan in the array. The wake behind this last fan represents the wake for the optimum case. Thus the optimum condition is obtained when the ultimate wake vortex pattern appears to move as a rigid body and the pitch of the inner helical vortex spiral is uniform along the radius. The problem, of course, is the determination of the single ducted fan which will yield the same wake configuration as the array.

APPENDIX II

VELOCITY FIELD OF THE UNIFORM BOUNDARY SHEET

The uniform boundary sheet of the ultimate wake vortex model consists of equal strength helical vortex filaments of constant and equal pitch wrapped on a right circular cylinder at the pitch angle φ_B . The strength of all filaments is the same and is given by $\tilde{\gamma}$, the sheet strength per unit length normal to the filaments.

This sheet can be divided into two sheets to be superposed. One sheet consists of a system of infinitesimal strength ring vortex elements whose axes are the axis of the cylindrical wake boundary surface. The strength of this sheet is given by $\tilde{\gamma} \cos \varphi_B$. The other sheet is a system of straight line filaments of infinitesimal strength lying on the cylindrical boundary surface and parallel to the wake axis. Again, the strength of all filaments is the same and the sheet strength per unit length normal to the filaments is given by $\tilde{\gamma} \sin \varphi_B$.

The velocity fields of these two sheets are calculated separately, in terms of a Biot-Savart integration of the filaments of the sheets, and then superposed to yield the velocity field of the entire uniform boundary sheet.

Ring Element Sheet

From considerations of symmetry, the angular and radial velocities associated with the ring element sheet are identically zero. The geometrical relationships necessary to calculate the axial velocity field of

this sheet are shown in Fig. 23. From the figure

$$d\gamma ds' = \tilde{\gamma} \cos \varphi_B R d\psi dz$$

$$h_2 = R - r \cos \psi$$

$$h^2 = (R - r \cos \psi)^2 + z^2$$

$$\bar{P}^2 = R^2 + r^2 - 2rR \cos \psi + z^2$$

$$\cos \beta = h/\bar{P}$$

$$\cos \alpha = h_2/h$$

so that

$$\begin{aligned} u_z &= 2 \int_0^\infty \int_0^{2\pi} \tilde{\gamma} \frac{\cos \varphi_B}{4\pi} \frac{\cos \beta}{\bar{P}^2} \cos \alpha R d\psi dz \\ &= 2 \int_0^\infty \int_0^{2\pi} \tilde{\gamma} \frac{\cos \varphi_B}{4\pi} \frac{(h/\bar{P})(h_2/h)}{\bar{P}^2} \\ &= 2 \int_0^\infty \int_0^{2\pi} \tilde{\gamma} \frac{\cos \varphi_B}{4\pi} \frac{(1 - \bar{r} \cos \psi) d\psi d\bar{z}}{(1 + \bar{r}^2 - 2\bar{r} \cos \psi + \bar{z}^2)^{3/2}} \end{aligned}$$

where \bar{r} and \bar{z} are nondimensionalized by R . Now look at the \bar{z} -integration and define, $a = (1 + \bar{r}^2 - 2\bar{r} \cos \psi)$ so that

$$2 \int_0^\infty \frac{d\bar{z}}{(a + \bar{z}^2)^{3/2}} = \frac{2\bar{z}}{a(a + \bar{z}^2)^{1/2}} \Big|_0^\infty = \frac{2}{a\left(\frac{a}{\bar{z}^2} + 1\right)^{1/2}} \Big|_0^\infty = 2/a$$

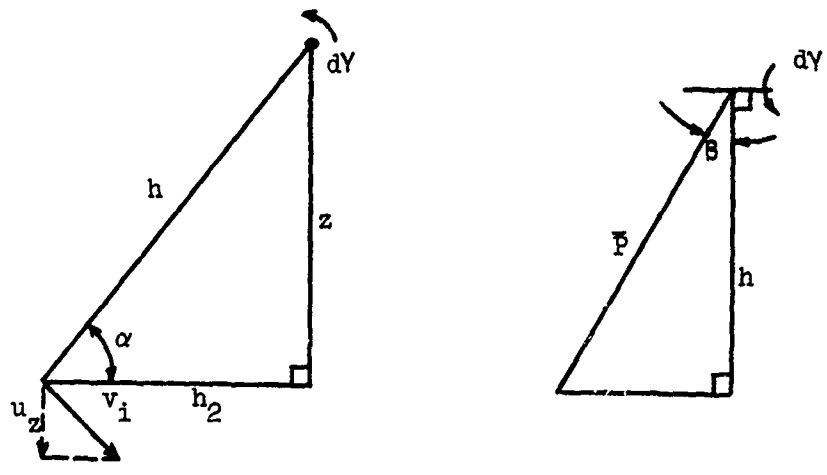
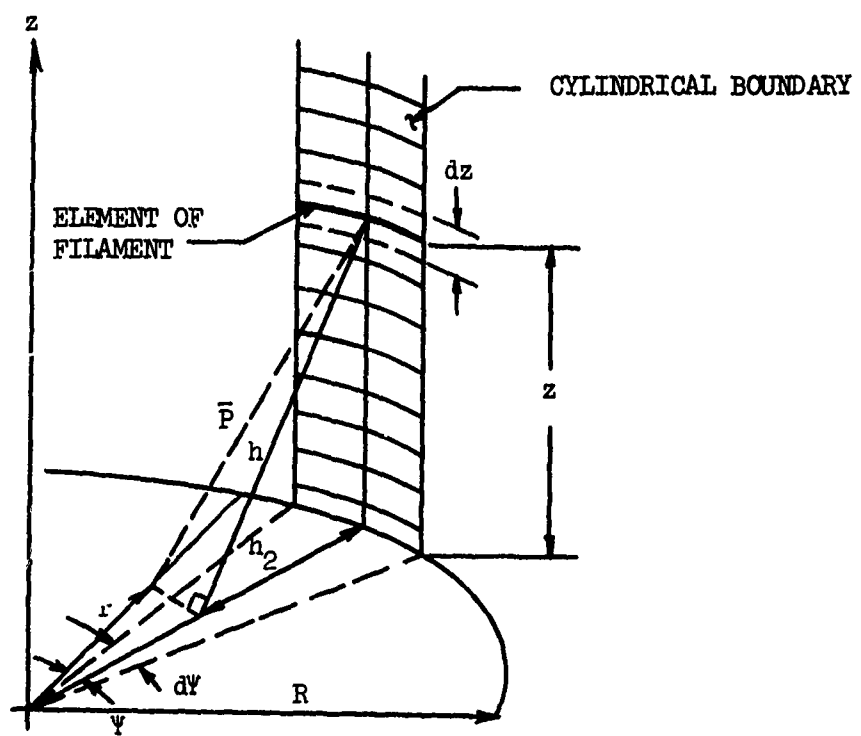


Figure 23. Geometry of the Ring-Element Sheet.

or

$$2 \int_0^{\infty} \frac{d\bar{z}}{(a + \bar{z}^2)^{3/2}} = 2/(1 + \bar{r}^2 - 2\bar{r} \cos \Psi) .$$

This integral may be found in reference 15.

Then u_z becomes

$$\begin{aligned} u_z &= \int_0^{2\pi} \tilde{\gamma} \frac{\cos \varphi_B}{2\pi} \frac{(1 - \bar{r} \cos \Psi)}{(1 + \bar{r}^2 - 2\bar{r} \cos \Psi)} d\Psi \\ &= \tilde{\gamma} \frac{\cos \varphi_B}{2\pi} \left\{ \int_0^{2\pi} \frac{d\Psi}{\bar{a} + \bar{b} \cos \Psi} - \bar{r} \int_0^{2\pi} \frac{\cos \Psi d\Psi}{\bar{a} + \bar{b} \cos \Psi} \right\} \end{aligned}$$

where $\bar{a} = 1 + \bar{r}^2$ and $\bar{b} = -2\bar{r}$. But

$$\frac{\cos \Psi}{\bar{a} + \bar{b} \cos \Psi} = \frac{1}{\bar{b}} \frac{\bar{b} \cos \Psi}{\bar{a} + \bar{b} \cos \Psi} = \frac{1}{\bar{b}} \left\{ 1 - \frac{\bar{a}}{\bar{a} + \bar{b} \cos \Psi} \right\} ,$$

so that

$$u_z = \tilde{\gamma} \frac{\cos \varphi_B}{2\pi} \left\{ \int_0^{2\pi} -\frac{\bar{r}}{\bar{b}} d\Psi + \left(1 + \frac{\bar{r}\bar{a}}{\bar{b}}\right) \int_0^{2\pi} \frac{d\Psi}{\bar{a} + \bar{b} \cos \Psi} \right\} .$$

Now

$$\int_0^{2\pi} \frac{d\Psi}{\bar{a} + \bar{b} \cos \Psi} = \frac{1}{\bar{a}} \int_0^{2\pi} \frac{d\Psi}{1 + \frac{\bar{b}}{\bar{a}} \cos \Psi} , \text{ which is of}$$

the form

$$\int_0^{2\pi} \frac{dx}{1 + a \cos x} , \text{ which yields from reference 15}$$

$$\int_0^{2\pi} \frac{dx}{1 + a \cos x} = \frac{2\pi}{(1 - a^2)^{1/2}} \text{ for } a^2 < 1 \text{ or, } \bar{r} < 1 \text{ (inside the wake).}$$

Then

$$\int_0^{2\pi} \frac{d\psi}{a + b \cos \psi} = \frac{1}{a} \frac{2\pi}{(1 - (\frac{b}{a})^2)^{1/2}} \text{ and}$$

$$\begin{aligned} u_z &= \tilde{\gamma} \frac{\cos \varphi_B}{2\pi} \left\{ 2\pi \left(\frac{-\bar{r}}{-2\bar{r}} \right) + \left(1 + \frac{\bar{r}a}{-2\bar{r}} \right) \left[\frac{1}{1 + \bar{r}^2} \left(2\pi / \left(1 - \left(\frac{-2\bar{r}}{1 + \bar{r}^2} \right)^2 \right)^{1/2} \right) \right] \right\} \\ &= \tilde{\gamma} \frac{\cos \varphi_B}{2\pi} \left\{ \pi + \frac{1}{2} (1 - \bar{r}^2) \left(\frac{2\pi}{(1 - \bar{r}^2)} \right) \right\} = \tilde{\gamma} \frac{\cos \varphi_B}{2\pi} (\pi + \pi) \end{aligned}$$

or

$$u_z = \tilde{\gamma} \cos \varphi_B .$$

Straight Line Element Sheet

From considerations of symmetry, the axial and radial velocities associated with the straight line element sheet are identically zero. The geometrical relationships necessary to calculate the angular velocity field of this sheet are shown in Fig. 24.

The velocity at a point due to the filament can be evaluated directly from reference 16 as

$$V = \frac{\Gamma}{2\pi h} , \text{ or } v_i = \tilde{\gamma} \frac{\sin \varphi_B dS}{2\pi \bar{r}} = \tilde{\gamma} \frac{\sin \varphi_B R d\psi}{2\pi \bar{r}}$$

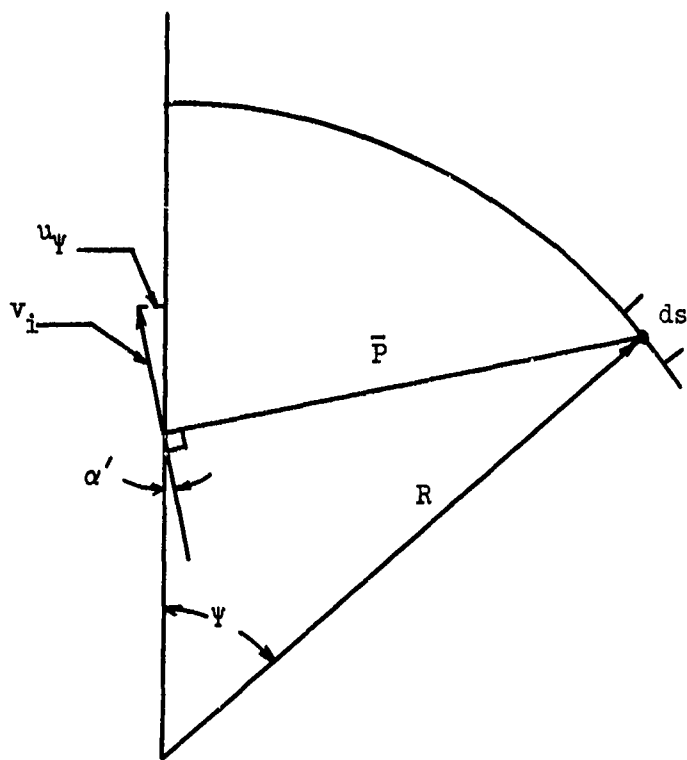


Figure 24. Geometry of the Straight-Line-Element Sheet.

From the figure $\bar{P}^2 = r^2 + R^2 - 2Rr \cos \Psi$

$$\sin \alpha = \frac{R^2 - r^2 - \bar{P}^2}{2r\bar{P}} .$$

Then

$$du_{\Psi} = \frac{1}{2\pi\bar{P}} \left(\frac{r^2 - R^2 + \bar{P}^2}{2r\bar{P}} \right) \tilde{\gamma} \sin \phi_B R d\Psi$$

so that

$$u_{\Psi} = \tilde{\gamma} \frac{\sin \phi_B}{4\pi} \left\{ \frac{2\pi}{\bar{r}} + \frac{\bar{r}^2 - 1}{\bar{r}} \int_0^{2\pi} \frac{d\Psi}{\bar{a} + \bar{b} \cos \Psi} \right\}$$

where $\bar{a} = 1 + \bar{r}^2$ and $\bar{b} = -2\bar{r}$. Again, the integral is of the form

$$\int_0^{2\pi} \frac{dx}{1 + a \cos x} = \frac{2\pi}{(1 - a^2)^{1/2}} , \quad a^2 < 1, \text{ or } \bar{r} < 1$$

so that

$$\begin{aligned} \frac{\bar{r}^2 - 1}{\bar{r}} \int_0^{2\pi} \frac{d\Psi}{(1 + \bar{r}^2 - 2\bar{r} \cos \Psi)} &= \frac{\bar{r}^2 - 1}{\bar{r}} \left(\frac{1}{1 + \bar{r}^2} \right) \left(2\pi / \left(1 - \left(\frac{2\bar{r}}{1 + \bar{r}^2} \right)^2 \right)^{1/2} \right) \\ &= \frac{\bar{r}^2 - 1}{\bar{r}} \left(2\pi / (1 - 2\bar{r}^2 + \bar{r}^2)^{1/2} \right) = \frac{\bar{r}^2 - 1}{\bar{r}} \left(\frac{2\pi}{1 - \bar{r}^2} \right) = \frac{-2\pi}{\bar{r}} \end{aligned}$$

Thus

$$u_{\Psi} = \tilde{\gamma} \frac{\sin \phi_B}{4\pi} \left\{ \frac{2\pi}{\bar{r}} - \frac{2\pi}{\bar{r}} \right\} = 0$$

Superposition

From the results for the two sheets the velocity field inside the wake due to the uniform boundary sheet is given by

$$\left. \begin{aligned} u_z &= \tilde{\gamma} \cos \varphi_B , \\ u_r &= 0 , \\ u_\psi &= 0 . \end{aligned} \right\} \quad (57)$$

APPENDIX III

CHECK CASES FOR THE NUMERICAL PROCEDURES

In developing the computer programs to handle the numerical calculations required for the solution of the wake vorticity distribution and the numerical calculation of thrust and power coefficients, a number of check cases were developed in order to obtain accuracy criteria for the various approximations required for a solution. The first of these checks involves the replacement of helical vortex sheets by a number of finite strength vortices.

The solution for the blade bound vorticity of an optimum free propeller is well-established and has been solved for a number of cases by Goldstein¹⁰. A numerical model similar to the one employed for the ducted fan was developed in order to check the accuracy of the integration of the velocity contributions of the finite strength helical vortex filaments and to establish a criterion for a minimum number of filaments required to adequately represent a helical vortex sheet. The conditions placed on the solution were as follows. The velocity normal to a helical sheet must be proportional to the local pitch of the sheet along a radial line on the sheet, and the vorticity of a single blade trailing sheet must sum to zero. The blade trailing sheets were divided into J strips, the strips replaced by filaments lying along the centerlines of the strips. Control points at which the normal velocity component was summed and specified were placed

at $(J-1)$ points midway between the filaments representing the sheet oriented at $\Psi = 0$. The arrangement for $J = 4$ is shown schematically in Fig. 25. The result is a set of 3 linear equations in 4 unknowns. The 4th equation is supplied by the zero net vorticity constraint. The system is illustrated as follows.

$$\begin{aligned} A_{1,1} \bar{v}_1 + A_{1,2} \bar{v}_2 + \dots + A_{1,J} \bar{v}_J &= \cos \varphi_{r_1} \\ &\vdots \\ A_{J-1,1} \bar{v}_1 + \dots + A_{J-1,J} \bar{v}_J &= \cos \varphi_{r_{J-1}} \\ \bar{v}_1 + \dots + \bar{v}_J &= 0 \end{aligned}$$

Where, for example, $A_{1,1}$ is the sum of the geometrical integrations of f_{ζ} for the inboard most filament of the b helical sheets. The system was calculated and solved for $\lambda = 1/2$ and $b = 2$ for values of $J = 4, 6, 8, 10, 12,$ and 18 . The results are shown in Fig. 26. Based on these results, it was decided that the ten filament system represents an adequate approximation to the vortex sheets. Greater numbers of filaments improve the solution very slowly and it was felt that the correspondingly larger computation times were not justified.

In order to provide a check on the calculation and integration of the functions of velocity in the ultimate wake, the integral for \bar{u}_z was set up in the manner described in Chapter V and evaluated for several cases of b at $\lambda = 1/2$. The result was compared to the exact value provided by equation (42) according to

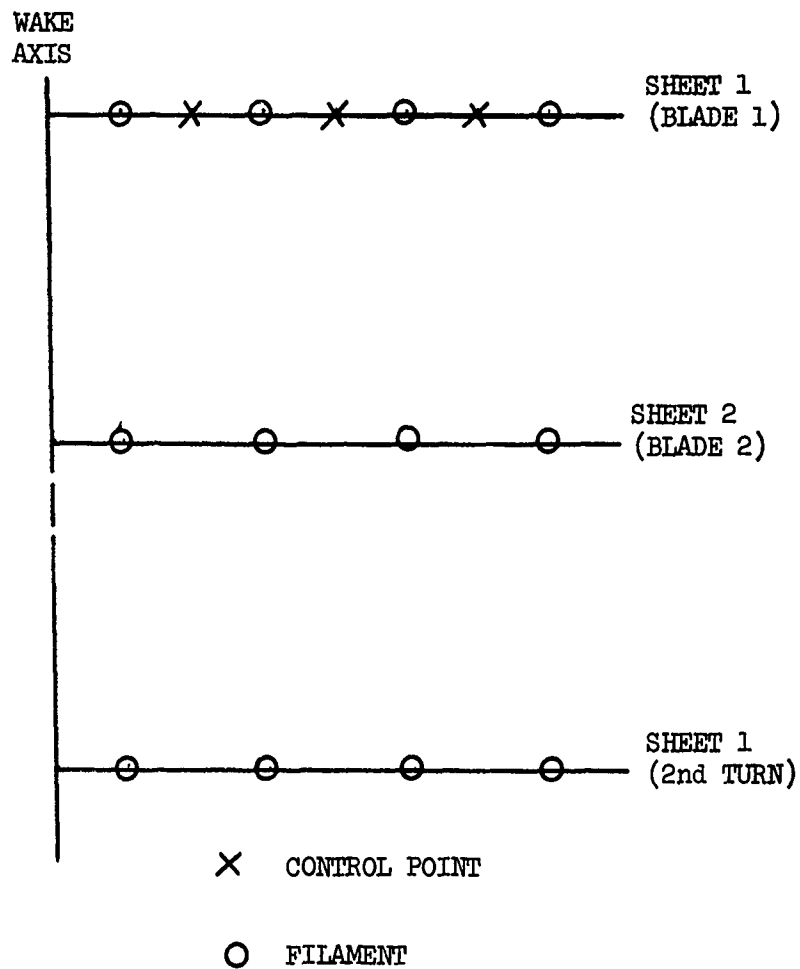


Figure 25. Schematic Diagram of the Arrangement of Filaments and Control Points in the Ultimate Wake of a Free Propeller.

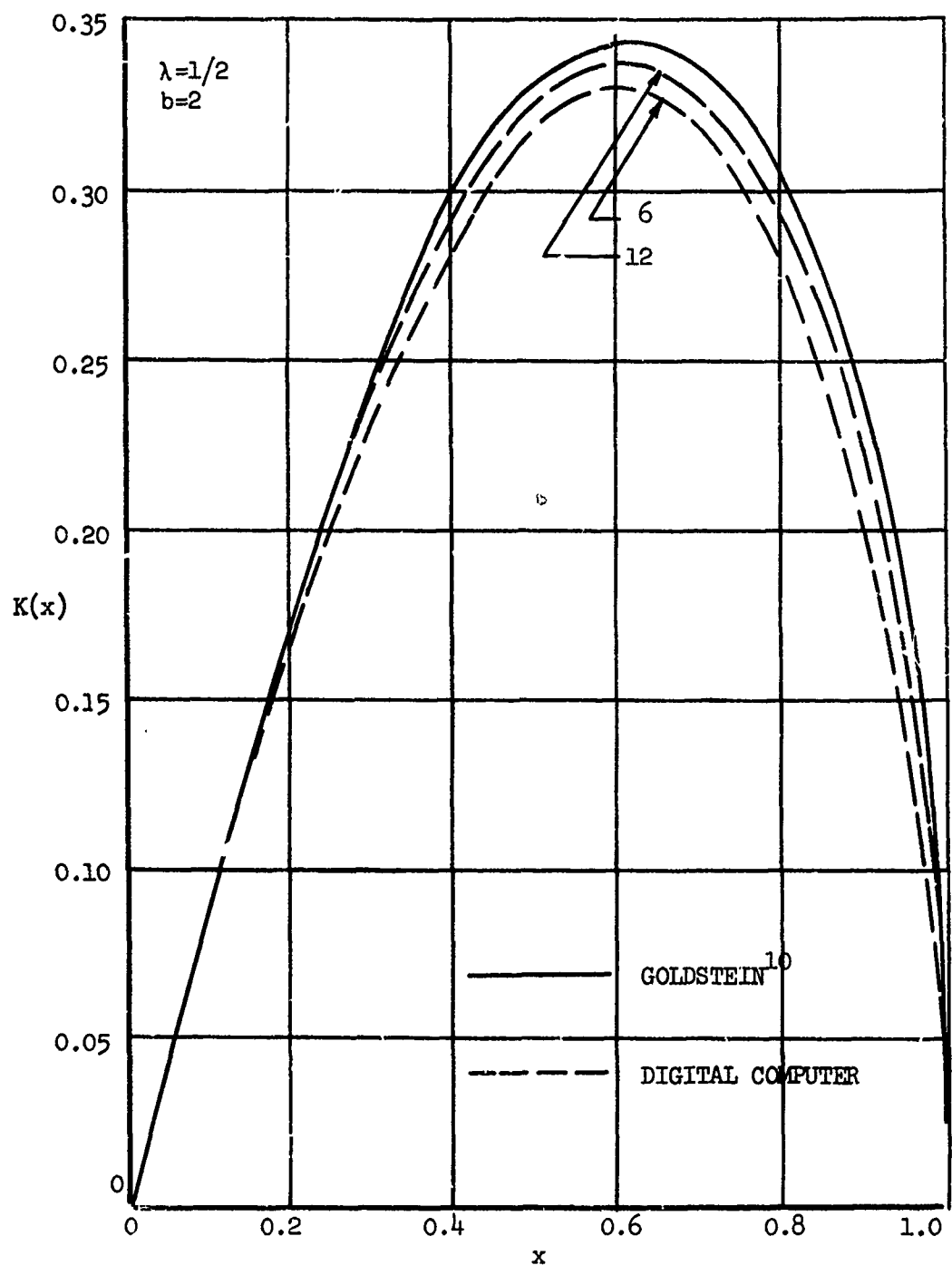


Figure 26. Comparison of Two Methods for Calculating the Blade Bound Vorticity for a Free Propeller.

$$\int_0^1 \int_0^1 \int_0^{2\pi} \bar{u}_z \bar{r} \, d\bar{r} \, d\bar{z} \, d\bar{\psi} / 2\pi = \frac{1}{2} [\mathcal{N} + u_{\xi_0}]$$

The comparisons are listed and reduced to a percent difference in Table 1, where

$$\text{percent difference} = \left| \frac{\int \bar{u}_z \, d \text{ vol}_{\text{exact}} - \int \bar{u}_z \, d \text{ vol}_{\text{numerical}}}{\int \bar{u}_z \, d \text{ vol}_{\text{exact}}} \right|$$

As the table shows, the difference in all cases was of the order of 1 percent or less so that the calculation and integration methods were considered to be sufficiently accurate.

As an additional check on the volume integrations, the values of ϵ_r , ϵ_ψ and ϵ_z were calculated for $\lambda = 1$ and $b = 2, 4, 8,$ and 12 . These results are compared to the values for an infinite blade fan. As can be seen in Fig. 27 the results show satisfactory convergence for increasing blade number.

Table 1. Accuracy of the Wake Integrations

b	$\int \bar{u}_z \, d \text{ vol}$ numerical	$\int \bar{u}_z \, d \text{ vol}$ exact	Difference	% Difference
2	.520	.526	.006	1.14
3	.552	.557	.005	0.90
4	.569	.572	.003	0.53
8	.589	.590	.001	0.17

$$\lambda = 1/2, \bar{w} = 0$$

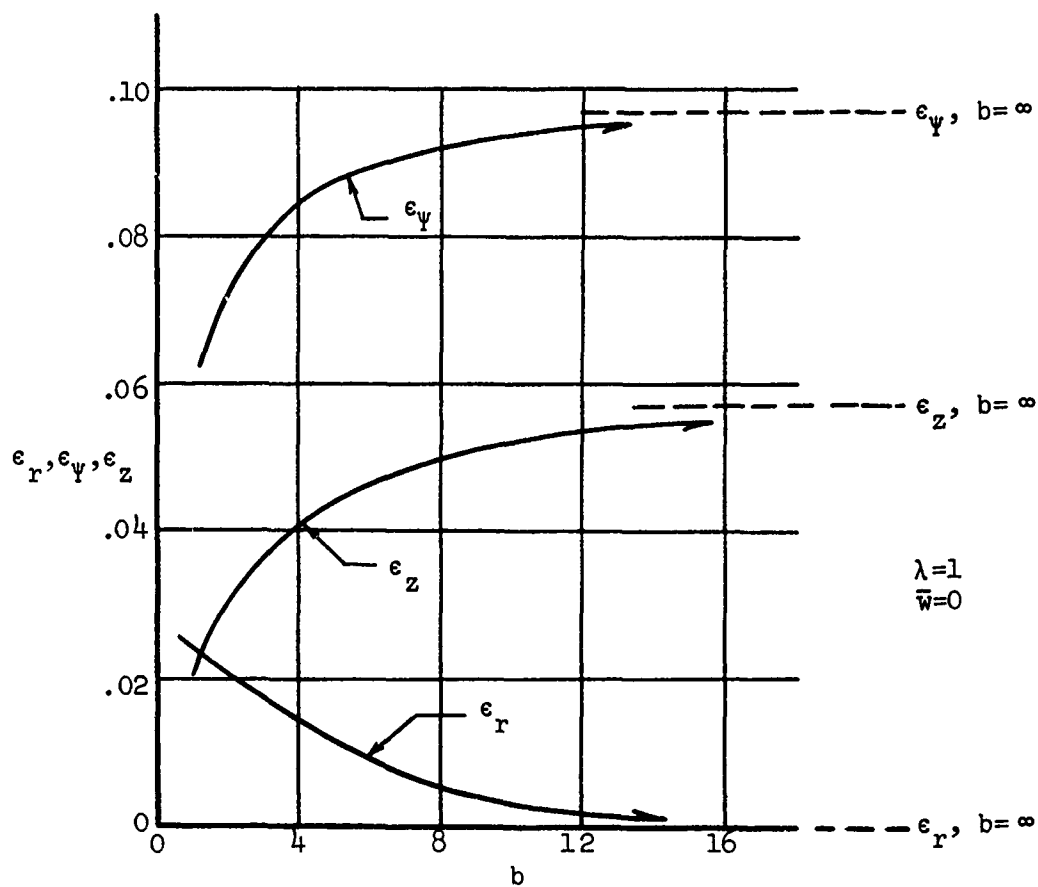


Figure 27. Convergence of the Wake Integration to the Exact Results¹³ for the Infinite Blade Case.

APPENDIX IV

PERFORMANCE AND DESIGN PARAMETERS

$\lambda = 1/8 \quad b = 2$						
X	$K_0(x)$	\bar{W}/λ	C_T	C_P	C_{TP}/C_T	G
0	0	0	0	0	1.0	1.0
		.05	.000719	.0000877	.9767	.9754
0.1	.4413	.10	.001435	.0001705	.9532	.9507
		.15	.002148	.0002486	.9294	.9260
0.2	.6920	.20	.002858	.0003219	.9052	.9012
		.25	.003567	.0003904	.8809	.8765
0.3	.8208	.30	.004275	.0004544	.8563	.8517
		.35	.004982	.0005317	.8315	.8268
0.4	.8894	.40	.005689	.0005685	.8064	.8020
		.45	.006396	.0006187	.7812	.7771
0.5	.9277	.50	.007105	.0006643	.7559	.7522
		.55	.007815	.0007058	.7304	.7272
0.6	.9501	.60	.008527	.0007427	.7047	.7023
		.65	.009242	.0007751	.6790	.6773
0.7	.9637	.70	.009961	.0008032	.6532	.6523
		.75	.01068	.0008270	.6273	.6273
0.8	.9723	.80	.01141	.0008464	.6013	.6022
		.85	.01214	.0008614	.5753	.5772
0.9	.9773	.90	.01288	.0008722	.5493	.5515
		.95	.01362	.0008786	.5233	.5270
1.0	.9795	1.0	.01437	.0008808	.4972	.5019

$\lambda = 1/8 \quad b = 3$						
x	$K_0(x)$	\bar{w}/λ	C_T	C_D	C_{Tp}/C_T	G
0	0	0	0	0	1.0	1.0
		.05	.000723	.0000881	.9765	
0.1	.4250	.10	.001443	.0001714	.9527	
		.15	.002160	.0002498	.9287	
0.2	.7006	.20	.002875	.0003234	.9045	
		.25	.003588	.0003923	.8800	
0.3	.8341	.30	.004300	.0004566	.8553	
		.35	.005012	.0005162	.8309	
0.4	.9001	.40	.005724	.0005712	.8054	
		.45	.006436	.0006217	.7802	
0.5	.9352	.50	.007149	.0006677	.7548	
		.55	.007864	.0007092	.7293	
0.6	.9548	.60	.008581	.0007463	.7037	
		.65	.009300	.0007789	.6780	
0.7	.9670	.70	.01002	.0008071	.6523	
		.75	.01075	.0008310	.6264	
0.8	.9745	.80	.01148	.0008505	.6006	
		.85	.01221	.0008656	.5747	
0.9	.9796	.90	.01295	.0008764	.5487	
		.95	.01369	.0008829	.5228	
1.0	.9818	1.0	.01444	.0008850	.4969	

$\lambda = 1/8 \quad b = 4$						
x	$K_0(x)$	\bar{w}/λ	C_T	C_P	C_{TP}/C_T	G
0	0	0	0	0	1.0	1.0
		.05	.000724	.0000883	.9764	
0.1	.4130	.10	.001445	.0001717	.9526	
		.15	.002164	.0002502	.9285	
0.2	.7063	.20	.002881	.0003240	.9042	
		.25	.003596	.0003930	.8796	
0.3	.8411	.30	.004310	.0004574	.8549	
		.35	.005023	.0005171	.8300	
0.4	.9050	.40	.005737	.0005723	.8049	
		.45	.006451	.0006289	.7797	
0.5	.9378	.50	.007166	.0006689	.7544	
		.55	.007883	.0007105	.7289	
0.6	.9561	.60	.008601	.0007476	.7033	
		.65	.009322	.0007803	.6777	
0.7	.9678	.70	.01005	.0008084	.6519	
		.75	.01077	.0008324	.6261	
0.8	.9752	.80	.01150	.0008520	.6003	
		.85	.01224	.0008671	.5744	
0.9	.9801	.90	.01298	.0008780	.5485	
		.95	.01372	.0008845	.5226	
1.0	.9828	1.0	.01447	.0008866	.4968	

$\lambda = 1/4 \quad b = 2$						
x	$K_0(x)$	\bar{w}/λ	C_T	C_P	C_{TP}/C_T	G
0	0	0	0	0	1.0	1.0
		.05	.002453	000599	.9802	.9764
0.1	.2420	.10	.004874	001161	.9596	.9527
		.15	.007266	001687	.9382	.9288
0.2	.4407	.20	.009636	002177	.9160	.9048
		.25	.01199	002633	.8931	.8807
0.3	.5866	.30	.01433	003055	.8695	.8565
		.35	.01667	003445	.8453	.8321
0.4	.6899	.40	.01901	003803	.8204	.8077
		.45	.02135	004129	.7949	.7831
0.5	.7626	.50	.02370	004425	.7689	.7585
		.55	.02607	004691	.7425	.7337
0.6	.8139	.60	.02846	004927	.7156	.7089
		.65	.03088	005134	.6884	.6839
0.7	.8500	.70	.03333	005313	.6609	.6589
		.75	.03582	005464	.6331	.6339
0.8	.8747	.80	.03835	005586	.6052	.6087
		.85	.04094	005682	.5771	.5835
0.9	.8899	.90	.04357	005750	.5490	.5582
		.95	.04627	005790	.5208	.5329
1.0	.8958	1.0	.04903	.005804	.4927	.5076

$\lambda = 1/4 \quad b = 3$						
x	$K_0(x)$	\bar{w}/λ	C_T	C_P	C_{TP}/C_T	G
0	0	0	0	0	1.0	1.0
		.05	.002500	.000610	.9794	
0.1	.2020	.10	.004971	.001182	.9580	
		.15	.007416	.001718	.9360	
0.2	.4195	.20	.009842	.002217	.9133	
		.25	.01225	.002682	.8900	
0.3	.5839	.30	.01465	.003112	.8661	
		.35	.01705	.003509	.8416	
0.4	.6989	.40	.01944	.003874	.8166	
		.45	.02185	.004207	.7911	
0.5	.7780	.50	.02426	.004508	.7652	
		.55	.02668	.004779	.7388	
0.6	.8324	.60	.02913	.005020	.7121	
		.65	.03160	.005232	.6852	
0.7	.8696	.70	.03410	.005414	.6579	
		.75	.03664	.005568	.6305	
0.8	.8948	.80	.03922	.005693	.6029	
		.85	.04184	.005790	.5751	
0.9	.9104	.90	.04451	.005860	.5474	
		.95	.04724	.005901	.5196	
1.0	.9170	1.0	.05002	.005915	.4919	

$\lambda = 1/4 \quad b = 4$						
x	$K_0(x)$	\bar{w}/λ	C_T	C_P	C_{TP}/C_T	G
0	0	0	0	0	1.0	1.0
		.05	.002519	.000614	.9790	
0.1	.1783	.10	.005010	.001191	.9573	
		.15	.007478	.001730	.9350	
0.2	.4084	.20	.009927	.002233	.9121	
		.25	.01236	.002701	.8886	
0.3	.5838	.30	.01479	.003135	.8645	
		.35	.01721	.003535	.8399	
0.4	.7045	.40	.01963	.003903	.8149	
		.45	.02205	.004238	.7894	
0.5	.7856	.50	.02449	.004542	.7634	
		.55	.02694	.004815	.7371	
0.6	.8402	.60	.02941	.005058	.7105	
		.65	.03191	.005271	.6836	
0.7	.8772	.70	.03443	.005455	.6565	
		.75	.03698	.005610	.6292	
0.8	.9024	.80	.03958	.005736	.6017	
		.85	.04222	.005834	.5742	
0.9	.9185	.90	.04490	.005904	.5466	
		.95	.04764	.005946	.5190	
1.0	.9258	1.0	.05044	.005960	.4914	

$\lambda = 1/4 \quad b = 6$						
x	$K_0(x)$	\bar{w}/λ	C_T	C_P	C_{TP}/C_T	G
0	0	0	0	0	1.0	1.0
		.05	.002534	.000618	.9787	
0.1	.1492	.10	.005042	.001198	.9567	
		.15	.007527	.001740	.9341	
0.2	.4007	.20	.009995	.002246	.9110	
		.25	.01245	.002717	.8874	
0.3	.5905	.30	.01490	.003154	.8632	
		.35	.01734	.003556	.8385	
0.4	.7079	.40	.01978	.003926	.8134	
		.45	.02223	.004263	.7879	
0.5	.7890	.50	.02468	.004569	.7619	
		.55	.02715	.004844	.7357	
0.6	.8508	.60	.02964	.005089	.7091	
		.65	.03215	.005303	.6823	
0.7	.8851	.70	.03469	.005488	.6553	
		.75	.03727	.005644	.6281	
0.8	.9026	.80	.03988	.005771	.6008	
		.85	.04253	.005870	.5733	
0.9	.9235	.90	.04523	.005940	.5459	
		.95	.04797	.005982	.5184	
1.0	.9381	1.0	.05078	.005996	.4910	

$\lambda = 3/8 \quad b = 2$						
x	$K_0(x)$	\bar{w}/λ	C_T	C_P	C_{TP}/C_T	G
0	0	0	0	0	1.0	1.0
		.05	.004320	.001656	.9832	.9779
0.1	.1615	.10	.008944	.003198	.9652	.9556
		.15	.01339	.004629	.9461	.9330
0.2	.3078	.20	.01757	.005955	.9257	.9102
		.25	.02180	.007178	.9043	.8871
0.3	.4307	.30	.02590	.008303	.8816	.8638
		.35	.03018	.009333	.8579	.8402
0.4	.5292	.40	.03436	.01027	.8331	.8164
		.45	.03857	.01112	.8073	.7929
0.5	.6059	.50	.04281	.01189	.7806	.7682
		.55	.04710	.01257	.7530	.7438
0.6	.6644	.60	.05147	.01318	.7247	.7171
		.65	.05593	.01371	.6957	.6943
0.7	.7078	.70	.06050	.01416	.6662	.6693
		.75	.06520	.01454	.6362	.6442
0.8	.7384	.80	.07005	.01485	.6058	.6189
		.85	.07506	.01509	.5752	.5935
0.9	.7575	.90	.08027	.01526	.5446	.5679
		.95	.08568	.01536	.5139	.5422
1.0	.7649	1.0	.09132	.01539	.4833	.5162

$\lambda = 3/8 \quad b = 3$						
x	$K_0(x)$	\bar{w}/λ	C_T	C_P	C_{TP}/C_T	G
0	0	0	0	0	1.0	1.0
		.05	.004692	.001719	.9827	
0.1	.1223	.10	.009795	.003321	.9643	
		.15	.01382	.004808	.9448	
0.2	.2775	.20	.01827	.006186	.9242	
		.25	.02268	.007459	.9025	
0.3	.4172	.30	.02706	.008629	.8798	
		.35	.03142	.009701	.8560	
0.4	.5317	.40	.03578	.01068	.8312	
		.45	.04016	.01157	.8055	
0.5	.6214	.50	.04457	.01236	.7790	
		.55	.04903	.01308	.7516	
0.6	.6898	.60	.05356	.01371	.7236	
		.65	.05818	.01426	.6949	
0.7	.7408	.70	.06291	.01473	.6657	
		.75	.06775	.01513	.6361	
0.8	.7770	.80	.07274	.01545	.6062	
		.85	.07789	.01570	.5761	
0.9	.8002	.90	.08322	.01588	.5459	
		.95	.08874	.01598	.5156	
1.0	.8097	1.0	.09448	.01602	.4855	

$\lambda = 3/8 \quad b = 4$						
x	$K_0(x)$	\bar{w}/λ	C_T	C_P	C_{TP}/C_T	G
0	0	0	0	0	1.0	1.0
		.05	.009773	.001747	.9819	
0.1	.1000	.10	.009459	.003375	.9629	
		.15	.01407	.004987	.9428	
0.2	.2589	.20	.01862	.006288	.9216	
		.25	.02313	.007582	.8905	
0.3	.4080	.30	.02760	.008772	.8764	
		.35	.03206	.009864	.8524	
0.4	.5312	.40	.03653	.01086	.8275	
		.45	.04100	.01176	.8018	
0.5	.6276	.50	.04552	.01257	.7753	
		.55	.05008	.01330	.7480	
0.6	.7010	.60	.05470	.01394	.7202	
		.65	.05942	.01450	.6917	
0.7	.7556	.70	.06423	.01499	.6629	
		.75	.06916	.01539	.6336	
0.8	.7948	.80	.07422	.01572	.6040	
		.85	.07944	.01597	.5743	
0.9	.8203	.90	.08482	.01615	.5444	
		.95	.09040	.01626	.5146	
1.0	.8344	1.0	.09618	.01630	.4848	

$\lambda = \frac{3}{8} \quad b = 6$						
x	$K_0(x)$	\bar{w}/λ	C_T	C_P	C_{TP}/C_T	G
0	0	0	0	0	1.0	1.0
		.05	.004837	.001770	.9816	
0.1	.07953	.10	.009589	.003419	.9623	
		.15	.01427	.004952	.9419	
0.2	.2409	.20	.01889	.006372	.9206	
		.25	.02346	.007684	.8983	
0.3	.3991	.30	.02801	.008892	.8751	
		.35	.03254	.01000	.8511	
0.4	.5308	.40	.03708	.01101	.8261	
		.45	.04163	.01192	.8009	
0.5	.6331	.50	.04621	.01275	.7732	
		.55	.05084	.01349	.7468	
0.6	.7103	.60	.05553	.01414	.7190	
		.65	.06031	.01471	.6907	
0.7	.7676	.70	.06518	.01520	.6620	
		.75	.07017	.01561	.6329	
0.8	.8093	.80	.07529	.01594	.6039	
		.85	.08055	.01620	.5740	
0.9	.8375	.90	.08599	.01638	.5441	
		.95	.09160	.01649	.5147	
1.0	.8512	1.0	.09742	.01653	.4852	

$\lambda = 1/2 \quad b = 2$						
x	$K_0(x)$	\bar{w}/λ	C_T	C_P	C_{TP}/C_T	G
0	0	0	0	0	1.0	1.0
		.05	.00648	.003162	.9854	.9798
0.1	.1172	.10	.01279	.006077	.9671	.9592
		.15	.01896	.008754	.9520	.9382
0.2	.2274	.20	.02500	.01120	.9332	.9168
		.25	.03096	.01343	.9128	.8950
0.3	.3259	.30	.03685	.01545	.8910	.8729
		.35	.04272	.01728	.8678	.8503
0.4	.4090	.40	.04859	.01891	.8430	.8274
		.45	.05451	.02036	.8169	.8091
0.5	.4780	.50	.06050	.02165	.7895	.7805
		.55	.06661	.02277	.7608	.7565
0.6	.5332	.60	.07287	.02374	.7309	.7322
		.65	.07933	.02456	.7001	.7075
0.7	.5757	.70	.08603	.02525	.6681	.6826
		.75	.09301	.02581	.6360	.6574
0.8	.6067	.80	.1003	.02625	.6031	.6319
		.85	.1080	.02657	.5699	.6062
0.9	.6266	.90	.1161	.02678	.5366	.5803
		.95	.1247	.02688	.5032	.5542
1.0	.6319	1.0	.1338	.02688	.4701	.5279

$\lambda = 1/2 \quad b = 3$						
x	$K_0(x)$	\bar{w}/λ	C_T	C_D	C_{TP}/C_T	G
0	0	0	0	0	1.0	1.0
		.05	.00686	.003342	.9857	
0.1	.08357	.10	.01353	.006420	.9700	
		.15	.02004	.009246	.9528	
0.2	.1979	.20	.02643	.01183	.9342	
		.25	.03272	.01418	.9142	
0.3	.3099	.30	.03894	.01632	.8927	
		.35	.04513	.01825	.8697	
0.4	.4095	.40	.05132	.01998	.8452	
		.45	.05754	.02153	.8194	
0.5	.4935	.50	.06384	.02290	.7923	
		.55	.07025	.02410	.7640	
0.6	.5617	.60	.07681	.02515	.7345	
		.65	.08356	.02604	.7041	
0.7	.6150	.70	.09054	.02679	.6728	
		.75	.09780	.02741	.6408	
0.8	.6673	.80	.1054	.02790	.6084	
		.85	.1133	.02827	.5755	
0.9	.6801	.90	.1217	.02852	.5426	
		.95	.1305	.02865	.5096	
1.0	.6912	1.0	.1398	.02867	.4768	

$\lambda = 1/2 \quad b = 4$						
x	$K_0(x)$	\bar{w}/λ	C_T	C_P	C_{TP}/C_T	G
0	0	0	0	0	1.0	1.0
		.05	.00705	.003938	.9859	
0.1	.0648	.10	.01392	.006606	.9699	
		.15	.02063	.009516	.9520	
0.2	.1791	.20	.02722	.01218	.9332	
		.25	.03370	.01461	.9130	
0.3	.2979	.30	.04012	.01682	.8914	
		.35	.04650	.01882	.8684	
0.4	.4065	.40	.05288	.02062	.8490	
		.45	.05929	.02223	.8183	
0.5	.4993	.50	.06578	.02365	.7913	
		.55	.07237	.02491	.7631	
0.6	.5754	.60	.07911	.02601	.7339	
		.65	.08609	.02695	.7037	
0.7	.6354	.70	.09319	.02775	.6727	
		.75	.1006	.02841	.6411	
0.8	.6803	.80	.1083	.02894	.6090	
		.85	.1164	.02933	.5765	
0.9	.7102	.90	.1249	.02961	.5439	
		.95	.1339	.02976	.5113	
1.0	.7241	1.0	.1433	.02979	.4788	

$\lambda = 1/2 \quad b = 6$						
x	$K_0(x)$	\bar{w}/λ	C_T	C_P	C_{TP}/C_T	G
0	0	0	0	0	1.0	1.0
		.05	.00720	.003509	.9897	
0.1	.0482	.10	.01422	.006747	.9682	
		.15	.02109	.009725	.9504	
0.2	.1588	.20	.02784	.01246	.9312	
		.25	.03449	.01495	.9106	
0.3	.2826	.30	.04107	.01722	.8888	
		.35	.04762	.01928	.8656	
0.4	.3992	.40	.05417	.02114	.8411	
		.45	.06075	.02280	.8153	
0.5	.5003	.50	.06740	.02429	.7884	
		.55	.07416	.02560	.7604	
0.6	.5839	.60	.08106	.02674	.7314	
		.65	.0884	.02773	.7015	
0.7	.6505	.70	.09544	.02857	.6708	
		.75	.1030	.02926	.6396	
0.8	.7014	.80	.1109	.02982	.6078	
		.85	.1191	.03025	.5758	
0.9	.7366	.90	.1277	.03054	.5435	
		.95	.1367	.03071	.5113	
1.0	.7542	1.0	.1462	.03076	.4792	

$\lambda = 1/2 \quad b = 8$						
x	$K_0(x)$	\bar{w}/λ	C_T	C_P	C_{TP}/C_T	G
0	0	0	0	0	1.0	1.0
		.05	.00729	.003550	.9844	
0.1	.0425	.10	.01440	.006829	.9675	
		.15	.02136	.009849	.9493	
0.2	.1506	.20	.02820	.01262	.9299	
		.25	.03494	.01516	.9092	
0.3	.2764	.30	.04162	.01747	.8871	
		.35	.04827	.01956	.8638	
0.4	.3968	.40	.05492	.02146	.8393	
		.45	.06160	.02316	.8135	
0.5	.5016	.50	.06835	.02467	.7866	
		.55	.07520	.02602	.7587	
0.6	.5884	.60	.08219	.02719	.7298	
		.65	.08936	.02821	.7000	
0.7	.6579	.70	.09675	.02907	.7696	
		.75	.1044	.02979	.6385	
0.8	.7119	.80	.1123	.03037	.6070	
		.85	.1206	.03082	.5751	
0.9	.7507	.90	.1293	.03113	.5432	
		.95	.1384	.03131	.5112	
1.0	.7720	1.0	.1479	.03136	.4793	

$\lambda = 5/8 \quad b = 2$						
x	$K_0(x)$	\bar{w}/λ	C_T	C_P	C_{TP}/C_T	G
0	0	0	0	0	1.0	1.0
		.05	.008111	.004943	.9861	.9818
0.1	.00808	.10	.01599	.009487	.9709	.9630
		.15	.02366	.01365	.9542	.9438
0.2	.1723	.20	.03118	.01745	.9360	.9240
		.25	.03856	.02090	.9162	.9037
0.3	.2425	.30	.04586	.02402	.8947	.8828
		.35	.05313	.02683	.8715	.8615
0.4	.3178	.40	.06091	.02935	.8466	.8396
		.45	.06776	.03159	.8201	.8172
0.5	.3762	.50	.07525	.03358	.7918	.7913
		.55	.08292	.03532	.7621	.7709
0.6	.4244	.60	.09085	.03684	.7308	.7470
		.65	.09911	.03814	.6983	.7227
0.7	.4627	.70	.1078	.03923	.6646	.6979
		.75	.1169	.04014	.6301	.6727
0.8	.4912	.80	.1267	.04087	.5948	.6470
		.85	.1370	.04143	.5592	.6210
0.9	.5095	.90	.1482	.04183	.5239	.5947
		.95	.1602	.04206	.4877	.5681
1.0	.5172	1.0	.1731	.04214	.4523	.5411

$\lambda = 5/8 \quad b = 3$						
x	$K_0(x)$	\bar{w}/λ	C_T	C_P	C_{TP}/C_T	G
0	0	0	0	0	1.0	1.0
		.05	.008731	.005331	.9878	
0.1	.06086	.10	.01718	.01023	.9742	
		.15	.02540	.01473	.9590	
0.2	.1477	.20	.03341	.01883	.9421	
		.25	.04128	.02257	.9235	
0.3	.2366	.30	.04903	.02595	.9032	
		.35	.05673	.02900	.8810	
0.4	.3195	.40	.06443	.03173	.8569	
		.45	.07219	.03417	.8311	
0.5	.3926	.50	.08007	.03633	.8035	
		.55	.08814	.03822	.7742	
0.6	.4542	.60	.09646	.03987	.7439	
		.65	.1051	.04129	.7111	
0.7	.5040	.70	.1142	.04249	.6777	
		.75	.1237	.04348	.6433	
0.8	.5417	.80	.1338	.04428	.6082	
		.85	.1446	.04489	.5726	
0.9	.5668	.90	.1561	.04532	.5367	
		.95	.1685	.04557	.5009	
1.0	.5774	1.0	.1817	.04566	.4655	

$\lambda = 5/8 \quad b = 4$						
x	$K_0(x)$	\bar{w}/λ	C_T	C_P	C_{TP}/C_T	G
0	0	0	0	0	1.0	1.0
		.05	.002045	.005525	.9881	
0.1	.04530	.10	.01280	.01061	9746	
		.15	.02631	.01527	9596	
0.2	.1301	.20	.03461	.01953	9429	
		.25	.04274	.02341	9245	
0.3	.2239	.30	.05077	.02692	9044	
		.35	.05873	.03009	8824	
0.4	.3148	.40	.06669	.03294	8585	
		.45	.07470	.03547	8329	
0.5	.3968	.50	.08283	.03772	8055	
		.55	.09114	.03969	7765	
0.6	.4672	.60	.09970	.04141	7460	
		.65	.1086	.04289	7140	
0.7	.5249	.70	.1179	.0444	6809	
		.75	.1277	.04518	6468	
0.8	.5692	.80	.1380	.04601	6119	
		.85	.1490	.04665	5766	
0.9	.5994	.90	.1607	.04710	5410	
		.95	.1732	.04737	5054	
1.0	.6128	1.0	.1867	.04746	4701	

$\lambda = 5/8 \quad b = 6$						
x	$K_0(x)$	\bar{w}/λ	C_T	C_P	C_{TP}/C_T	G
0	0	0	0	0	1.0	1.0
		.05	.002357	.005703	.9858	
0.1	.03219	.10	.01846	.01095	.9701	
		.15	.02733	.01577	.9535	
0.2	.1117	.20	.03603	.02018	.9352	
		.25	.04458	.02419	.9154	
0.3	.2080	.30	.05303	.02783	.8941	
		.35	.06143	.03111	.8713	
0.4	.3058	.40	.06983	.03406	.8469	
		.45	.07829	.03669	.8210	
0.5	.3967	.50	.08686	.03902	.7936	
		.55	.09561	.04107	.7648	
0.6	.4765	.60	.1046	.04286	.7347	
		.65	.1139	.04439	.7035	
0.7	.5434	.70	.1236	.04570	.6713	
		.75	.1337	.04677	.6382	
0.8	.5962	.80	.1444	.04764	.6045	
		.85	.1557	.04831	.5703	
0.9	.6334	.90	.1676	.04878	.5360	
		.95	.1804	.04906	.5016	
1.0	.6512	1.0	.1941	.04915	.4648	

$\lambda = 5/8 b = 8$						
x	$K_0(x)$	\bar{w}/λ	C_T	C_F	C_{TP}/C_T	G
0	0	0	0	0	1.0	1.0
		.05	0	.005780	.9874	
0.1	.02782	.10	.009467	.01110	.9733	
		.15	.02758	.01599	.9577	
0.2	.1036	.20	.03631	.02046	.9405	
		.25	.07487	.02452	.9218	
0.3	.1999	.30	.05332	.02822	.9013	
		.35	.06171	.03155	.8791	
0.4	.3003	.40	.07010	.03454	.8553	
		.45	.07853	.03721	.8297	
0.5	.3950	.50	.08707	.03958	.8026	
		.55	.09580	.04167	.7739	
0.6	.4790	.60	.1048	.04348	.7437	
		.65	.1140	.04503	.7123	
0.7	.5503	.70	.1237	.04637	.6798	
		.75	.1339	.04747	.6464	
0.8	.6078	.80	.1445	.04835	.6122	
		.85	.1558	.04903	.5776	
0.9	.6498	.90	.1679	.04950	.5428	
		.95	.1807	.04979	.5079	
1.0	.6711	1.0	.1944	.04988	.4732	

$\lambda = 3/4 \quad b = 2$						
x	$K_0(x)$	\bar{w}/λ	C_T	C_P	C_{TP}/C_T	G
0	0	0	0	0	1.0	1.0
		.05	.00944	.00689	.9867	.9837
0.1	.0677	.10	.01859	.01319	.9720	.9668
		.15	.02749	.01893	.9559	.9493
0.2	.1340	.20	.03619	.02414	.9382	.9312
		.25	.04473	.02883	.9188	.9125
0.3	.1963	.30	.05316	.03305	.8977	.8931
		.35	.06156	.03681	.8777	.8730
0.4	.2516	.40	.06997	.04015	.8498	.8523
		.45	.07849	.04309	.8229	.8309
0.5	.2995	.50	.08719	.04567	.7940	.8089
		.55	.09616	.04790	.7633	.7862
0.6	.3406	.60	.1055	.04982	.7308	.7628
		.65	.1153	.05145	.6967	.7389
0.7	.3746	.70	.1258	.05280	.6611	.7143
		.75	.1369	.05392	.6244	.6891
0.8	.4002	.80	.1480	.05480	.5869	.6634
		.85	.1620	.05547	.5488	.6371
0.9	.4161	.90	.1762	.05594	.5106	.6103
		.95	.1918	.05622	.4725	.5832
1.0	.4227	1.0	.2088	.05631	.4350	.5556

$\lambda = 3/4 \quad b = 3$						
x	$K_0(x)$	\bar{w}/λ	C_T	C_P	C_{TP}/C_T	G
0	0	0	0	0	1.0	1.0
		.05	.01030	.00754	.9895	
0.1	.0463	.10	.02023	.01494	.9776	
		.15	.02984	.02074	.9640	
0.2	.1190	.20	.03919	.02645	.9486	
		.25	.04832	.03161	.9313	
0.3	.1853	.30	.05731	.03624	.9121	
		.35	.06621	.04038	.8907	
0.4	.2536	.40	.07512	.04106	.8672	
		.45	.08410	.04731	.8414	
0.5	.3156	.50	.09326	.05015	.8135	
		.55	.1027	.05262	.7835	
0.6	.3694	.60	.1125	.05474	.7514	
		.65	.1228	.05655	.7176	
0.7	.4138	.70	.1337	.05806	.6821	
		.75	.1453	.05929	.6453	
0.8	.4482	.80	.1578	.06028	.6075	
		.85	.1713	.06102	.5690	
0.9	.4715	.90	.1861	.06155	.5303	
		.95	.2021	.06186	.4917	
1.0	.4816	1.0	.2196	.06196	.4535	

$\lambda = 3/4 \quad b = 4$						
x	$K_0(x)$	\bar{w}/λ	C_T	C_P	C_{TP}/C_T	G
0	0	0	0	0	1.0	1.0
		.05	.01075	.00788	.9902	
0.1	.0321	.10	.02111	.01510	.9788	
		.15	.03113	.02168	.9658	
0.2	.1016	.20	.04085	.02766	.9510	
		.25	.05035	.03306	.9343	
0.3	.1704	.30	.05969	.03792	.9156	
		.35	.06893	.04276	.8947	
0.4	.2531	.40	.07816	.04612	.8716	
		.45	.08715	.04953	.8462	
0.5	.3160	.50	.09692	.05252	.8187	
		.55	.1066	.05512	.7890	
0.6	.3851	.60	.1167	.05736	.7573	
		.65	.1273	.05926	.7237	
0.7	.4323	.70	.1385	.06083	.6885	
		.75	.1505	.06216	.6519	
0.8	.4773	.80	.1633	.06320	.6143	
		.85	.1771	.06378	.5760	
0.9	.5035	.90	.1921	.06454	.5374	
		.95	.2084	.06487	.4988	
1.0	.5180	1.0	.2262	.06498	.4607	

$\lambda = 3/4 \quad b = 6$						
x	$K_0(x)$	\bar{w}/λ	C_T	C_P	C_{TP}/C_T	G
0	0	0	0	0	1.0	1.0
		.05	.01119	.00821	.9903	
0.1	.02301	.10	.02198	.01573	.9791	
		.15	.03240	.02259	.9662	
0.2	.08265	.20	.04253	.02883	.9516	
		.25	.05242	.03447	.9350	
0.3	.1586	.30	.06213	.03954	.9164	
		.35	.07174	.04409	.8957	
0.4	.2397	.40	.08133	.04813	.8728	
		.45	.09099	.05170	.8477	
0.5	.3187	.50	.1008	.05484	.8205	
		.55	.1109	.05756	.7911	
0.6	.3909	.60	.1213	.05991	.7597	
		.65	.1322	.06191	.7265	
0.7	.4535	.70	.1438	.06359	.6917	
		.75	.1560	.06496	.6555	
0.8	.5042	.80	.1692	.06606	.6183	
		.85	.1833	.06689	.5804	
0.9	.5407	.90	.1986	.06747	.5421	
		.95	.2152	.06782	.5039	
1.0	.5582	1.0	.2333	.06794	.4660	

$\lambda = 3/4 \quad b = 8$						
x	$K_0(x)$	\bar{w}/λ	C_T	C_P	C_{TP}/C_T	G
0	0	0	0	0	1.0	1.0
		.05	.01139	.00835	.9900	
0.1	.01960	.10	.02238	.01601	.9785	
		.15	.03300	.02300	.9654	
0.2	.07545	.20	.04333	.02935	.9506	
		.25	.05342	.03510	.9338	
0.3	.1506	.30	.06333	.04027	.9151	
		.35	.07314	.04490	.8943	
0.4	.2334	.40	.08293	.04903	.8714	
		.45	.09278	.05267	.8464	
0.5	.3158	.50	.1028	.05587	.8192	
		.55	.1131	.05865	.7900	
0.6	.3927	.60	.1237	.06106	.7588	
		.65	.1348	.06311	.7258	
0.7	.4606	.70	.1465	.06482	.6915	
		.75	.1589	.06623	.6554	
0.8	.5171	.80	.1722	.06735	.6185	
		.85	.1865	.06820	.5809	
0.9	.5591	.90	.2020	.06880	.5429	
		.95	.2187	.06916	.5049	
1.0	.5805	1.0	.2369	.06928	.4673	

$\lambda = 3/4 \quad b = 12$						
x	$K_0(x)$	\bar{w}/λ	C_T	C_P	C_{TP}/C_T	G
0	0	0	0	0	1.0	1.0
		.05	.01156	.00847	.9896	
0.1	.01784	.10	.02272	.01629	.9777	
		.15	.03353	.02333	.9642	
0.2	.06979	.20	.04404	.02978	.9489	
		.25	.05431	.03562	.9319	
0.3	.1436	.30	.06441	.04088	.9129	
		.35	.07442	.04559	.8920	
0.4	.2272	.40	.08440	.04978	.8690	
		.45	.09444	.05349	.8439	
0.5	.3120	.50	.1046	.05675	.8167	
		.55	.1151	.05959	.7876	
0.6	.3923	.60	.1259	.06203	.7566	
		.65	.1372	.06412	.7238	
0.7	.4649	.70	.1491	.06587	.6896	
		.75	.1617	.06730	.6540	
0.8	.5272	.80	.1751	.06845	.6175	
		.85	.1896	.06932	.5802	
0.9	.5762	.90	.2051	.06993	.5427	
		.95	.2220	.07029	.5050	
1.0	.6038	1.0	.2402	.07041	.4677	

$\lambda = 1 \quad b = 2$						
x	$K_0(x)$	\bar{w}/λ	C_T	C_R	C_{TR}/C_T	G
0	0	0	0	0	1.0	1.0
		.05	.01131	.01099	.9877	.9872
0.1	.04382	.10	.02227	.02098	.9742	.9737
		.15	.03290	.02999	.9594	.9595
0.2	.08653	.20	.04325	.03808	.9430	.9446
		.25	.05339	.04529	.9248	.9289
0.3	.1271	.30	.06337	.05167	.9047	.9124
		.35	.07329	.05726	.8825	.8951
0.4	.1647	.40	.08325	.06212	.8580	.8769
		.45	.09334	.06631	.8311	.8578
0.5	.1985	.50	.1037	.06987	.8017	.8377
		.55	.1145	.07287	.7696	.8167
0.6	.2280	.60	.1259	.07536	.7351	.7947
		.65	.1381	.07740	.6982	.7718
0.7	.2526	.70	.1514	.07909	.6591	.7479
		.75	.1659	.08034	.6182	.7230
0.8	.2719	.80	.1821	.08133	.5759	.6972
		.85	.2001	.08205	.5329	.6705
0.9	.2850	.90	.2203	.08255	.4896	.6430
		.95	.2432	.08283	.4467	.6198
1.0	.2910	1.0	.2690	.08293	.4097	.5858

$\lambda = 1 \quad b = 3$						
x	$K_0(x)$	\bar{w}/λ	C_T	C_P	C_{TP}/C_T	G
0	0	0	0	0	1.0	1.0
		.05	.01255	.01224	.9917	
0.1	.02915	.10	.02460	.02337	.9870	
		.15	.03621	.03342	.9708	
0.2	.07297	.20	.04743	.04246	.9578	
		.25	.05835	.05051	.9428	
0.3	.1204	.30	.06903	.05764	.9256	
		.35	.07958	.06391	.9059	
0.4	.1673	.40	.09010	.06936	.8837	
		.45	.1007	.07406	.8586	
0.5	.2113	.50	.1116	.07807	.8306	
		.55	.1229	.08145	.7996	
0.6	.2506	.60	.1348	.08427	.7657	
		.65	.1475	.08653	.7290	
0.7	.2841	.70	.1613	.08844	.6899	
		.75	.1764	.08991	.6485	
0.8	.3108	.80	.1932	.09104	.6056	
		.85	.2119	.09187	.5615	
0.9	.3299	.90	.2328	.09244	.5170	
		.95	.2564	.09277	.4728	
1.0	.3382	1.0	.2830	.09288	.4279	

$\lambda = 1 \quad b = 4$						
x	$K_0(x)$	\bar{w}/λ	C_T	C_P	C_{TP}/C_T	G
0	0	0	0	0	1.0	1.0
		.05	.01329	.01799	.9933	
0.1	.02018	.10	.02602	.02480	.9852	
		.15	.03824	.03549	.9755	
0.2	.06226	.20	.05007	.04508	.9640	
		.25	.06144	.05365	.9504	
0.3	.1122	.30	.07258	.06125	.9345	
		.35	.08356	.06792	.9160	
0.4	.1645	.40	.09448	.07373	.8948	
		.45	.1055	.07875	.8706	
0.5	.2154	.50	.1167	.08304	.8434	
		.55	.1284	.08666	.8130	
0.6	.2621	.60	.1407	.08968	.7796	
		.65	.1537	.09216	.7432	
0.7	.3028	.70	.1679	.09416	.7041	
		.75	.1834	.09575	.6628	
0.8	.3358	.80	.2006	.09697	.6197	
		.85	.2197	.09787	.5755	
0.9	.3594	.90	.2410	.09898	.5306	
		.95	.2651	.09884	.4859	
1.0	.3708	1.0	.2921	.09896	.4420	

$\lambda = 1 \quad b = 6$						
x	$K_0(x)$	\bar{w}/λ	C_T	C_F	C_{TF}/C_T	G
0	0	0	0	0	1.0	1.0
		.05	.01401	.01371	.991	
0.1	.01341	.10	.02741	.02618	.9868	
		.15	.04026	.03757	.9779	
0.2	.05020	.20	.05262	.04762	.9671	
		.25	.06452	.05668	.9543	
0.3	.09991	.30	.07626	.06473	.9390	
		.35	.08773	.07180	.9213	
0.4	.1562	.40	.09916	.07798	.9007	
		.45	.1106	.08331	.8771	
0.5	.2190	.50	.1223	.08787	.8505	
		.55	.1344	.09172	.8206	
0.6	.2695	.60	.1471	.09496	.7877	
		.65	.1606	.09762	.7518	
0.7	.3198	.70	.1752	.09977	.7131	
		.75	.1912	.1015	.6721	
0.8	.3619	.80	.2087	.1028	.6293	
		.85	.2283	.1038	.5852	
0.9	.3930	.90	.2501	.1041	.5402	
		.95	.2746	.1048	.4958	
1.0	.4088	1.0	.3021	.1049	.4517	

$\lambda = 1 \quad b = 8$						
x	$K_0(x)$	\bar{w}/λ	C_T	C_P	C_{TP}/C_T	G
0	0	0	0	0	1.0	1.0
		.05	.01438	.01406	.9942	
0.1	.01123	.10	.02812	.02687	.9869	
		.15	.04131	.03846	.9781	
0.2	.04485	.20	.05400	.04888	.9673	
		.25	.06678	.05820	.9543	
0.3	.09312	.30	.07824	.06698	.9394	
		.35	.09001	.07376	.9217	
0.4	.1502	.40	.1017	.08011	.9013	
		.45	.1134	.08561	.8779	
0.5	.2109	.50	.1254	.09032	.8514	
		.55	.1378	.09430	.8218	
0.6	.2709	.60	.1507	.09764	.7892	
		.65	.1645	.1004	.7533	
0.7	.3267	.70	.1794	.1026	.7152	
		.75	.1956	.1044	.6745	
0.8	.3751	.80	.2135	.1057	.6320	
		.85	.2333	.1067	.5882	
0.9	.4121	.90	.2553	.1074	.5438	
		.95	.2801	.1078	.4993	
1.0	.4320	1.0	.3078	.1080	.4554	

$\lambda = 1 \quad b = 12$						
x	$K_0(x)$	\bar{w}/λ	C_T	C_F	C_{TF}/C_T	G
0	0	0	0	0	1.0	1.0
		.05	.01465	.01428	.9939	
0.1	.01019	.10	.02867	.02719	.9863	
		.15	.04213	.03878	.9771	
0.2	.04091	.20	.05509	.04913	.9662	
		.25	.06764	.05830	.9531	
0.3	.08740	.30	.07988	.06837	.9378	
		.35	.09192	.07340	.9200	
0.4	.1441	.40	.1039	.07964	.8995	
		.45	.1159	.08464	.8761	
0.5	.2061	.50	.1281	.08900	.8497	
		.55	.1407	.09262	.8202	
0.6	.2693	.60	.1540	.09558	.7878	
		.65	.1680	.09793	.7521	
0.7	.3302	.70	.1831	.09976	.7195	
		.75	.1996	.1011	.6742	
0.8	.3850	.80	.2177	.1021	.6321	
		.85	.2377	.1027	.5887	
0.9	.4289	.90	.2600	.1030	.5497	
		.95	.2819	.1030	.5006	
1.0	.4542	1.0	.3127	.1028	.4570	

$\lambda = 1 \quad b = 1/6$						
x	$K_0(x)$	\bar{w}/λ	C_T	C_P	C_{TP}/C_T	G
0	0	0	0	0	1.0	1.0
		.05	.01479	.01446	.9936	
0.1	.00997	.10	.02896	.02764	.9857	
		.15	.04256	.03957	.9763	
0.2	.03950	.20	.05568	.05031	.9651	
		.25	.06838	.05992	.9518	
0.3	.08512	.30	.08077	.06845	.9363	
		.35	.09296	.07597	.9183	
0.4	.1415	.40	.1051	.08254	.8977	
		.45	.1172	.08823	.8743	
0.5	.2038	.50	.1296	.09310	.8479	
		.55	.1424	.09724	.8185	
0.6	.2679	.60	.1558	.1007	.7862	
		.65	.1700	.1036	.7510	
0.7	.3307	.70	.1852	.1059	.7132	
		.75	.2018	.1077	.6732	
0.8	.3889	.80	.2200	.1091	.6314	
		.85	.2402	.1102	.5883	
0.9	.4377	.90	.2626	.1109	.5446	
		.95	.2876	.1113	.5007	
1.0	.4680	1.0	.3155	.1115	.4579	

CITED LITERATURE

1. Sacks, A. H., Burnell, J. A., "Ducted Propellers - A Critical Review of the State of the Art," Progress in Aeronautical Sciences, Vol. III, pp. 87-135, Pergamon Press, Inc., New York, N. Y., 1962.
2. Tachmindji, A. J., "The Potential Problem of the Optimum Propeller with Finite Number of Blades Operating in a Cylindrical Duct," Report 1228, July 1958, David Taylor Model Basin, Washington, D. C.
3. Theodorsen, T., "Theoretical Investigation of Ducted Propeller Aerodynamics," Vol. III TREC TR 61-119, Sept. 1961, U. S. Army Transportation Research Command, Fort Eustis, Va.
4. Gray, R. B., "An Investigation of an Approach to the Problem of Determining the Optimum Design of Shrouded Propellers," TREC 60-44, May 1960, U. S. Army Transportation Research Command, Fort Eustis, Va.
5. Gray, R. B., "An Investigation of a Digital Computer Method of Determining the Optimum Design Parameters of Shrouded Propellers," TREC 61-124, Oct. 1961, U. S. Army Transportation Research Command, Fort Eustis, Va.
6. Morgan, W. B., "Theory of the Annular Airfoil and Ducted Propeller," Fourth Symposium on Naval Hydrodynamics, Office of Naval Research, Department of the Navy, Washington, D.C., ACR-73, Vol. I, pp. 161-212.
7. Ordway, D. C., Sluyter, M. M., and Sonnerup, B. O. U., "Three-Dimensional Theory of Ducted Propellers," TAR-TR 602, Aug. 1960, Therm Advanced Research Division of Therm Corporation, Ithaca, New York.
8. Chaplin, H. R., "A Method for Numerical Calculation of Slipstream Contraction of a Shrouded Impulse Disc in the Static Case with Application to Other Axisymmetric Flow Problems," Report 1857, June 1964, David Taylor Model Basin, Washington, D. C.
9. Betz, A., "Screw Propellers with Minimum Energy Loss," Technical Translation 736, National Research Council of Canada, Ottawa, Canada, 1958.

10. Goldstein, S., "On the Vortex Theory of Screw Propellers," Proceedings of the Royal Society (London), Ser. A., Vol. 112, pp. 440-465.
11. Theodorsen, T., Theory of Propellers, McGraw-Hill Book Company, Inc., New York, N. Y. 1948.
12. Lamb, H., Hydrodynamics, Dover Publications, New York, N. Y., 1945.
13. Gray, R. B., "Analysis of a Heavily Load Ducted Fan with an Infinite Number of Blades," to be published.
14. Fadeeva, V. N., Computational Methods of Linear Algebra, pp. 67-72, Dover Publications, Inc., New York, N. Y. 1959.
15. Hodgman, C. D., Standard Mathematical Tables, The Chemical Rubber Publishing Company, Cleveland, Ohio, 1959.
16. Keuthe, A. M., Schetzer, J. C., Foundations of Aerodynamics, John Wiley and Sons, Inc., New York, N. Y., 1959.

Unclassified
Security Classification

DOCUMENT CONTROL DATA - R & D

(Security classification of title, body of abstract and indexing annotation must be entered when the overall report is classified)

1. ORIGINATING ACTIVITY (Corporate author) Georgia Institute of Technology		2a. REPORT SECURITY CLASSIFICATION Unclassified	
		2b. GROUP NA	
3. REPORT TITLE Determination of the Design Parameters for Optimum Heavily Loaded Ducted Fans			
4. DESCRIPTIVE NOTES (Type of report and inclusive dates) Technical Report			
5. AUTHOR(S) (First name, middle initial, last name) Terry Wright			
6. REPORT DATE November 1969		7a. TOTAL NO. OF PAGES 140	7b. NO. OF REFS 16
8a. CONTRACT OR GRANT NO. DAHCO4 68 C 0004		8b. ORIGINATOR'S REPORT NUMBER(S) Report 69-3	
8. PROJECT NO.		8c. OTHER REPORT NO(S) (Any other numbers that may be assigned this report) T-2.8-E	
8.			
8.			
10. DISTRIBUTION STATEMENT This document has been approved for public release and sale; its distribution is unlimited.			
11. SUPPLEMENTARY NOTES		12. SPONSORING MILITARY ACTIVITY U. S. Army Research Office-Durham Box CM, Duke Station Durham, North Carolina 27706	
13. ABSTRACT Like the free propeller in axial flight, a single-rotation ducted fan of highest induced efficiency is characterized by an ultimate wake vortex system shed from the blade trailing edges whose apparent motion is that of rigid helical surfaces. In addition and concentric with this inner sheet system there is a cylindrical surface of helical vortex filaments shed from the duct training edge. For zero hub diameter and neglecting compressibility, viscosity and tip clearance, a consistent mathematical model of the constant-diameter vortex wake is developed and the compatibility relationships to be satisfied are presented. Using the Biot-Savart equation, the vortex strength distribution in the ultimate wake is determined and then related to the blade bound vortex strength distribution. In addition, expressions are developed for the thrust, power and induced efficiency which depend on numerical integrations of velocity profiles in the ultimate wake. It is shown that the wake vorticity and the velocity distribution in the wake for all loadings from the lightly loaded limit to the heavily loaded static thrust condition may be extracted from the lightly loaded result through the use of a simple algebraic scale factor. The performance parameters, thrust, power and blade bound vortex strength are thus expressed in terms of a lightly loaded solution for a given freestream velocity, blade tip speed, blade number and the loading parameter. The lightly loaded case is compared to existing theoretical and experimental results. Some sample results for heavily loaded performance parameters and design parameters are presented and compared to the exact results for a heavily loaded ducted fan with an infinite number of blades. Results for the heavily loaded system over a broad range of conditions are presented.			

DD FORM 1473
NOV 65

REPLACES DD FORM 1473, 1 JAN 64, WHICH IS OBSOLETE FOR ARMY USE.

Unclassified

Security Classification

Security Classification

14. KEY WORDS	LINK A		LINK B		LINK C	
	ROLE	WT	ROLE	WT	ROLE	WT
Ducted fans Vortices Wakes Aerodynamics						